Title
THE (p,t) AND (p, 3He) REACTIONS ON (2s-ld) SHELL NUCLEI

Author
Brunnader, Heinz.

Publication Date
1969

UCRL-18716

eq I

THE (p, t) AND (p, ^{3}He) REACTIONS ON (2s-1d) SHELL NUCLEI

Heinz Brunnader
(Ph. D. Thesis)

January 1969

LAWRENCE RADIATION LABORATORY
UNIVERSITY of CALIFORNIA BERKELEY

UCRL-18716

eq I

DISCLAIMER

UCRL-18716

UNIVERSITY OF CALIFORNIA

Lawrence Radiation Laboratory
Berkeley, California 94720

AEC Contract No. W-7405-eng-48

THE (p,t) AND (p,^{3}He) REACTIONS ON (2s-1d) SHELL NUCLEI

Heinz Brunnader
(Ph.D. Thesis)

January 1969

TABLE OF CONTENTS

THE (p,t) AND (p,^{3}He) REACTIONS ON (2s-1d) SHELL NUCLEI

Heinz Brunnader

Department of Chemistry and Lawrence Radiation Laboratory
University of California, Berkeley, California 94720

January 1969

ABSTRACT

The excitations of high isospin (T=2) analogue states in the T_z=0 and the T_z=+1 A=4n nuclei have been measured for the entire (sd) shell using the (p,t) and (p,^{3}He) reactions induced by 45 MeV protons. Also, the reactions ^{40}Ar(p,t)^{38}Ar and ^{40}Ar(p,^{3}He)^{38}Cl were utilized to observe the first T=3 analogue states in the T_z=1 and T_z=2 nuclei. In addition to these high T states, a number of T=1 analogue states were also observed. The ratio of the observed cross sections for these T=1 analogue states was compared with the ratio predicted from the DWBA cross section expressions. This predicted ratio is found to depend on the type of transition by which the final analogue states are formed, and hence may be used to provide structural information on the analogues without the use of detailed wave functions. The (p,t) reaction was further utilized to extend the range of known excitations in the nuclei ^{18}Ne and ^{34}Ar. All Coulomb displacement data in the (1p) and ($1d_{5/2}$) shells, including those derived from this work, were fitted to parameterized Coulomb displacement energy formulae derived in the jj-coupling low seniority and Wigner supermultiplet schemes. The results were used to predict the masses of yet unmeasured neutron deficient nuclei in this region.

I. INTRODUCTION

There has been an increasing utilization of two nucleon transfer reactions in recent years to determine nuclear level structure and to obtain spectroscopic information. Much of this information has been derived from a comparison of characteristic shapes of angular distributions of reaction products. However, the increasing application of distorted wave Born approximation (DWBA) caluclations[1-5] has permitted the interpretation of the results in terms of detailed nuclear structure.

The differential cross section for a two nucleon transfer reaction, neglecting spin-orbit forces, can be written as:

$$\left(\frac{d\sigma}{d\Omega}\right) \propto \sum_{LSJT} f(S,T)\left|\sum_{N}^{\ell_1\ell_2} \mathcal{S}^{1/2}\,(\ell_1\ell_2;\ LSJT)\cdot B^{M}_{NL}(E,\theta,Q)\right|^2 \qquad \text{(I-1)}$$

where ℓ_1 and ℓ_2 are the angular momenta of the transferred nucleons which can be coupled to states of LSJT; $\mathcal{S}^{1/2}$ is the spectroscopic factor, and B is the transition probability of a structureless pair of particles. As a result of this coherent sum over $\mathcal{S}^{1/2}$ and B, the detailed comparison with experiment is strongly dependent upon accurate wave functions.

Some spectroscopic information, however, can be obtained without detailed wave functions from the comparisons of the cross sections of analogue final states (same $J^{\pi};T$) produced by mirror reactions; an example would be the (p,t) and (p,^{3}He) reactions. For final states with a final isospin, $T_f = T_i + 1$ both reactions are restricted to S=0, T=1 transfer. Consequently, the angular distributions observed for the outgoing tritons and ^{3}He particles populating such states should be

identical in shape and differ only in magnitude by a factor depending on the reaction kinematics and on an isospin Clebsch-Gordan coupling coefficient. This fact has been utilized previously[6,7] to identify the T=3/2 and T=2 states produced by these reactions. This thesis extends such comparison to states of high isospin ($T_f=T_i+1$) in (sd)-shell nuclei.

For final states with $T_f=T_i$ ($T_i=1,2$), the cross section ratios for analogue states are found to depend on the type of transition by which they are produced. Hence the ratios can be used to distinguish states produced by the pickup of two particles from the same shell (i.e., j^2 pickup) or different shells (j_1j_2-pickup). In certain favorable cases, the cross section ratio observed for j_1j_2 pickup may also be used to determine the spin and parity of the final states. A comparison of the observed cross section ratios with those predicted from nuclear configurations is made for $T_f=T_i$ states in nuclei of the (sd)-shell.

Assuming the charge independence of nuclear forces analogue states will have identical nuclear configurations, the differences in their masses, corrected for the neutron-hydrogen mass difference, should, therefore be due simply to the Coulomb interaction. Recently, Hecht[8] has derived Coulomb energy formulae for two limiting coupling schemes: the jj-coupling low seniority scheme, and the Wigner supermultiplet scheme. These energy formulae have been utilized to obtain a general Coulomb displacement energy formula for each of the coupling schemes. In principle, any deviations observed between the calculated and experimental displacement energies can be interpreted as non-Coulomb charge-dependent effects, including the charge-dependence of nuclear forces. In this work, however,

the general displacement formulae have been parameterized and fitted to the experimental data.

Multiplets based on ground states with $T=T_z > 0$ which lie entirely within either the (1p)- or $(1d_{5/2})$-shells were used to obtain the displacement energies. The data for each shell were treated separately to minimize unrelated effects. Both the seniority and the supermultiplet formulae were used in the $(1d_{5/2})$-shell in order to determine the effect of the different coupling schemes. Only the supermultiplet scheme was used to fit the (1p)-shell, because the seniority scheme is not valid over the combined $(1p_{3/2})$- and $(1p_{1/2})$-shells.

The good agreement obtained in fitting the experimental data indicate that these formulae may be used to predict the masses of yet unmeasured nuclei and their analogues from the known mass of any one member of a multiplet. Such predictions have been tabulated for multiplets of $T \geq 2$. In cases where no members of a multiplet have been reported, the Coulomb displacement energies have been listed instead.

II. THEORY

A. Cross Section Ratios of Analogue States

Several distorted wave theories of direct two-nucleon transfer reactions have been developed[1,2,9] and have been extensively applied to experimental data. Because of the coherent sum over structural and kinematic factors, the two-nucleon transfer DWBA theory requires the knowledge of detailed nuclear wave functions for the initial and final states of the reaction in order to calculate spectroscopic information. As a result, a comparison of observed intensities with predicted values provides a very sensitive test of the nuclear wave functions. No wave function information, however, can be obtained directly from the experiment using this approach because of these coherent effects.

However, by comparing the experimental cross section ratio obtained for the mirror pickup reactions, (p,t) and (p,^{3}He), proceeding to analogue final states (identical $J^\pi;T$), with the calculated ratio, some nuclear structure information can be obtained. Using the DWBA formalism of Glendenning,[1] the expression for the differential cross section, neglecting spin-orbit forces, can be written as follows:

$$\left(\frac{d\sigma}{d\Omega}\right) \propto \frac{k_f}{k_i} \sum_{LSJT} C^2_{ST} \sum_M \left| \sum_N G_{NLSJT} \cdot B^M_{NL}\ (k_i,k_f) \right|^2 \qquad \text{(II-1)}$$

where N is the principal quantum number, L is the angular momentum, and M is its projection, and k_f and k_i are the wave numbers of the light outgoing and incoming particles, respectively.

The term $C^2_{ST} = b^2_{ST}\ |\langle T_f\ T\ T_{zf} T_z | T_i T_{zi}\rangle|^2 [D(S,T)]^2$ for a pickup

reaction, where b^2_{ST} is an overlap integral involving the spin-isospin wave functions of the transferred pair of nucleons, and the A=3 ground state wave functions.

$$b^2_{ST} = \begin{cases} (\delta_{S0}\ \delta_{T1}) & \text{for } (p,t) \\ 1/2[(\delta_{S0}\ \delta_{T1}) + (\delta_{S1}\ \delta_{T0})] & \text{for } (p,{}^3He) \end{cases} \qquad \text{(II-2)}$$

The Clebsch-Gordan coefficient relates the isospins of the initial and final nuclear states produced by the transfer of the nucleon pair with isospin T and a projection T_z where T_z is defined as $\frac{1}{2}(N-Z)$. The spin factor [D(S,T)] is a function of S and T and results from introducing spin and isospin exchange terms in the interaction potential.[5] The nuclear structure factor, G_{NLSJT}, is given by:

$$G_{NLSJT} = \Omega_n \sum^{[n_1\ell_1 j_1][n_2\ell_2 j_2]} g\, \mathcal{A}^{1/2}_{AB}([n_1\ell_1 j_1][n_2\ell_2 j_2];\ JT) \begin{bmatrix} \ell_1 & \ell_2 & L \\ \frac{1}{2} & \frac{1}{2} & S \\ j_1 & j_2 & J \end{bmatrix}$$

$$\times \langle \bar{n}_1\ell_1\bar{n}_2\ell_2 : L \,|\, \bar{n}\ 0\ \bar{N}\ L : L \rangle \qquad \text{(II-3)}$$

where Ω_n is the overlap of the relative motion in the target of the transferred pair with the motion in the light nuclide which is formed and can be evaluated by the following relationship:

$$\Omega_n = \frac{[(2n-1)!]^{1/2}}{2^{n-1}(n-1)!} \left(\frac{2\sqrt{6}\,\nu^{1/2}\,\eta}{6\eta^2+\nu}\right)^{3/2} \cdot \left(1 - \frac{2\nu}{6\eta^2+\nu}\right)^{n-1} \quad n = 1,2,\ldots \qquad \text{(II-4)}$$

The size parameter η of the light residual nuclide[1] is related to its mean square radius by $\eta^2 = 1/6\langle r^2\rangle$ for mass 3 particles. ν is the strength parameter of the harmonic oscillator wave functions of the transferred pair of nucleons.

$$g = \begin{cases} 1 & \text{if } [n_1\ell_1 j_1] = [n_2\ell_2 j_2] \\ \sqrt{2} & \text{otherwise} \end{cases} \qquad \text{(II-5)}$$

$\mathcal{S}_{AB}^{1/2}([n_1\ell_1 j_1][n_2\ell_2 j_2]; JT)$ is the spectroscopic factor for the production of a final state with J,T by pickup of 2 particles with quantum numbers $[n_1\ell_1 j_1]$ and $[n_2\ell_2 j_2]$ respectively. The factor, [LSJ] is defined as:

$$\begin{bmatrix} \ell_1 & \ell_2 & L \\ \frac{1}{2} & \frac{1}{2} & S \\ j_1 & j_2 & J \end{bmatrix} = [(2L+1)(2S+1)(2j_1+1)(2j_2+1)]^{1/2} \begin{Bmatrix} \ell_1 & \ell_2 & L \\ \frac{1}{2} & \frac{1}{2} & S \\ j_1 & j_2 & J \end{Bmatrix} \qquad \text{(II-6)}$$

where {L,S,J} is a standard 9-j coefficient as defined in de Shalit and Talmi[10] and comes from the transformation from j-j to L S coupling; and $\langle \bar{n}_1\ell_1\bar{n}_2\ell_2{:}L \mid \bar{n}0\bar{N}L{:}L \rangle$ represents the transformation from the individual coordinates of the two nucleons to center-of-mass and relative coordinates. The values for these transformation brackets have been tabulated by Brody and Moshinsky.[11] (Note that the values tabulated in Ref. 11 use the radial quantum number $\bar{n}$, which is related to the principal quantum number n by $n=\bar{n}+1$.) The term B_{NL}^{M} is the transfer amplitude representing the probability of transferring a structureless pair of nucleons from the

target to the incident particle. Although there is a slight kinematic dependence in this term, it will be treated as identical for both (p,t) and (p,^{3}He) pickup to analogue states. This assumption has been shown to be acceptable in the comparison of (p,t) and (p,^{3}He) cross sections for S=0, T=1 transitions from T=1/2 states to T=3/2 states, where agreement to better than 10% is obtained for the (1p)shell and the (1d)shell.[4,12]

In order to derive spectroscopic information from cross section data without the use of detailed wave functions one can employ the magnitude ratios of analogue states observed in mirror reactions. If the (p,t) and (p,^{3}He) mirror reactions are observed on the same target and populate analogue final states, then the ratio of the differential cross sections can be written as:

$$\frac{(d\sigma/d\Omega)_{(p,t)}}{(d\sigma/d\Omega)_{(p,^3He)}} = \frac{k_t}{k_{^3He}} \cdot \frac{\sum_{LSJT} C^2_{ST}(t) \sum_N \left| G_{NLSJT}(t) \right|^2}{\sum_{LSJT} C^2_{ST}(^3He) \sum_N \left| G_{NLSJT}(^3He) \right|^2} \qquad \text{(II-7)}$$

Restricting these pickup reactions to even-even targets ($J^\pi_i = 0^+$) and assuming for the derivation, single initial and final configurations the summation over M disappears and a further simplification can be made in the above expression. Since $\vec{J}_f = \vec{J}_i + \vec{J}$, then for even-even targets, $J_f = J$. Thus the summation over J required to evaluate the ratio reduces to a single term for both reactions. Similarly, for the (p,t) reaction, the transition can proceed only by S=0, T=1 transfer. From the equation $\vec{J} = \vec{L} + \vec{S}$, it is evident that for S=0, J=L, and hence the summations over

L, S, and T are also replaced by a single term. The (p,^{3}He) reaction, however, can in general proceed by both S=0, T=1 and S=1, T=0 transfer. This reduces the summation over S and T to two terms. Since, in this comparison, only the ratio for natural parity states is considered (the (p,t) reaction on 0^+ targets can populate only natural parity states, i.e., states with $\pi=(-)^J$), again only a single L can contribute, eliminating the sum over L. (In principle, for (p,^{3}He) reactions, J=L, L±1, but since $\pi_f=(-)^L\pi_i$ a transfer of L±1 would change the parity of the states produced and hence results in unnatural parity states. Thus the expression for the cross section ratio, R_c, can be simplified to give:

$$R_c(t/^3He) = \frac{(d\sigma/d\Omega)_{(p,t)}}{(d\sigma/d\Omega)_{(p,^3He)}} = \frac{k_t}{k_{^3He}} \quad \frac{C^2_{ST}(t)\left|G_{NLSJT}(t)\right|^2}{\sum_{S,T} C^2_{ST}(^3He)\left|G_{NLSJT}(^3He)\right|^2} \tag{II-8}$$

From the definition of G_{NLSJT} given by Eq. (II-3), it is evident that only two factors, the spectroscopic factor ($\mathcal{S}^{1/2}_{AB}$) and the [9j]-factor can depend on S or T, and hence differ for (p,t) and (p,^{3}He).

By evaluating the summation, substituting for C^2_{ST} and G_{NLSJT} and cancelling common factors, Eq. (II-8) can be rewritten as follows:

$$R_c(t/^3He) = \frac{k_t}{k_{^3He}} \cdot \frac{\left|\langle T_f\ 1\ T_{zf}\ 1 \left|\ T_i T_{zi}\right\rangle\right|^2}{\frac{1}{2}\left|\langle T_f\ 1 T_{zf}\ 0 \left| T_i T_{zi}\right\rangle\right|^2 + \frac{3}{2}R\left|\langle T_f\ 0 T_{zf}\ 0 \left| T_i T_{zi}\right\rangle\right|^2 \left|f(\mathcal{S})\right|^2} \tag{II-9}$$

where

$$f(\mathcal{L}) = \frac{\mathcal{L}_{AB}^{1/2}\ (T=0) \begin{Bmatrix} \ell_1 & \ell_2 & L \\ \frac{1}{2} & \frac{1}{2} & 1 \\ j_1 & j_2 & J \end{Bmatrix}}{\mathcal{L}_{AB}^{1/2}\ (T=1) \begin{Bmatrix} \ell_1 & \ell_2 & L \\ \frac{1}{2} & \frac{1}{2} & 0 \\ j_1 & j_2 & J \end{Bmatrix}} \qquad \text{(II-10)}$$

and

$$R = \left\{ \frac{[D(10)]}{[D(01)]} \right\}^2 \qquad \text{(II-11)}$$

R is the ratio of strengths of the singlet and triplet spin terms, and is usually taken to be 1/3.[4,5]

Using the relationship*

$$\begin{Bmatrix} \ell_1 & \ell_2 & L \\ \frac{1}{2} & \frac{1}{2} & 1 \\ j_1 & j_2 & J \end{Bmatrix} = (-) \frac{[\ell_1(\ell_1+1)-\ell_2(\ell_2+1)] - [j_1(j_1+1)-j_2(j_2+1)]}{[3L(L+1)]^{1/2}} \begin{Bmatrix} \ell_1 & \ell_2 & L \\ \frac{1}{2} & \frac{1}{2} & 0 \\ j_1 & j_2 & J \end{Bmatrix} \qquad \text{(II-12)}$$

and recognizing the following equalities:

(i) For all stable targets; $T_i = T_{zi}$

(ii) For (p,t); $T_{zf} = T_{zi} - 1 = T_i - 1$

---

* The equality as given by M. Rotenberg, R. Bivins, N. Metropolis, and J. K. Wooten, Jr., Table of 3n-j Symbols, Technology Press, M.I.T., Cambridge (1959), and by de Shalit and Talmi,[10] are erroneous. The correct equation has been derived by W. E. Rose and L. C. Biedenharn, in report number (ORNL-1779) and J. M. Kennedy and W. T. Sharp in the AECL report number (CRT-580).

(iii) For $(p,{}^3He)$; $T_{zf} = T_{zi} = T_i$

(iv) For $(p,{}^3He)$, S = 1 term; $T_f = T_i$

$$\therefore \langle T_f T\ T_{zf} T_z | T_i T_{zi} \rangle = \langle T_i\ 0\ T_i\ 0 | T_i T_i \rangle = 1$$

Hence

$$R_c(t/{}^3He) = \frac{2k_t}{k3_{He}} \cdot \frac{|\langle T_f\ 1\ T_i\ -1\ 1 | T_i T_i \rangle|^2}{|\langle T_f 1 T_i 0 | T_i T_i \rangle|^2 + \frac{1}{3}\delta_{S1} \left| \frac{\mathcal{J}_{AB}^{1/2}(T=0)}{\mathcal{J}_{AB}^{1/2}(T=1)} \cdot \frac{\lambda}{\sqrt{L(L+1)}} \right|^2} \tag{II-13}$$

where

$$\lambda = [\ell_1(\ell_1 + 1) - \ell_2(\ell_2 + 1)] - [j_1(j_1 + 1) - j_2(j_2 + 1)] \tag{II-14}$$

1. j^2 Pickup

For a pickup involving two particles from the same shell (i.e., j^2 pickup), $\ell_1 = \ell_2$ and $j_1 = j_2$. Hence $\lambda = 0$, so that there is no S = 1 component to the transition amplitude for the $(p,{}^3He)$ reaction between such initial and final states. Thus, the cross section ratio becomes

$$R_c(j^2;\ t/{}^3He) = \frac{2k_t}{k3_{He}} \frac{|\langle T_f 1 T_i\ -1\ 1 | T_i T_i \rangle|^2}{|\langle T_f 1 T_i\ 0 \mid T_i T_i \rangle|^2} \tag{II-15}$$

A j^2 pickup can produce final analogue states of $T_f = T_i + 1$ and $T_f = T_i$ configurations. For these two cases, the Clebsch-Gordan coefficients can be evaluated to give the following results:

$$T_f = T_i + 1 \qquad R_c(T_+;t/^3He) = \frac{k_t}{k3_{He}} \cdot \frac{2}{(2T_f-1)} \tag{II-16}$$

$$T_f = T_i \qquad R_c(j^2;t/^3He) = \frac{k_t}{k3_{He}} \cdot \frac{2}{T_f} \tag{II-17}$$

2. $j_1 j_2$ Pickup

The pickup of two particles from different shells (i.e., $j_1 j_2$ pickup) can again proceed to two types of final states: those with $T_f=T_i+1$ and those with $T_f=T_i$. Because the structure dependent term can contribute only for the latter, the cross section ratio expression for states of $T_f=T_i+1$ is identical to that given in Eq. (II-16). For the case of $T_f=T_i$, however, the S=1, T=0 term can now contribute to the transfer amplitude of the (p,^{3}He) reaction. In order to evaluate the spectroscopic factors in the structure term, a particular configuration for the final state must be assumed.

Algebraic expressions for the spectroscopic factors are given by Towner and Hardy[13] for two-nucleon pickup reactions. If one considers the pickup of one particle from the outer shell, and one particle from the second shell, with lower shells filled, e.g., for a ^{22}Ne target

$$[(1p\ 1/2)^4_{j_i=0;t_i=0}(1d\ 5/2)^6_{j_i'=0;t_i'=1}]_{J_i=0,T_i=1} \tag{II-18}$$

$$\uparrow\downarrow$$

$$[(1p\ 1/2)^3_{j_f=1/2;t_f=1/2}(1d\ 5/2)^5_{j_f'=5/2;t_f'=1/2}]_{J_f;T_f}$$

(residual nucleus)

$$+\ [(1p\ 1/2)^1_{j_1=1/2;t_1=1/2}(1d\ 5/2)^1_{j_2=5/2;t_2=1/2}]_{J;T}$$

(transferred pair)

then:

$$\mathcal{S}_{AB}^{1/2} = (-)^{n_2-1}\binom{n_1}{1}^{1/2}\binom{n_2}{1}^{1/2} \langle (1p\ 1/2)^{n_1}(j_i;t_i)\{|(1p\ 1/2)^{n_1-1}(j_f;t_f);(1p\ 1/2)^1\rangle$$

$$\times \langle (1d\ 5/2)^{n_2}(j_i';t_i')\{|(1d\ 5/2)^{n_2-1}(j_f';t_f');(1d\ 5/2)^1\rangle$$

$$\times \begin{bmatrix} j_f & j_1 & j_i \\ j_f' & j_2 & j_i' \\ J_f & J & J_i \end{bmatrix} \begin{bmatrix} t_f & t_1 & t_i \\ t_f' & t_2 & t_i' \\ T_f & T & T_i \end{bmatrix} \qquad \text{(II-19)}$$

where $\langle \{| \rangle$'s are single particle coefficients of fractional parentage.

Since the shell-model configurations are identical for analogue final states, the cfp's are the same for both reactions, as are the binomial coefficients. Also, the [9j] coefficient in J is found to be identical in both the (p,t) and the (p,^{3}He) reactions. Hence, for a transition of the form described above

$$\frac{\mathcal{S}_{AB}^{1/2}(T=0)}{\mathcal{S}_{AB}^{1/2}(T=1)} = \frac{\begin{bmatrix} t_f & \frac{1}{2} & t_i \\ t_f' & \frac{1}{2} & t_i' \\ T_f & 0 & T_i \end{bmatrix}}{\begin{bmatrix} t_f & \frac{1}{2} & t_i \\ t_f' & \frac{1}{2} & t_i' \\ T_f & 1 & T_i \end{bmatrix}} = \frac{\sqrt{T_f(T_f+1)}}{\tau} \qquad \text{(II-20)}$$

where

$$\tau = [t_i(t_i+1) - t_i'(t_i'+1)] - [t_f(t_f+1) - t_f'(t_f'+1)] \qquad \text{(II-21)}$$

t_i and t_i' and t_f and t_f' are the isospins given by Eq. (II-18). These t's are the isospins to which the particles in each active subshell of the initial and final configurations are coupled.

Substituting this result into Eq. (II-13), and evaluating the Clebsch-Gordan coefficients produces the following result

$$R_c(j_1 j_2; t/^3He) = \frac{k_t}{k3_{He}} \cdot \frac{2}{T_f} \left[1 + \frac{1}{3} \cdot \frac{\lambda^2}{\tau^2} \cdot \frac{(T_f + 1)^2}{L(L+1)} \right]^{-1} \qquad \text{(II-22)}$$

The ratio of differential cross sections to analogue states produced by both the (p,t) and (p,^{3}He) reactions is summarized below:

(a) Case 1: $T_f = T_i + 1$: both the (p,t) and (p,^{3}He) reactions can proceed only through the S=0, T=1 term in the transition amplitude. The ratio for this case is entirely general and totally independent of any assumed configurations for either the initial and final states.

$$R_c(T_+;\ t/3_{He}) = \frac{k_t}{k3_{He}} \cdot \frac{2}{(2T_f - 1)} \qquad \text{(II-16)}$$

(b) Case 2: $T_f = T_i$, pickup of j^2 configuration: Because the factor λ=0 for this type of transition on even-even targets, only the S=0, T=1 term can again contribute to the reaction cross section. In this case the value of the ratio is again independent of any configuration assumed for either the initial or final states. It should also be noted that this ratio is independent of any mixture of j^2 transfers, provided essentially all transfers between initial and final states proceed by some j^2 process.

$$R_c(j^2;\ t/^3He) = \frac{k_t}{k^3He} \cdot \frac{2}{T_f} \qquad \text{(II-17)}$$

(c) Case 3: $T_f = T_i$, pickup of $j_1 j_2$ configuration: Both the S=0, T=1 term and the S=1, T=0 term can contribute to the cross section of the $(p,^3He)$ reaction in this case. In addition to the restriction to even-even ($J_i^\pi = 0^+$) targets, this ratio depends on the assumed initial and final configurations, because τ is related to the isospins of the sub-shells - see Eq. (II-21).

$$R_c(j_1 j_2; t/^3He) = \frac{k_t}{k^3He} \cdot \frac{2}{T_f} \left[1 + \frac{1}{3} \frac{\lambda^2}{\tau^2} \frac{(T_f + 1)^2}{L(L+1)} \right]^{-1} \qquad \text{(II-22)}$$

In the case of a $j_1 j_2$ transition, the cross section ratio is seen to depend strongly on the angular momentum transfer, L. Hence, for states with relatively pure initial and final configurations, related by a simple $j_1 j_2$ transfer, the cross section ratio could be used to assign spins to final states. For example, consider a pair of states in mass 40, produced by a transition such as:

$$[(1d\ 3/2)^8_{00} (1f\ 7/2)^2_{01}]_{01} \rightarrow [(1d\ 3/2)^7_{3/2\ 1/2} (1f\ 7/2)^1_{7/2\ 1/2}]_{J1}$$

Since the parity change is odd for such a transition, only odd J analogues will be produced by both the (p,t) and $(p,^3He)$ reactions. Hence, the J of the final state is either 3^- or 5^-. For $J^\pi = 3^-$, the cross section ratio is expected to be k_t/k^3He; for a $J^\pi = 5^-$ it is $1.42\ k_t/k^3He$. These differences should be readily observable.

It should also be noted, however, that a mixture of $j_1 j_2$ transitions between the same initial and final states can produce a cross section ratio less than that calculated for either component, through interference in the coherent sum over G_{NLSJT}. Under no circumstances, however, can the $j_1 j_2$ ratio exceed that for j^2: it must always be less. Thus, a transition can be unambiguously identified as j^2, even without the knowledge of precise initial and final state wave functions.

B. Selection Rules for Two Nucleon Pickup Reactions

The selection rules pertaining to two nucleon transfer reactions have been extensively discussed previously[1,13,14] and only those applying to the reactions treated in this work will be given here. Since all experiments discussed are restricted to $J_i^\pi = 0^+$ targets,

$$\vec{J}_f = \vec{J} = \vec{L} + \vec{S} \qquad \text{(II-23)}$$

Also, only pure relative S pickup for the nucleon pair is considered. Thus the angular momentum and parity transferred by the reaction are

$$\vec{J} = \vec{L} + \vec{S} = \vec{\Lambda} + \vec{S} \qquad \text{(II-24)}$$

and

$$\Delta\pi = (-)^L = (-)^\Lambda$$

where $\vec{\Lambda} = \vec{l}_1 + \vec{l}_2$ = the center-of-mass angular momentum of the pair. Since the deuteron has spin 1, and the α-particle is spinless, the (d,α) reaction is restricted to S=1, T=0 transfer. Since the wave function of the pair must be antisymmetric, then for j^2 pickup, J must be odd if T is even. Thus, since T=0 for the (d,α) reaction, even spin states should not be produced from 0^+ targets in this manner.

Summarizing the selection rules for even-even targets, the following is obtained:

(p,t)	S=0,T=1 only	j^2 pickup → J^π = even$^+$ only $j_1 j_2$ pickup → natural π states	(II-25)
(p,^{3}He)	S=0,T=1 and S=1,T=0[a]	j^2 pickup → $j_1 j_2$ pickup → no restriction[b]	(II-26)
(d,α)	S=1,T=0 only	j^2 pickup → J^π = odd$^+$ only $j_1 j_2$ pickup → no restrictions[b]	(II-27)

(a) If only S=0, T=1 can contribute, the (p,^{3}He) selection rules are identical to those for (p,t).

(b) No restrictions imposed by the reaction beyond those imposed by the J and π of the picked-up pair of nucleons.

III. EXPERIMENTAL PROCEDURE

A. Cyclotron and External Beam Facilities

The experiments discussed in this work were carried out using 45 MeV proton and deuteron beams in the Cave 2 external beam facility of the 88-in. cyclotron.[15] A schematic diagram of the cyclotron and experimental facilities is shown in Fig. 1.

The charged particle beams were extracted at a radius of 39.3 inches by an electrostatic deflector, and were subsequently centered using vertical and radial steering magnets located immediately after the vertical collimator. The beams were then magnetically analyzed by being deflected through an angle of 39.5 degrees, onto a 0.040-inch tantalum analyzing slit, located at the vault wall. The typical beam-energy resolution obtained after analysis was approximately 0.14%. After passing into the experimental cave, the beams were brought to a radial and vertical focus in the center of an 18-inch scatter chamber, using two sets of doublet quadrupole magnets. The beam spots obtained ranged from 0.060×0.060 to 0.100×0.100 inches in size. To permit positioning and focusing of the beam in the center of the scatter chamber, a luminous foil[16] marked with grid lines 0.063-inches apart and viewed by remote television was used. A second such foil was placed 28 inches behind the chamber to permit a determination of beam angle deviations from the optic axis of the system. The beam energy for each experiment was determined using a series of five remotely-controlled ten-position foil wheels, containing aluminum degrader foils of varying thicknesses. The range-energy tables of C. C. Maples[17] were used to obtain particle

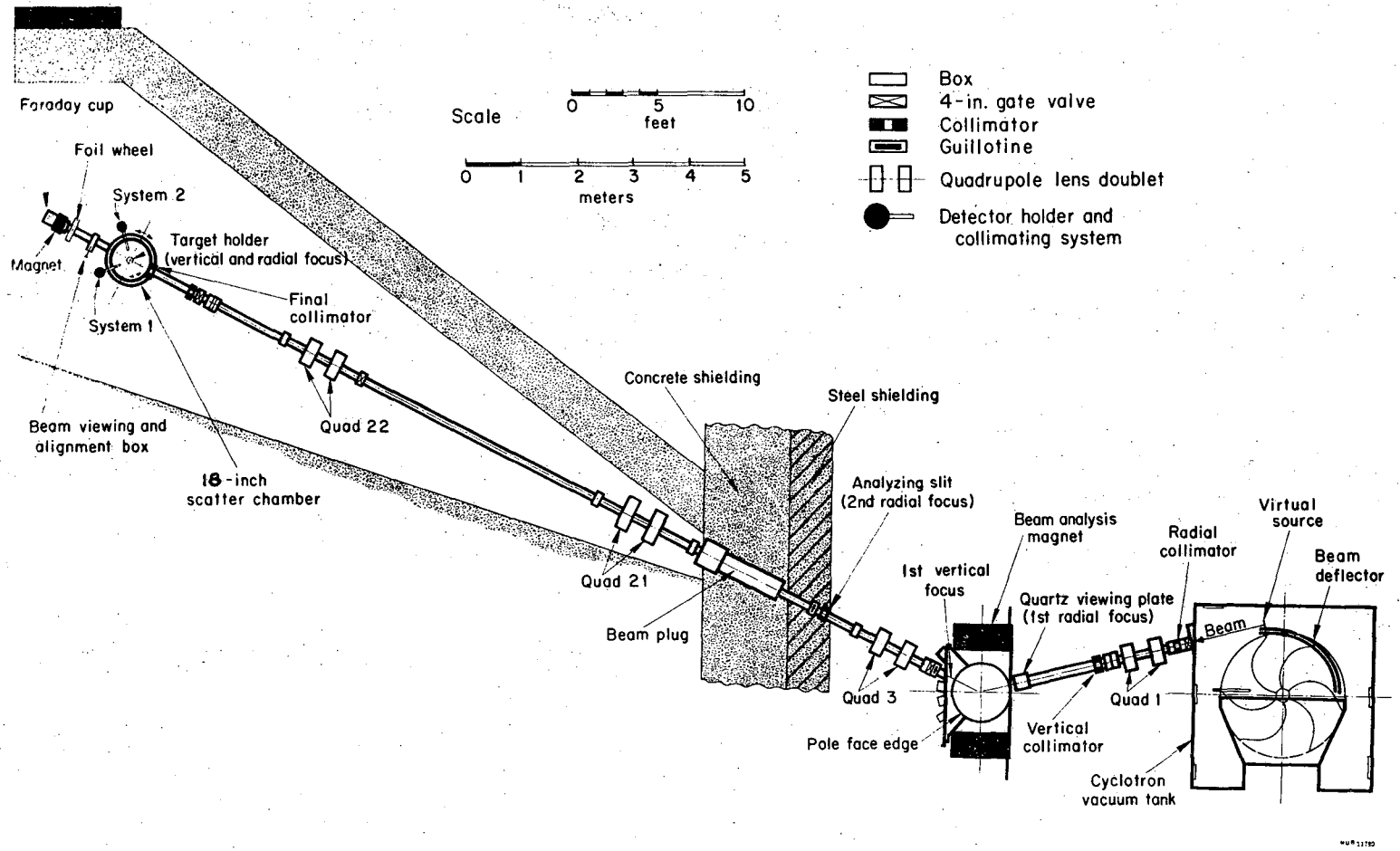
Faraday cup
Foil wheel
System 2
Magnet
Target holder
(vertical and radial focus)
Final
collimator
System 1
Beam viewing and
alignment box
18-inch
scatter chamber
Quad 22
Quad 21
Concrete shielding
Steel shielding
Beam plug
Analyzing slit
(2nd radial focus)
Beam analysis
magnet
1st vertical
focus
Quartz viewing plate
(1st radial focus)
Radial
collimator
Virtual
source
Beam
deflector
Beam
Quad 3
Quad 1
Pole face edge
Vertical
collimator
Cyclotron
vacuum tank
Scale
0 5 10
feet
0 1 2 3 4 5
meters
Box
4-in. gate valve
Collimator
Guillotine
Quadrupole lens doublet
Detector holder and
collimating system

Figure 1

energies from the measured aluminum ranges. The beam current, which ranged from 50 nA. to 1.0 μA. depending on the target and the scattering angle, was monitored using a Faraday cup in conjunction with an integrating beam electrometer. The precision of the beam integration system was measured to be about 1%.

B. Targets

A detailed diagram of the scatter chamber, gas target and gas handling apparatus is shown in Fig. 2. Since many of the gases used as target materials in these experiments were separated isotopes available only in limited supply, every effort was made to keep the volume of the gas cell and gas handling apparatus to a minimum, in order to give maximum pressure in the gas cell from small initial amounts of gas. An additional consideration in minimizing volumes was to permit efficient recovery of the gas after use. The gas cell used consisted of a stainless steel cylindrical frame 2.50-inches in diameter and 0.875-inches high. It had a 315 degree continuous window of 0.0001-inch Havar foil,[18] and conical inserts top and bottom (see insert in Fig. 2) to further reduce the volume. The inserts were required to be conical to permit the detection of particles by counters placed 10 degrees out of the horizontal plane. The cell volume excluding small entrance tubing was measured to be 47.0 cm^3. The operating gas pressure in the cell was determined by a mercury U-tube manometer, and ranged from 20-30 cm. of mercury.

The gas temperature was measured using a thermometer placed near the scatter chamber.

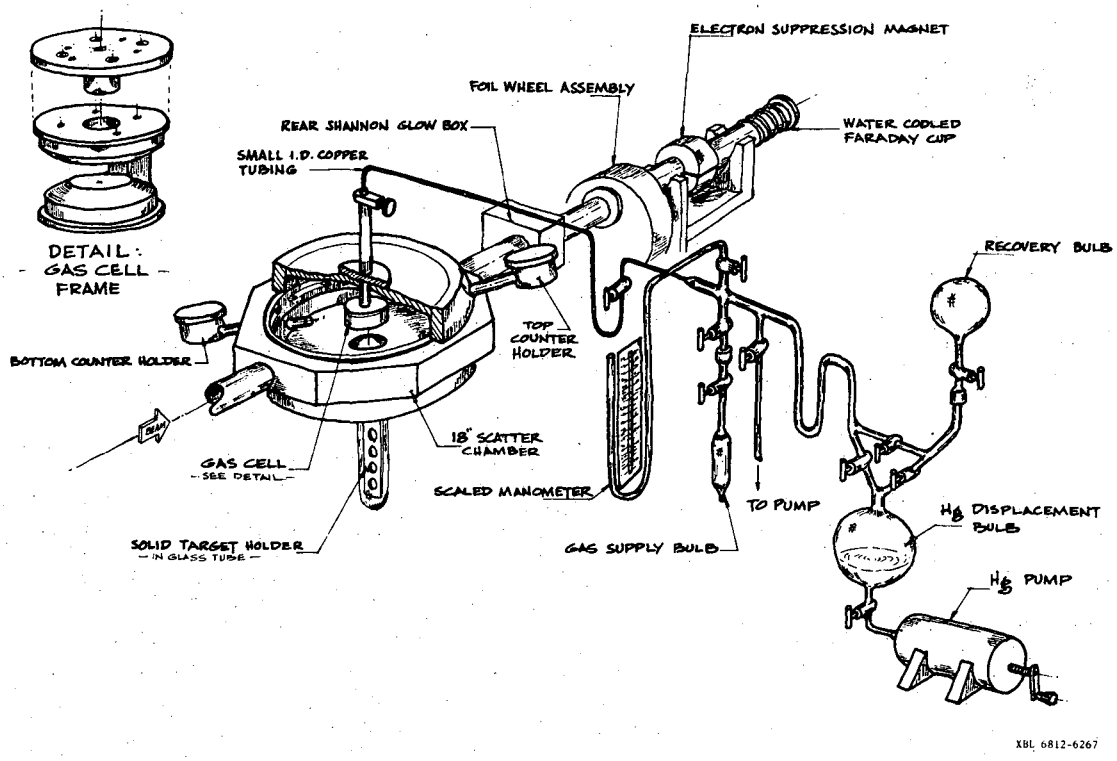
DETAIL:
GAS CELL
FRAME
ELECTRON SUPPRESSION MAGNET
FOIL WHEEL ASSEMBLY
REAR SHANNON GLOW BOX
WATER COOLED
FARADAY CUP
SMALL I.D. COPPER
TUBING
RECOVERY BULB
TOP
COUNTER
HOLDER
BOTTOM COUNTER HOLDER
BEAM
18" SCATTER
CHAMBER
GAS CELL
SEE DETAIL
SCALED MANOMETER
TO PUMP
Hg DISPLACEMENT
BULB
SOLID TARGET HOLDER
IN GLASS TUBE
GAS SUPPLY BULB
Hg PUMP
XBL 6812-6267

Figure 2

In order to recover separated isotope gases after use, the gases were expanded into a large expansion flask, which could subsequently be pumped full of mercury, compressing the gas into previously evacuated recovery bottles. Repeating this pumping process about 3 times permitted the recovery of essentially all the gas used in the experiment.

The solid targets used in this series of experiments were all self-supporting evaporated foils, ranging in thickness from $\sim$100 $\mu g/cm^2$ to $\sim$1 mg/cm^2. With the exception of the CdS targets used for the reactions $^{34}S(p,t)^{32}S$ and $^{34}S(p,^3He)^{32}P$, the targets were essentially pure. (A small amount of carbon and oxygen was usually present; these impurities were used as internal calibrations.)

The targets were mounted on target frames which were subsequently placed in a movable target ladder, capable of accepting up to five targets. This ladder could be raised and lowered by remote control, to permit the use of several targets without the need to open the scatter chamber. This target ladder could also be rotated to any angle with respect to the beam, but since two telescopes at opposite sides of the chamber were used to collect data, the target angle was usually set at 90 degrees with respect to the beam.

C. Detectors and Electronics

Two independent counter assemblies, mounted 10 degrees above and below the horizontal scattering plane were used to detect the reaction products. These assemblies could be set independently to any scatter chamber angle, the upper assembly from θ_{LAB} = 10 degrees to θ_{LAB} = 170 degrees, and the lower assembly from θ_{LAB} = 10 degrees to

θ_{LAB} = 110 degrees. Each counter assembly consisted of a 3 counter-telescope holder, which was mounted externally about 18 inches from the target, and could be isolated from the scatter chamber by a vacuum valve. A set of tantalum collimators 0.085-inches wide, 0.200-inches high and of adequate thickness to stop elastically scattered particles was mounted at a distance of 18.75 inches from the center of the target. In addition, for gas targets, a second radial collimator 0.085-inches wide was installed 4.50 inches from the target center to completely define the solid angle. The solid angle subtended by each counter telescope was found to be 5×10^{-5}sr., with an angular resolution of 0.26 degrees.

For these experiments, a three detector counter telescope was used in each of the systems. Each telescope consisted of a 6.1 mil phosphorus diffused silicon ΔE transmission detector, a 120 mil lithium drifted silicon stopping (E) detector, and a 20 mil lithium drifted silicon E-reject detector, operated in anti-coincidence to eliminate long range particles penetrating the E detector. The E detector was rotated, with its normal at an angle of 30 degrees to the incident particles, in order to provide a greater effective counter thickness for stopping high energy tritons.

The detectors were connected to fast-rise charge sensitive pre-amplifiers, which were mounted as close as possible in order to minimize signal losses and reduce pickup noise. The preamplified signals were subsequently transmitted from the experimental area to a remote counting area, where they were delay-line shaped and further amplified. A schematic diagram of the counting equipment is shown in Fig. 3. The

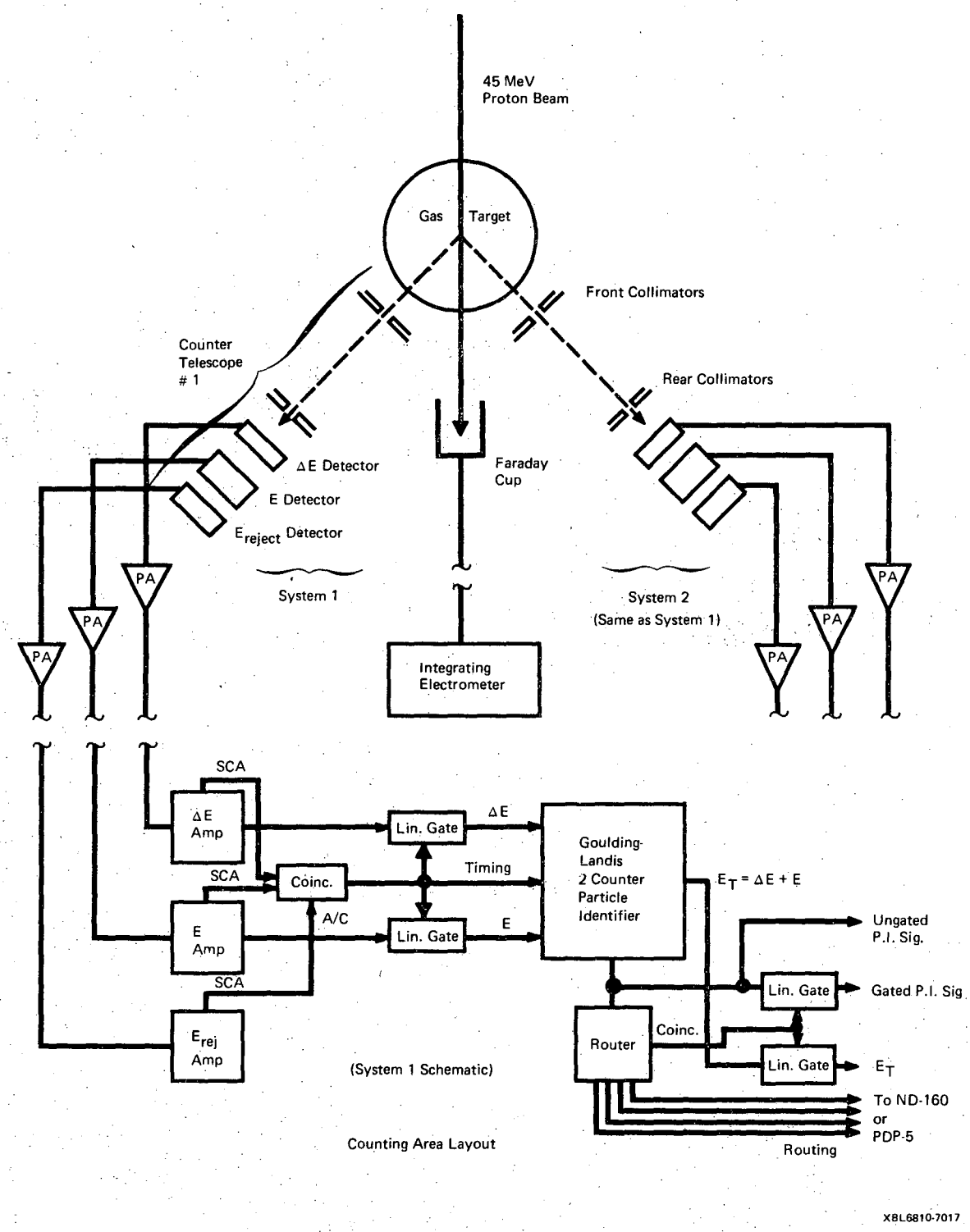
45 MeV
Proton Beam
Gas
Target
Front Collimators
Counter
Telescope
1
Rear Collimators
ΔE Detector
E Detector
E reject Detector
Faraday
Cup
System 1
System 2
(Same as System 1)
PA
Integrating
Electrometer
SCA
ΔE
Amp
Lin. Gate
ΔE
Goulding-
Landis
2 Counter
Particle
Identifier
Timing
Coinc.
E = ΔE + E
A/C
E
Amp
Lin. Gate
E
Ungated
P.I. Sig.
Lin. Gate
Gated P.I. Sig
Router
Coinc.
Lin. Gate
E
To ND-160
or
PDP-5
E rej
Amp
(System 1 Schematic)
Counting Area Layout
Routing
XBL6810-7017

Figure 3

ΔE and E signals, after satisfying slow (2τ=2 μsec.) coincidence requirements, were fed into a Goulding-Landis two-counter particle identifier.[19] Using the empirical range-energy relationship

$$R = aE^{1.73}$$

this identifier produced an output logic pulse which was proportional to the particle type, in coincidence with the total energy signal of the particle obtained by summing the ΔE and E signals. A typical particle identifier spectrum is shown in Fig. 4. The particle-type logic signals were fed into a 4-channel router, each channel consisting of a single channel analyzer, which triggered a routing signal when fired. The router S.C.A.'s were set around tritons, ^{3}He and α-particle signals, as well as a safety group in the deuteron-triton valley, and were subsequently used to route the coincident energy signal into the appropriate segment of a pulse-height analyzer, permitting the simultaneous accumulation of triton, ^{3}He and α-particle spectra. One system utilized a Nuclear Data ND-160 4096 channel pulse-height analyzer, operating in a 4×1024 channel mode. The other system used a 4096 channel analogue-to-digital converter, with up to 8 logic (router) buffers, to feed a PDP-5 computer, programmed to accumulate data.

The router single channel analyzer for tritons was set to exclude any deuteron component, and hence also excluded "leak-through" tritons, i.e., those normally rare tritons which channel through the relatively thin ΔE detector, producing particle identifier signals

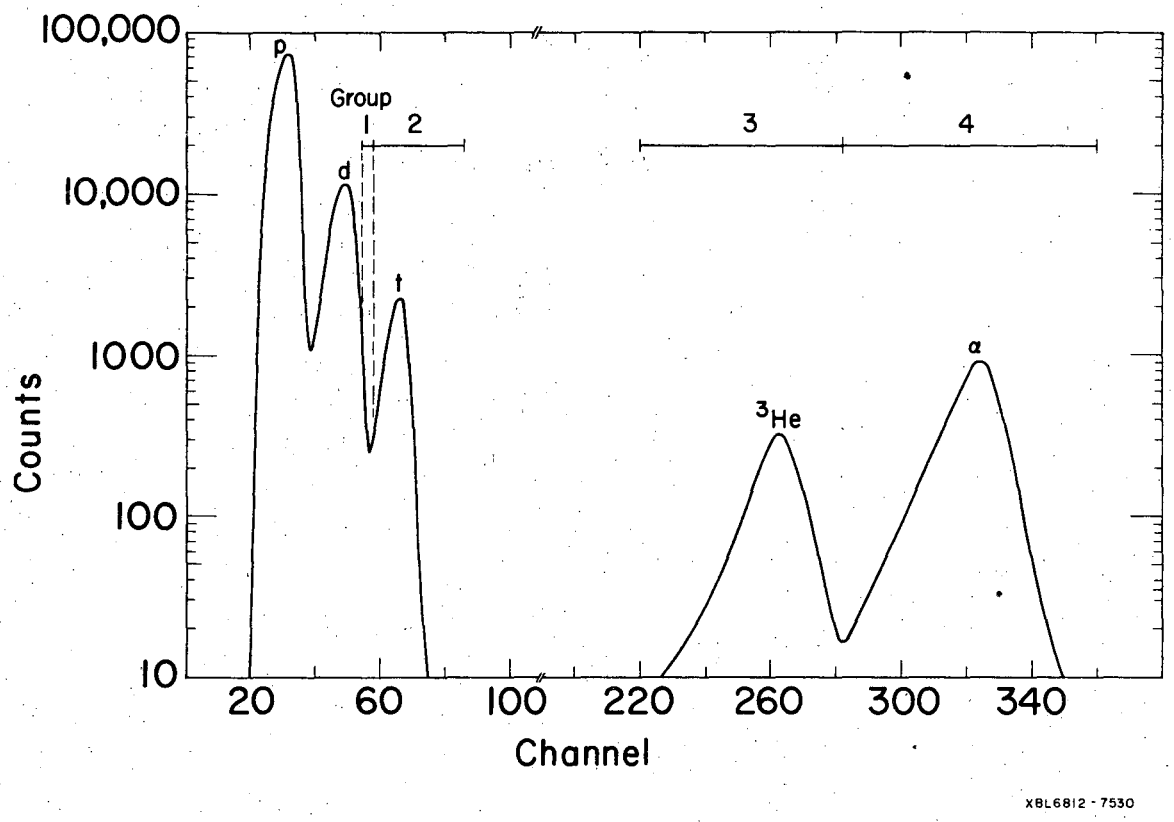
100,000
10,000
1000
100
10
Counts
p
Group
1
2
3
4
d
t
α
^{3}He
20
60
100
220
260
300
340
Channel
XBL6812-7530

Figure 4

somewhat smaller than expected. In order to obtain a measure of the amount of these leakthrough tritons, the deuteron-triton valley was monitored, and any contribution added to the triton spectra. Less than 10% leakthrough was detected for the highest energy triton observed (∿36 MeV), and essentially none was observed for tritons of less than 30 MeV.

The particle identification signals, both free and gated by the router, were monitored on RIDL 400 channel analyzers. The overall energy resolution (FWHM) typically obtained from this system was 110-150 keV for tritons, and 120-170 keV for ^{3}He particles, depending on target thickness and kinematics.

A monitor counter, mounted in the horizontal plane, at a fixed angle of θ_{LAB} = 27.5 degrees, was used in addition to the two counter telescopes, to check targets for decomposition, and to observe any changes in beam energy. The collimator used with this counter had a 0.200-inch circular aperture and was mounted 23.94 inches from the target center, giving it approximately the same angle of acceptance as that of the counter telescopes. The monitor counter was usually used to monitor the (p,α) reaction since the positive Q-value of the reaction renders it virtually free from interferences at high particle energies.

D. Data Handling

After accumulation on the PDP-5 computer, the data were stored on DEC-555 magnetic tapes, which could be reread to produce printouts and graphs. The data accumulated in the ND-160 analyzer could also be transferred to the PDP-5, where it could be handled in the same manner.

Facilities were also available to transfer data to an IBM compatable magnetic tape, to permit further analysis using a CDC-6600 computer.

After correcting appropriately for leakthrough, the differential cross section at each angle was obtained using the formulae given below.

(a) Solid Target:

$$\left(\frac{d\sigma}{d\Omega}\right)_{cm} = J_{\theta_L} \times \frac{C}{B} \times \frac{(ZMR)^2}{NAt} \times 2.660\times10^{-4} \ \mu b/sr.$$

(b) Gas Target

$$\left(\frac{d\sigma}{d\Omega}\right)_{cm} = J_{\theta_L} \times \frac{C}{B} \times \left[\frac{Z \times (T + 273) \times (L_1 + L_2)^2 \times \sin\theta}{NAPW_1 \times (1 + L_1/L_2)}\right] \times 6.530\times10^{-4} ub/sr$$

J_{θ_L} = Jacobian for the transformation from lab to center-of-mass

C/B = counts /μ oulomb

Z = charge of the incident particle

M = molecular weight of the target (gm/mole)

R = distance to the front of the rear collimator from target

N = number of target nuclei per molecule

A = area of the rear collimator (cm^2)

t = target thickness (mg/cm^2)

L_1 = distance to the back of front collimator from target center

L_2 = distance from L_1 to the front of the rear collimator

P = pressure of the gas (cm Hg)

W_1 = width of front collimator

T = temperature of the gas (°C)

The errors shown on the experimental points in all the angular distributions are pure counting statistical errors.

The excitation energies of the states observed in this series of experiments were determined by the computer program, LORNA.[20] This program established an energy scale by finding a least squares fit to peaks whose Q-values were known, after correcting all incoming and outgoing particles for kinematic effects and absorber losses. For the data described, contaminants were often present or introduced to provide calibrations. In particular, states produced from the reactions $^{12}C(p,t)^{10}C$ and $^{12}C(p,^{3}He)^{10}B$ were especially useful throughout: the masses of the ground and first excited states of ^{10}C were taken from a recent re-evaluation by Brunnader et al.,[21] while the level information for ^{10}B levels was taken from Ajzenberg-Selove and Lauritzen.[22]

IV. EXPERIMENTAL RESULTS

If a target nucleus has isospin T_i, then the ratio of the differential cross-section for the (p,t) and (p,^{3}He) reactions leading to analogue final states with isospin $T_f = T_i + 1$ can, as derived in Sec. II, be expressed simply where charge-dependent effects are neglected:

$$\frac{(d\sigma/d\Omega)_{(p,t)}}{(d\sigma/d\Omega)_{(p,^3He)}} = \frac{k_t}{k3_{He}} \cdot \frac{2}{2T_f - 1} \qquad \text{(IV-1)}$$

Thus, in this approximation, the differential cross sections to analogue states should be identical in shape, and their magnitudes should be in the ratio of $(k_t/k3_{He})$ when $T_f = 3/2$; $(^{2k}t/^{3k}3_{He})$ when $T_f = 2$; and $(^{2k}t/^{5k}3_{He})$ when $T_f = 3$. These properties provide an unambiguous experimental method for identifying analogue states.[12]

The series of experiments discussed here included a remeasurement of the (p,t) reaction on ^{22}Ne and ^{26}Mg targets in which carbon impurities had been added to provide an energy calibration. In particular, the ground and first excited states of ^{10}C, produced in the reaction ^{12}C(p,t)^{10}C, resulted in triton peaks whose energies bracket that of the T=2 states in ^{20}Ne and ^{24}Mg. Since the ground-state mass excess of ^{10}C taken from the then current mass tables[23] was 15.658±0.013 MeV, it was therefore surprising to observe a discrepancy of ∿45 keV with the accepted energies of the T=2 states in ^{20}Ne and ^{24}Mg (which were known to ±2.4 keV and ±5.0 keV resp.). This led to a re-evaluation of the ^{10}C mass excess,[21] giving agreement with a new experimentally determined value

of 15.7025±0.0018 MeV for the ground state. The excitation energy of the first excited state in ^{10}C was found to be 3.344±0.008 MeV. Using these remeasured values for the ^{10}C states, good agreement with the accepted values of the ^{20}Ne and ^{24}Mg states was obtained.

A. ^{20}Ne (p,t) ^{18}Ne and ^{20}Ne (p,^{3}He) ^{18}F Reactions

In order to calibrate the ^{21}Ne (p,t) ^{19}Ne and ^{21}Ne (p,^{3}He) ^{19}F data which will be discussed in Sec. IV-B, it was necessary to establish the excitation energies and relative magnitudes of the states produced by the (p,t) and (p,^{3}He) reactions on the ^{20}Ne present in the ^{21}Ne-enriched target. For this purpose, targets consisting of pure neon and a neon-methane (40-60% resp.) mixture were used, the neon being 99.9% enriched in ^{20}Ne. A single set of spectra were obtained for each tele- at θ_{LAB} = 22.3 degrees, using the pure neon target. Accurate excitation energies were then obtained from the neon-methane mixed target, with the known mass-10 states providing internal calibrations, in addition to the known states in mass-18.

A series of four sets of spectra on the mixed target were taken at angles ranging from θ_{LAB} = 22.3 degrees to θ_{LAB} = 41.0 degrees; the spectra collected at θ_{LAB} = 26.8 degrees for 2570 microcoulombs are shown in Fig. 5. The states whose energies are marked without brackets in the figure, were used to establish the mass-18 calibration; the bracketed energies represent the best value determined for the states marked. The final excitation energies determined from this experiment for ^{18}Ne are listed in Table 1, together with previous measurements.[24-26]

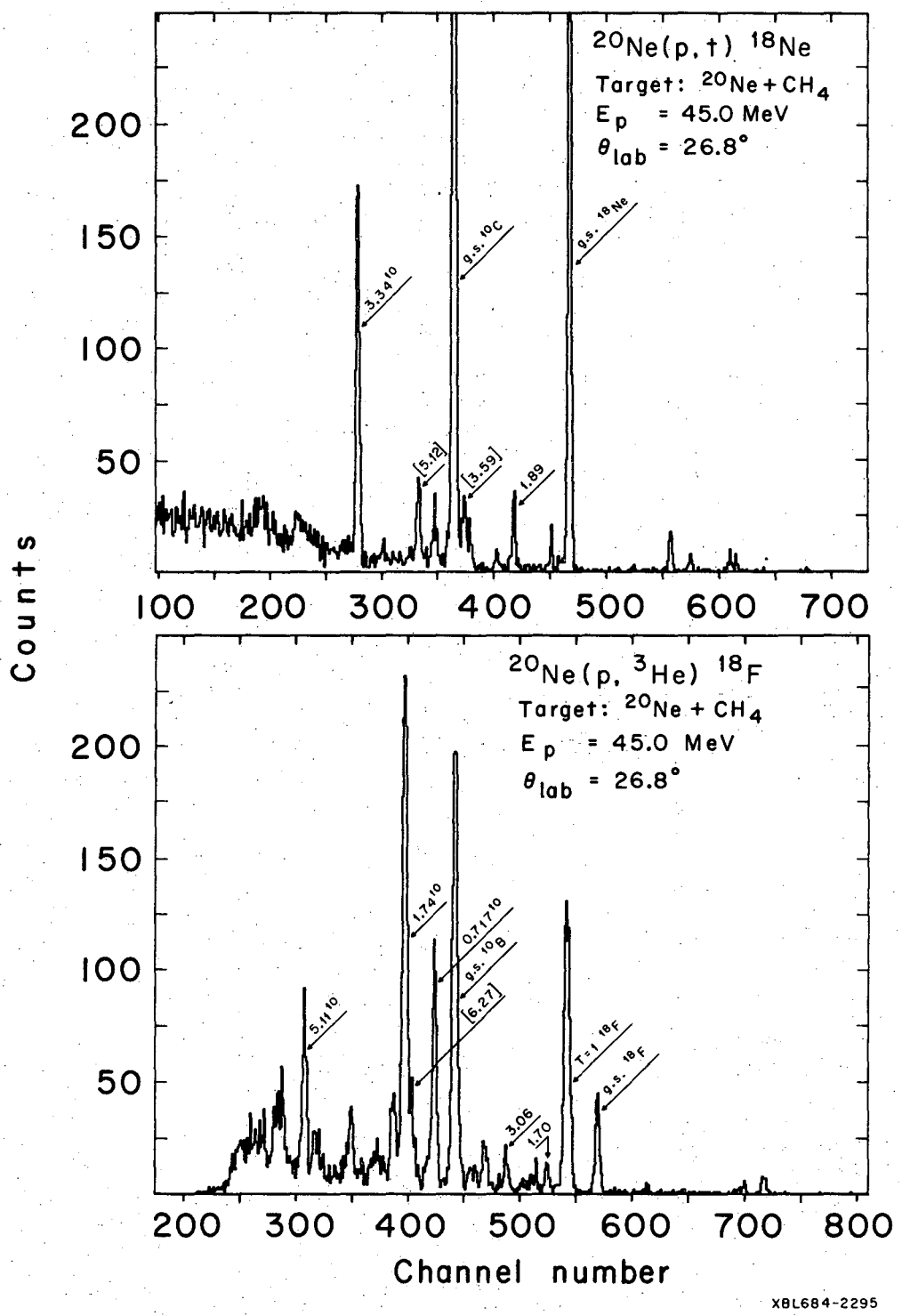
^{20}Ne(p,t) ^{18}Ne
Target: ^{20}Ne + CH$_4$
E_p = 45.0 MeV
θ_{lab} = 26.8°
3.34 10
g.s. ^{10}C
g.s. ^{18}Ne
[5.12]
[3.59]
1.89
^{20}Ne(p, ^{3}He) ^{18}F
Target: ^{20}Ne + CH$_4$
E_p = 45.0 MeV
θ_{lab} = 26.8°
1.74 10
0.717 10
g.s. ^{10}B
[6.27]
5.11 10
T=1 ^{18}F
g.s. ^{18}F
3.06
1.70
Counts
Channel number
XBL684-2295

Figure 5

Table 1. Excited states of ^{18}Ne.

This Work (MeV ± keV)	Previous Work (MeV ± keV)	Ref.	Average (MeV ± keV)
g.s.	g.s.		---
1.890 ± 20	1.8873 ± 0.2	(a)	1.8873 ± 0.2*
3.375 ± 30	3.3762 ± 0.4	(a)	3.3762 ± 0.4
3.588 ± 25*†	3.5763 ± 2.0	(a)	3.5763 ± 2.0
	3.6164 ± 0.6	(a)	3.6164 ± 0.6
4.580 ± 30	4.558 ± 13.5	(b,c)	4.562 ± 12.2
5.115 ± 25	5.140 ± 18.0	(b)	5.132 ± 15*

*These values were used as known in the analysis of ^{21}Ne (p,t) ^{19}Ne .

†This value was used in the analysis of ^{21}Ne(p,t)^{19}Ne because it represents the effective energy of the unresolved mixture of the (0^+) state at 3.5673 MeV and the $2^{(+)}$ state at 3.6164 MeV, both populated by the (p,t) reaction.

(a)R. D. Gill, B. C. Robertson, J. L'Ecuyer, R. A. I. Bell, and H. J. Rose, Phys. Lett. 28B, 116 (1968).

(b)E. Adelberger, Thesis, California Institue of Technology, unpublished.

(c)J. H. Towle, and G. J. Wall, Nucl. Phys. A118, 500 (1968).

Since the density of states in ^{18}F is large at higher excitations, it is difficult to make a meaningful comparison of states observed in these experiments with those observed previously. There is, however, only one state which is necessary for subsequent calibrations, and the excitation energy obtained for it from these measurements is 6.270±0.030 MeV. (Although this peak is not clearly resolved in Fig. 5 from the $^{10}B^*$ 1.74-MeV state, this was not the case at other angles observed.) This value should be compared with 6.265±0.013 MeV, measured in the reaction ^{27} $^{16}O(^3He,p)^{18}F$, and because of the greater accuracy of the latter, it was used in the following sections.

Since the primary purpose of obtaining these data was to provide energy calibrations for subsequent experiments, the range of angles covered was small with large increments between successive angles. Hence, the available data were considered inadequate to provide meaningful angular distributions and, as a result, no attempt was made to extract this type of information.

B. $^{21}Ne\ (p,t)\ ^{19}Ne$ and $^{21}Ne\ (p,^3He)\ ^{19}F$; T = 3/2 States

The neon target used in these experiments was enriched in ^{21}Ne, with an isotopic composition of 21.1% ^{20}Ne, 56.3% ^{21}Ne and 22.6% ^{22}Ne. Seven angles, ranging from θ_{LAB} = 11.7° to θ_{LAB} = 31.5°, were studied in order to obtain angular distribution data. A pair of spectra collected at θ_{LAB} = 22.3° for 4880 microcoulombs, is shown in Fig. 6.

Rough coulomb energy calculations assuming a uniformly charged sphere predict the T = 3/2 analogue levels in ^{19}Ne and ^{19}F to lie at an excitation of approximately 7.5 MeV. The peaks marked as T = 3/2* in

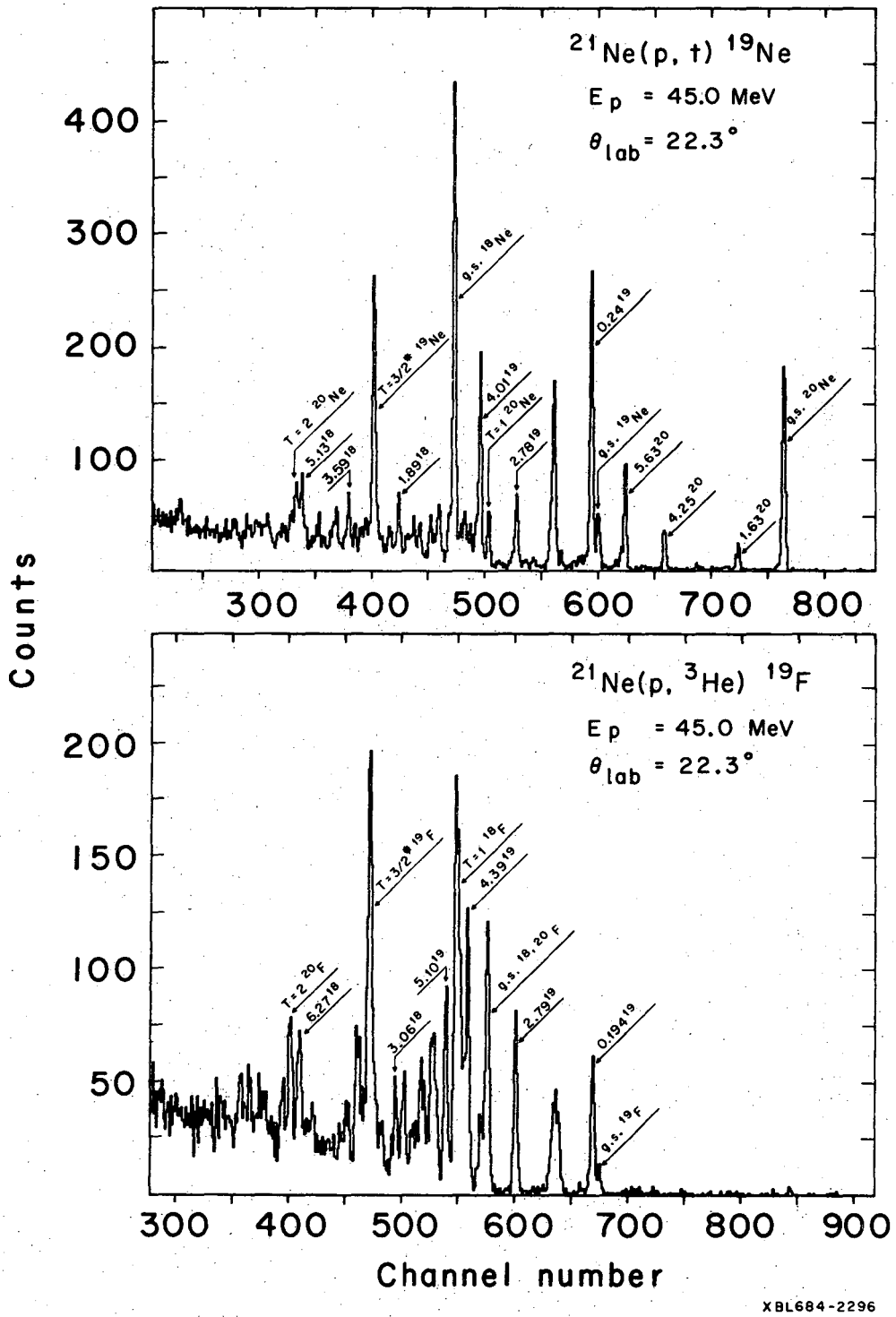
^{21}Ne(p, t) ^{19}Ne
Ep = 45.0 MeV
θlab = 22.3°
T = 2 20Ne
5.13 18
3.59 18
T=3/2* 19Ne
1.89 18
g.s. 18Ne
4.01 19
T=1 20Ne
2.78 19
0.24 19
g.s. 19Ne
5.63 20
4.25 20
1.63 20
g.s. 20Ne
^{21}Ne(p, ^{3}He) ^{19}F
Ep = 45.0 MeV
θlab = 22.3°
T=2 20F
6.27 18
T=3/2* 19F
3.06 18
5.10 19
T=1 18F
4.39 19
g.s. 18, 20 F
2.79 19
0.194 19
g.s. 19F
Counts
Channel number
XBL684-2296

Figure 6

Fig. 6 are consistent with these values. The angular distributions of the tritons and ^{3}He-particles corresponding to the T = 3/2* analogue states are shown in the upper protion of Fig. 7. The experimental ^{3}He data have been multiplied by $k_t/k3_{He}$ (=0.93) in order to facilitate the comparison of cross section magnitudes. The shape and magnitudes of the distributions are indeed identical, within the expected accuracy of the approximations used in the derivation of Eq. (IV-1), and thus, the T = 3/2 character of the levels is established. Triton angular distributions characteristic of L=0 and L=2 transfer are also shown for two T = 1/2 levels in ^{19}Ne; in addition, the L=0 distribution is included for the (p,t) reaction on ^{20}Ne leading to the ground state of ^{18}Ne. (There were no states in ^{19}Ne known to be $3/2^{+}$, and since the J^{π} of ^{21}Ne is $3/2^{+}$, there could be no "known" L=0 angular distributions to states in that nucleus. Instead, for comparison the L=0 distribution of tritons leading to the ^{18}Ne ground state from the reaction ^{20}Ne(p,t)^{18}Ne g.s., has been included.) From the characteristic L=0 distribution shape, it is possible to identify both the 4.013 MeV state in ^{19}Ne, as well as the analogue states, to be $3/2^{+}$. To provide additional verification, distorted wave Born approximation (DWBA) calculations were performed using a modified version of the computer program DWUCK[28] and the optical-model potentials listed in Table 2.[29] The results of the computations, which assumed pure L=0 or L=2 transfer, are shown as the dashed curves in Fig. 7. These curves were normalized to the experimental data, giving very good fits and confirming the above assignments. However, the J^{π} of ^{19}O, which is the T_z = 3/2 member of this analogue multiplet, is known to

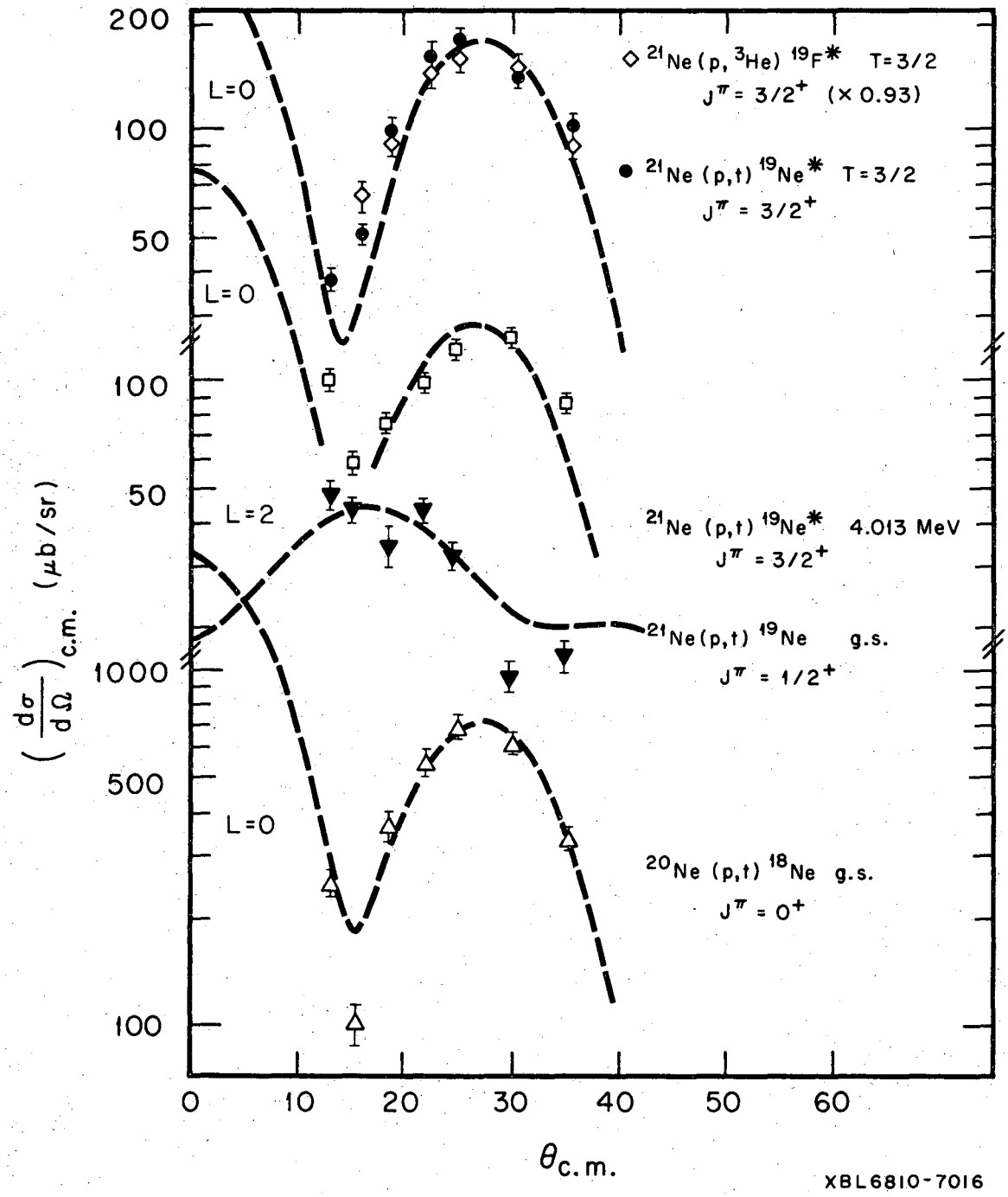
200
100
50
100
50
1000
500
100
L=0
L=0
L=2
L=0
◇ 21Ne (p, 3He) 19F* T=3/2
Jπ = 3/2+ (× 0.93)
● 21Ne (p,t) 19Ne* T=3/2
Jπ = 3/2+
21Ne (p,t) 19Ne* 4.013 MeV
Jπ = 3/2+
21Ne(p,t) 19Ne g.s.
Jπ = 1/2+
20Ne (p,t) 18Ne g.s.
Jπ = 0+
(dσ/dΩ)c.m. (μb/sr)
0
10
20
30
40
50
60
θc.m.
XBL6810-7016

Figure 7

Table 2. Optical model parameters[29] used in DWBA calculations

Target	Projectile	V(MeV)	W_s(MeV)	r(fm.)	a
	p	51.5	19.0	1.25	0.5
^{20}Ne, ^{21}Ne	t, ^{3}He	162.0	37.5	1.25	0.6
^{22}Ne	p	51.5	19.0	1.15	0.5
	t, ^{3}He	162.0	37.5	1.15	0.6
^{25}Mg	p	51.5	19.0	1.15	0.5
	t, ^{3}He	162.0	37.5	1.15	0.6
^{30}Si	p	51.5	19.0	1.15	0.5
	t, ^{3}He	160.0	38.5	1.15	0.6
^{36}Ar, ^{38}Ar, ^{40}Ar	p	51.5	19.0	1.15	0.5
	t, ^{3}He	160.0	38.5	1.15	0.6

R_c used throughout = 1.20 fm.

be $5/2^+$ indicating that the T = 3/2 levels produced in ^{19}Ne and ^{19}F by the (p,t) and (p,^{3}He) reactions must be analogues to the first excited state of ^{19}O - a $3/2^+$ state at 0.095 MeV.

The excitation energies of the analogue states were determined in the manner previously described and the final results are listed in Table 3. There have been no previously reported measurements of either T = $3/2^*$ state, although an observation has been reported[30] of the lowest T = 3/2 state in ^{19}F.

The calibration of the ^{3}He spectrum also yielded an energy for the lowest T = 2 state in ^{20}F, the accuracy of which depends largely upon the 6.265±0.013 MeV state in ^{18}F. This state will be discussed in greater detail in the next section (Sec. IV-C).

C. ^{22}Ne (p,t) ^{20}Ne and ^{22}Ne (p,^{3}He) ^{20}F; T = 2 States

Although the excitations of the lowest T=2 analogue states in mass 20 had been reported previously,[6,31-33] and although the experimental uncertainty on the lowest T=2 state in ^{20}Ne was sufficiently small to preclude any improvement by the present measurements, the (p,t) and (p,^{3}He) experiments on ^{22}Ne were repeated primarily to reduce the existing uncertainty on the excitation of the lowest T=2 state in ^{20}F. However, the good agreement between the present determination of the T=2 state in ^{20}Ne and previous data may be taken as a measure of the reliability of these methods.

In order to provide internal calibrations in the region of the T=2 states, a neon-methane mixed (50%-50%) target was used in addition

Table 3. Summary of experimental results for high T states.

Nucleus	Analogue State J^π ; T	Excitation energy This Work (MeV ± keV)	Previous Work (Ref.) (MeV ± keV)	Average (MeV ± keV)
^{19}F*	$3/2^+$;3/2	7.660±35	not reported	7.660±35
^{19}Ne*	$3/2^+$;3/2	7.620±25	not reported	7.620±25
^{20}F	0^+ ; 2	6.523±35	6.43±100 (a)	6.513±33
^{20}Ne	0^+ ; 2	16.722±25	16.732±2.4 (a,b,c,d)	16.732±2.4
^{23}Na	$5/2^+$;3/2	7.910±30	7.890±30 (e,f)	7.900±21
^{23}Mg	$5/2^+$;3/2	7.788±25	not reported	7.788±25
^{24}Na	0^+ ; 2	5.978±35	5.98±48 (g,h)	5.979±28
^{24}Mg	0^+ ; 2	15.426±30	15.436±5 (i,j,k)	15.436±5
^{28}Al	0^+ ; 2	5.983±25	not reported	5.983±25
^{28}Si	0^+ ; 2	15.206±25	not reported	15.206±25
^{32}P	0^+ ; 2	5.071±40	not reported	5.071±40
^{32}S	0^+ ; 2	12.034±40	not reported	12.034±40
^{36}Cl	0^+ ; 2	4.295±30	not reported	4.295±30
^{36}Ar	0^+ ; 2	10.858±35	not reported	10.858±35
^{38}Cl	0^+ ; 3	8.216±25	not reported	8.216±25
^{38}Ar	0^+ ; 3	18.784±30	not reported	18.784±30
^{40}K	0^+ ; 2	4.375±25	4.370±70 (g)	4.374±24
^{40}Ca	0^+ ; 2	11.978±25	11.970±65 (g)	11.977±23

*These levels are not the lowest T=3/2 levels in mass-19, but are analogous to the first excited state (0.095 MeV) of ^{19}O.

Table 3. Continued

(a) J. Cerny, R. H. Pehl, and G. T. Garvey, Phys. Lett. 12, 234 (1964).

(b) E. Adelberger and A. B. McDonald, Phys. Lett. 24B, 270 (1967).

(c) H. M. Kuan, D. W. Heikkinen, K. A. Snover, F. Riess and S. S. Hanna, Phys. Lett. 25B, 217 (1967).

(d) R. Bloch, R. E. Pixley, and P. Truöl, Phys. Lett. 25B, 215 (1967).

(e) S. Mubarakmand, and B. E. F. Macefield, Nucl. Phys. A98, 97 (1967) and private communication to J. C. Hardy.

(f) J. Dubois, Nucl. Phys. A104, 657 (1967).

(g) G. T. Garvey and J. Cerny, unpublished.

(h) F. G. Kingston, R. J. Griffiths, R. A. Johnston, W. R. Gibson and E. A. McClatchie, Phys. Lett. 22 458 (1966).

(i) G. T. Garvey, J. Cerny, and R. H. Pehl, Phys. Rev. Lett. 12 726 (1964).

(j) E. Adelberger, and A. B. McDonald, Phys. Lett. 24B, 270 (1967) and erratum Phys. Lett. 24B, 618 (1967).

(k) F. Riess, W. J. O'Connell, D. W. Heikkinen, H. M. Kuan, and S. S. Hanna, Phys. Rev. Lett. 19, 327 (1967).

to the pure neon target. The neon gas used was 92.0% enriched in ^{22}Ne, the proportions of the remaining isotopes being 7.6%^{20}Ne and 0.4%^{21}Ne. Figure 8 shows the triton and ^{3}He spectra taken at θ_{LAB} = 36.2 degrees for 9280 microcoulombs. Although the cross section for L=0 transfer is relatively low at this angle, it is greater than for any other angle at which the T=2 states in both ^{20}Ne and ^{20}F are simultaneously resolved from all the calibration peaks. The excitation energies of the observed analogue states were determined primarily by using the known states in ^{10}C and ^{10}B as calibrations.

Since angular distributions of the tritons and ^{3}He particles corresponding to the analogue T=2 states had been previously measured,[6] spectra were recorded only at θ_{LAB} = 36.2 degrees. Hence no further angular distribution information was obtained from this data.

The excitation obtained for the T=2 state in ^{20}Ne is given in Table 3, and is found to be in good agreement with the accepted value. Excitations for additional states, potentially of T=1 character, were determined in ^{20}Ne as well, with observed values of 10.890±0.050, 11.100±0.40 and 12.250±0.40 MeV. These will be discussed later in Sec. V-B-1.

The value for the excitation of the T=2 state in ^{20}F quoted in Table 3 is based on a weighted average of the value obtained from these experiments and the data discussed previously in Sec. IV-B.

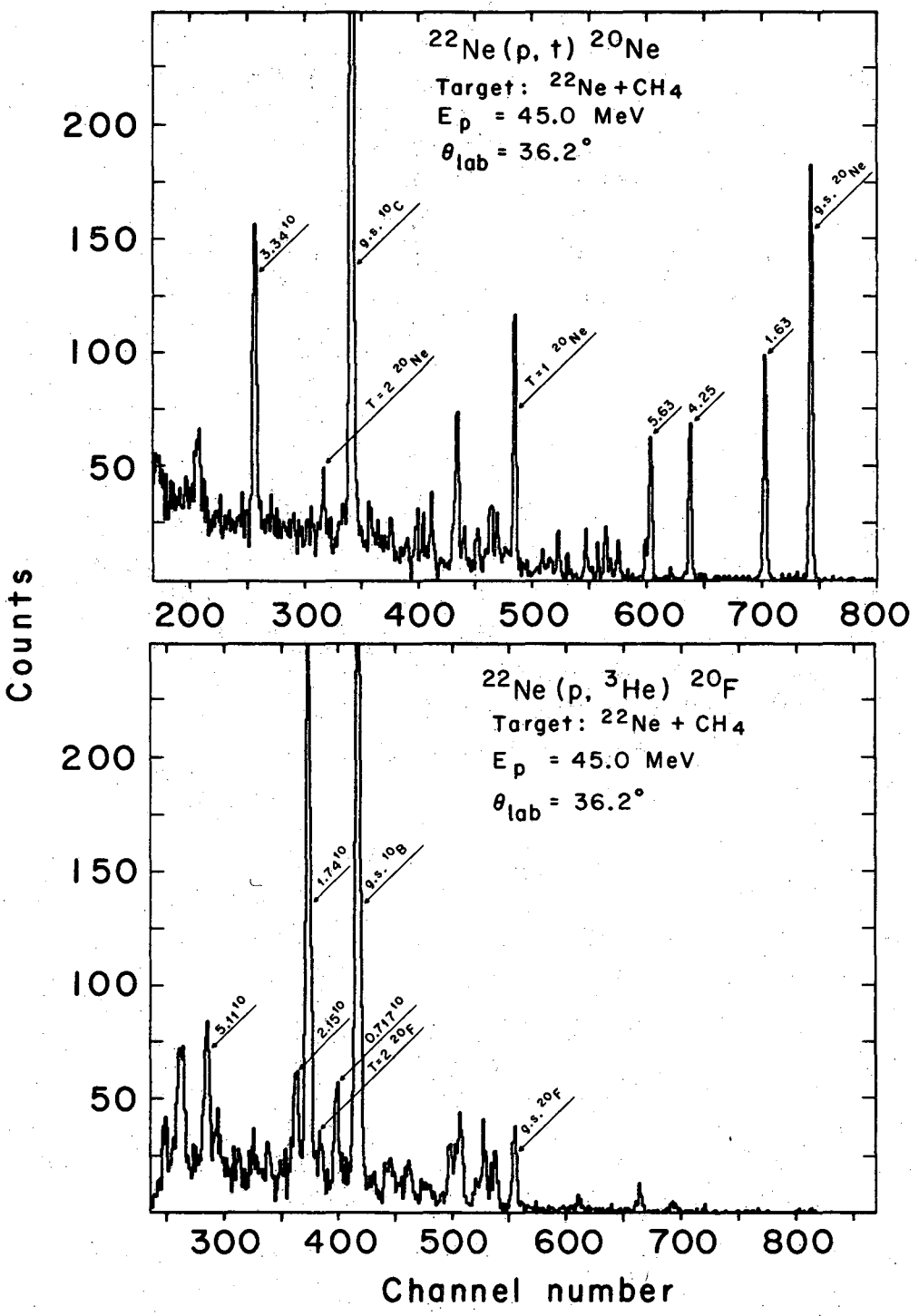
^{22}Ne(p, t) ^{20}Ne
Target: ^{22}Ne + CH$_4$
E_p = 45.0 MeV
θ_{lab} = 36.2°
3.34 ^{10}C
g.s. ^{10}C
T=2 ^{20}Ne
T=1 ^{20}Ne
5.63
4.25
1.63
g.s. ^{20}Ne
^{22}Ne(p, ^{3}He) ^{20}F
Target: ^{22}Ne + CH$_4$
E_p = 45.0 MeV
θ_{lab} = 36.2°
1.74 ^{10}B
g.s. ^{10}B
5.11 ^{10}B
2.15 ^{10}B
0.717 ^{10}B
T=2 ^{20}F
g.s. ^{20}F
Counts
Channel number
XBL684-2294

Figure 8

D. ^{25}Mg (p,t) ^{23}Mg and ^{25}Mg (p,^{3}He) ^{23}Na; T = 3/2 States

The target used in these experiments was a 500 $\mu g/cm^2$ self-supporting evaporated magnesium foil, enriched in ^{25}Mg. The components of this target were ^{24}Mg(8.29%), ^{25}Mg(91.54%), ^{26}Mg(0.17%), and, in addition, small amounts of oxygen and carbon impurities. Spectra were obtained at six angles between θ_{LAB} = 17.2 degrees and θ_{LAB} = 31.5 degrees, with the spectra obtained at θ_{LAB} = 24.1 degrees for 970 micro-coulombs being shown in Fig. 9.

Rough coulomb energy calculations indicated that the T = 3/2 analogue states should lie at an excitation of about 7.8 MeV in both ^{23}Mg and ^{23}Na. The peaks marked T = 3/2 in Fig. 9 are consistent with these expectations. The upper portion of Fig. 10 shows the angular distributions of the corresponding tritons and ^{3}He particles, the latter having been multiplied by $k_t/k3_{He}$(=0.92). The similarity of the distributions satisfies the requirements of Eq. (IV-1), and establishes these levels as being T = 3/2. Also shown in the lower portion of Fig. 10 are the angular distributions for the (p,t) reactions to the ground state ($3/2^+$) and 0.451 MeV state ($5/2^+$) of ^{23}Mg. Since the spin-parity of ^{25}Mg is $5/2^+$, the former transition should be characterized by predominantly L=2 transfer, while the latter should be L=0. By simple comparison, the angular momentum transfer to the analogue states is determined to be principally L=0. The dashed curves are again DWBA calculations, using the optical model parameters listed in Table 2, and normalized to the experimental data. Based on these L transfers, it is

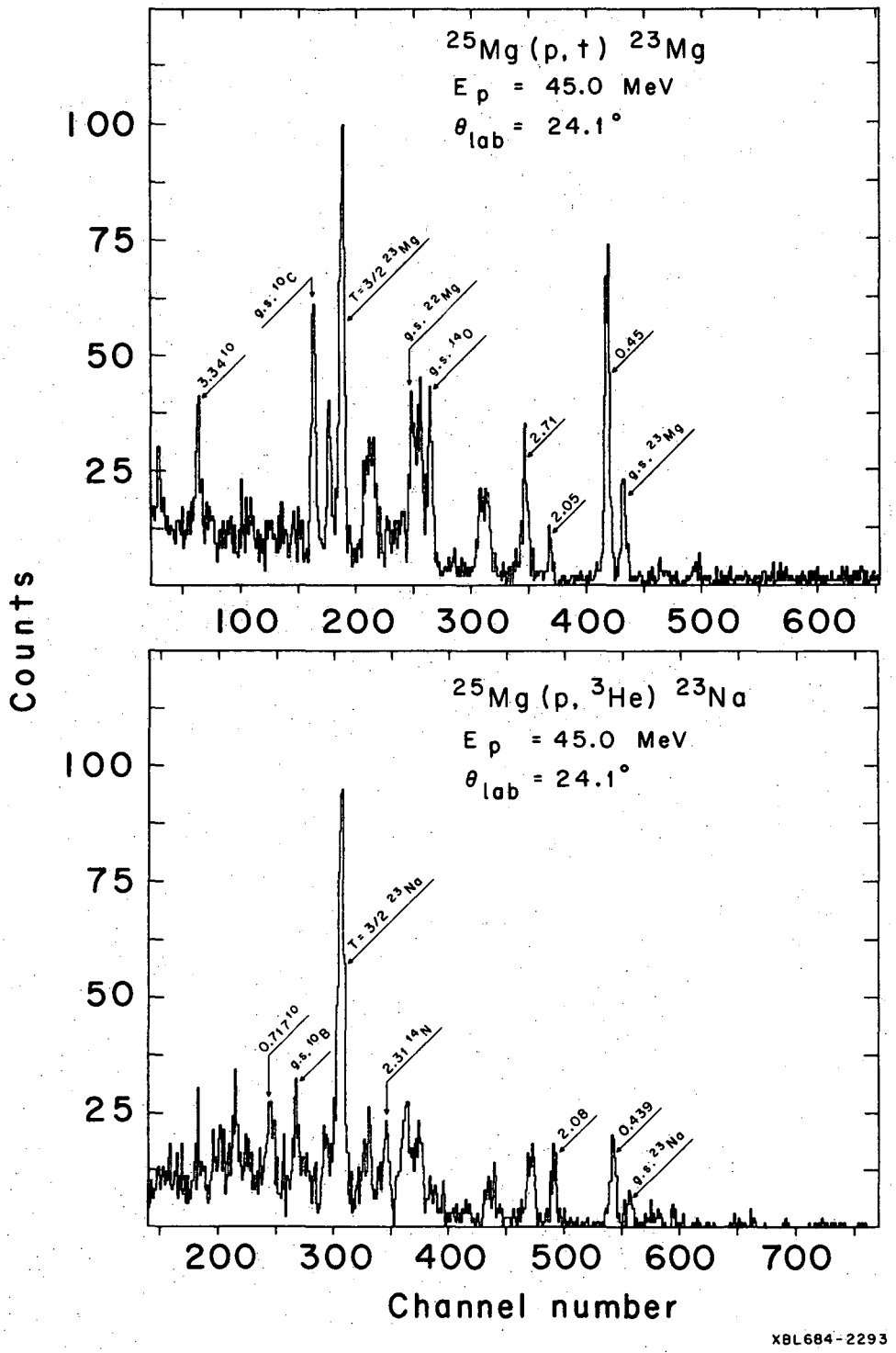
^{25}Mg (p, t) ^{23}Mg
E_p = 45.0 MeV
θ_{lab} = 24.1°
g.s. ^{10}C
T=3/2 ^{23}Mg
g.s. ^{22}Mg
g.s. ^{14}O
3.34 ^{10}
2.71
0.45
g.s. ^{23}Mg
2.05
^{25}Mg (p, ^{3}He) ^{23}Na
E_p = 45.0 MeV
θ_{lab} = 24.1°
T=3/2 ^{23}Na
0.717 ^{10}
g.s. ^{10}B
2.31 ^{14}N
2.08
0.439
g.s. ^{23}Na
Counts
Channel number
XBL684-2293

Figure 9

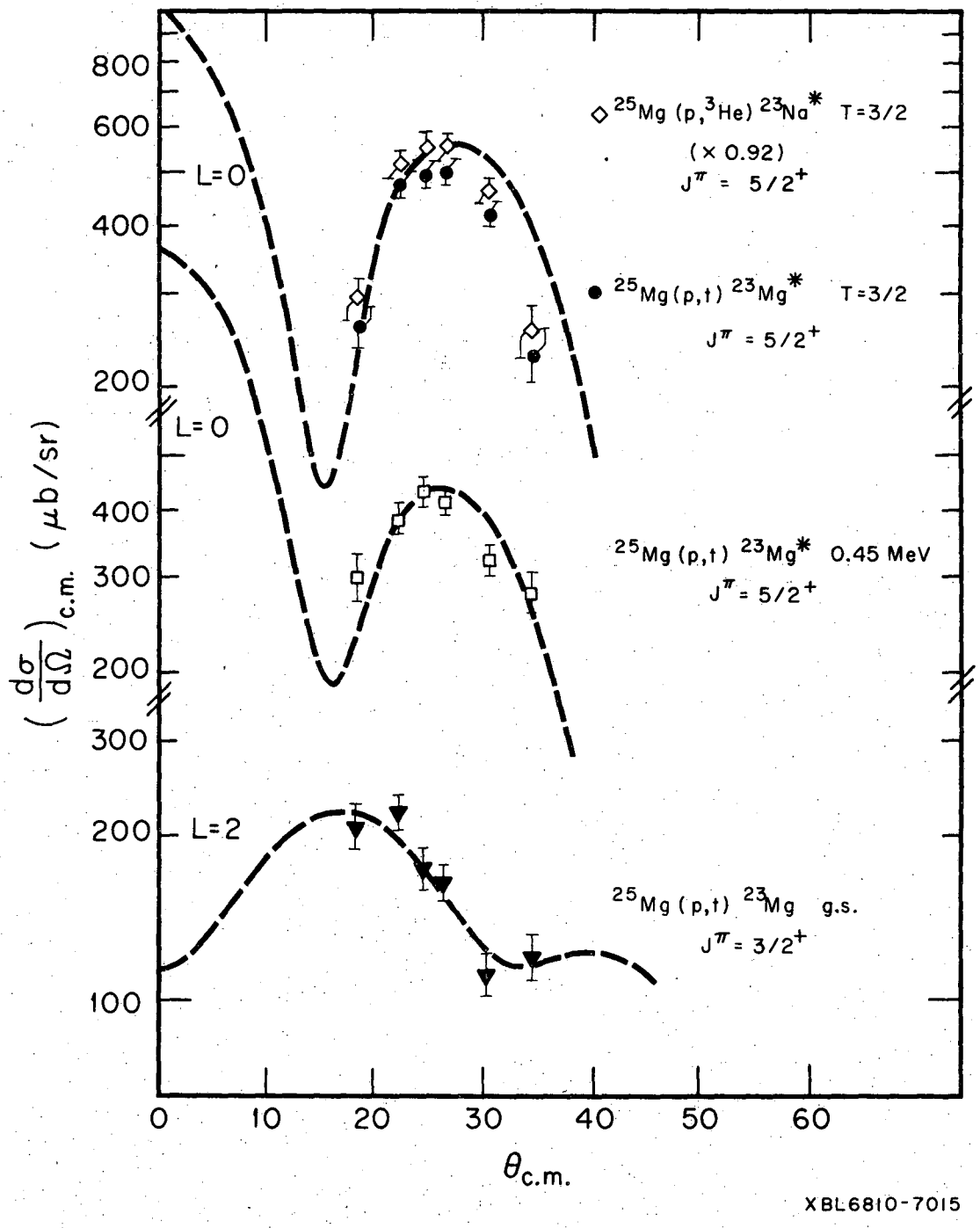
◇ 25Mg (p,3He) 23Na* T=3/2
(× 0.92)
Jπ = 5/2+
● 25Mg(p,t) 23Mg* T=3/2
Jπ = 5/2+
25Mg (p,t) 23Mg* 0.45 MeV
Jπ = 5/2+
25Mg (p,t) 23Mg g.s.
Jπ = 3/2+
L=0
L=0
L=2
(dσ/dΩ)c.m. (μb/sr)
θc.m.
XBL6810-7015

Figure 10

possible to assign a spin-parity to the T = 3/2 states of $5/2^+$, indicating that they are analogues to the ground state of ^{23}Ne.

The excitation energies of the analogue states were determined precisely by using as known those peaks whose energies are marked in Fig. 9; the primary calibration points in the (p,t) spectrum were the ground states of ^{10}C, ^{22}Mg, and ^{14}O, while in the (p,^{3}He) spectrum the principal points were the ground state of ^{10}B and the 2.31 MeV (T=1) first excited state in ^{14}N. The results obtained are given in Table 3 where, for the case of the T = 3/2 level in ^{23}Na, it can be seen that there is good agreement with earlier measurements.[34,35] The T = 3/2 analogue level in ^{23}Mg had not been reported previously.

E. ^{26}Mg (p,t) ^{24}Mg and ^{26}Mg (p,^{3}He) ^{24}Na; T=2 States

The target used for this work was a 1.26 mg/cm^2 self-supporting magnesium foil, enriched to 99.2% in ^{26}Mg. Figure 11 shows the triton and ^{3}He spectra observed at θ_{LAB} = 22.3 degrees for 3200 microcoulombs. It is evident from the figure that a significant amount of carbon was present in the target; the peaks corresponding to states in ^{10}C and ^{10}B provided the primary source of calibration, although all other peaks with (unbracketed) energies marked in the figure were also used.

As was the case with the T=2 states in mass-20, the lowest T=2 analogue states in ^{24}Mg and ^{24}Na, had been previously identified,[31,36-39] and in fact, the angular distributions of the (p,t) reaction to states in ^{24}Mg (including the T=2 analogue) had also been extensively studied.[29]

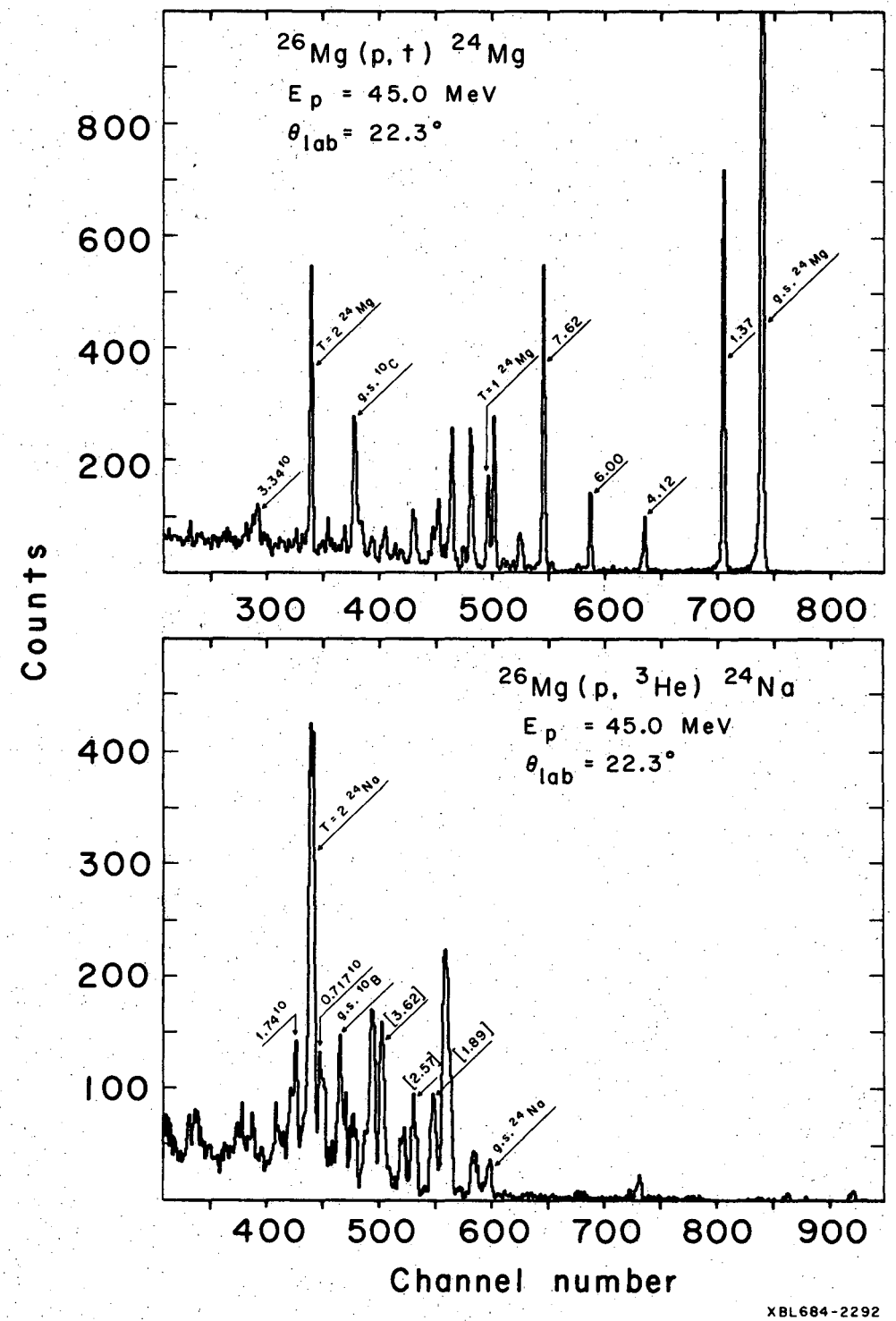
^{26}Mg (p, t) ^{24}Mg
E_p = 45.0 MeV
θ_{lab} = 22.3°
T=2 ^{24}Mg
g.s. ^{10}C
3.34 ^{10}
T=1 ^{24}Mg
7.62
6.00
4.12
1.37
g.s. ^{24}Mg
^{26}Mg (p, ^{3}He) ^{24}Na
E_p = 45.0 MeV
θ_{lab} = 22.3°
T=2 ^{24}Na
1.74 ^{10}
0.717 ^{10}
g.s. ^{10}B
[3.62]
[2.57]
[1.89]
g.s. ^{24}Na
Counts
Channel number
XBL684-2292

Figure 11

Consequently no attempt was made here to obtain angular distributions; both telescopes were set at θ_{LAB} = 22.3 degrees. This angle was chosen because it was near the maximum in the L=0 angular distribution, as well as being one at which the analogue states in both ^{24}Mg and ^{24}Na were resolved from nearby impurity levels.

Again, the experimental uncertainty on the excitation energy of the T=2 state in ^{24}Mg is too small, (±5.0 keV), to be improved by the present work, but its remeasurement provided another check on the accuracy of this method. Using the corrected mass for ^{10}C, excellent agreement was obtained with previous values as shown in Table 3. The excitation energy obtained for the analogue state in ^{24}Na is also given in Table 3, together with a weighted average of all previous data; the final overall average also includes the present results.

Excitation energies for states in ^{24}Mg of potential T=1 character were also determined from this work and are summarized in Table 4. A comparison of these states with observed ^{24}Na states will be discussed in detail in Sec. V-B-2.

F. ^{30}Si (p,t) ^{28}Si and ^{30}Si (p,^{3}He) ^{28}Al; T=2 States

The target used here was a self-supporting evaporated silicon foil, 420 μg/cm^2 thick obtained from ORNL^{40} and enriched to 89.12% in ^{30}Si; the remaining isotopic impurities were 10.16% ^{28}Si, and 0.72% ^{29}Si. Significant amounts of carbon and oxygen were also present, and provided useful calibrations at higher excitation energies. A sample set of triton and ^{3}He spectra obtained at θ_{LAB} = 18.0 degrees for 2150 microcoulombs is shown in Fig. 12.

Table 4. Summary of T=1 States observed in Mass-24

Nucleus	This Work (MeV ± keV)	J^π; T	Previous Work (MeV ± keV)	Ref.	Average (MeV ± keV)
^{24}Mg	9.526 ± 25	4^+;1	9.517 ± 6	(a)	9.517 ± 6*
	10.080 ± 30	(2^+;1)	10.072 ± 8	(a)	10.072 ± 8*
	10.337 ± 35	2^+;	10.353 ± 20	(a)	10.348 ± 17
	10.740 ± 35	1^+;(1)	10.737 ± 9	(a)	10.737 ± 9
	10.977 ± 40		not reported		10.977 ± 40
	11.160 ± 35	$(1,3)^-$;	11.165 ± 5	(a)	11.165 ± 5
	11.375 ± 40	1^-;	11.391 ± 4	(a)	11.391 ± 4
^{24}Na	g.s.	4^+;1	g.s*	(a)	-------
	0.546 ± 35	1^+;1	0.472 ± 0.2	(a)	0.472 ± 0.2
		2^+;1	0.563 ± 0.2	(a)	0.563 ± 0.2
	1.498 ± 35	;1	1.341 ± 0.2	(a)	1.341 ± 0.2
		;1	1.347 ± 0.3	(a)	1.347 ± 0.3
		;1	1.508 ± 10	(b)	1.508 ± 10
	1.890 ± 30	($\leq$4)$^+$;1	1.885 ± 0.3	(a)	1.885 ± 0.3

*These states were used as known, in addition to the other calibrations discussed in the text.

(a) P. M. Endt and C. Van der Leun, Nucl. Phys. A105, 1 (1967).

(b) R. Jahr, J. A. H. Pfleger and H. Zell, Phys. Lett. 25B, 113 (1967).

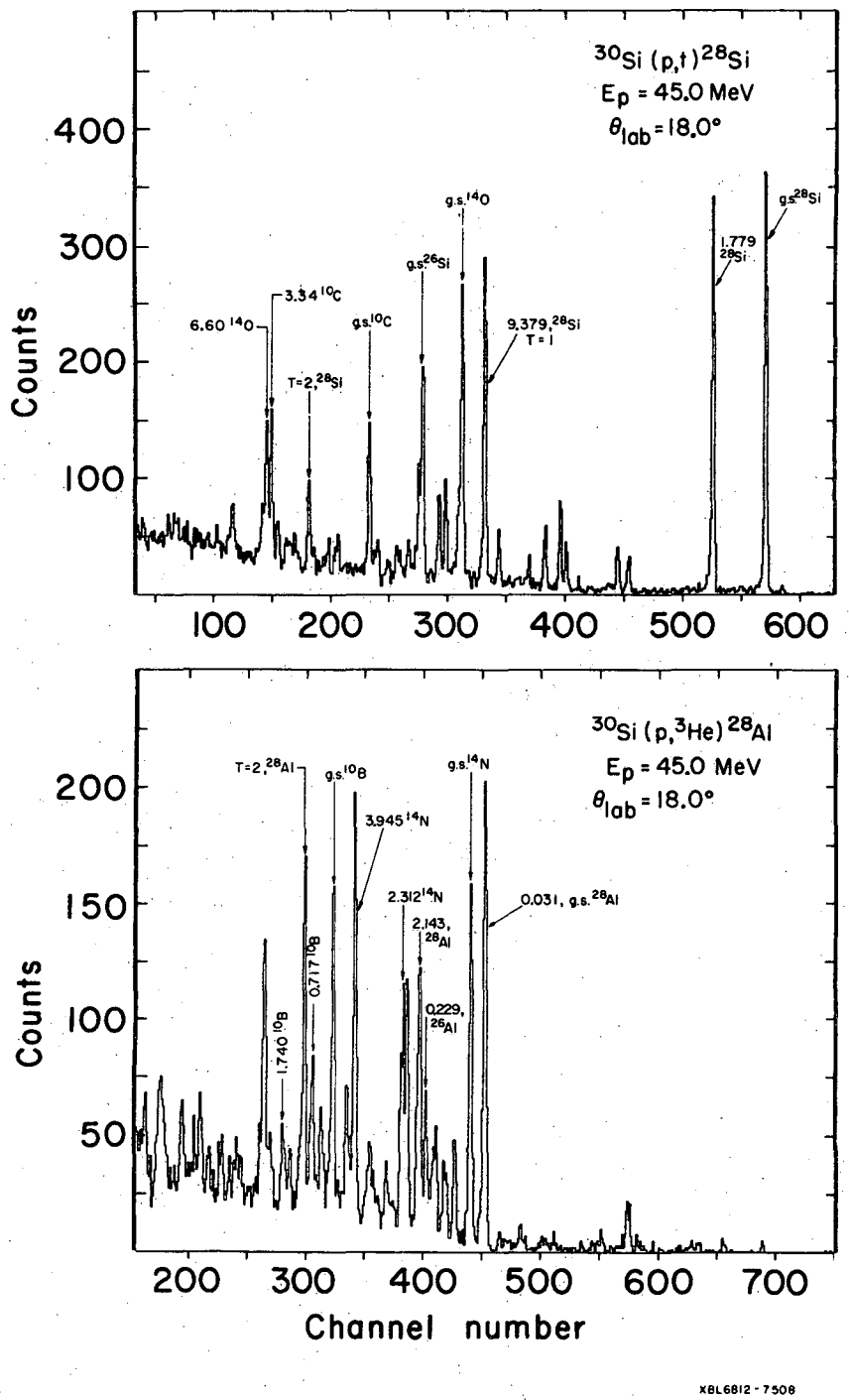
^{30}Si (p,t)^{28}Si
Ep = 45.0 MeV
θlab = 18.0°
g.s.^{14}O
g.s.^{28}Si
1.779 ^{28}Si
g.s.^{26}Si
3.34 ^{10}C
6.60 ^{14}O
g.s.^{10}C
9.379, ^{28}Si T=1
T=2, ^{28}Si
Counts
100
200
300
400
500
600
^{30}Si (p,^{3}He)^{28}Al
Ep = 45.0 MeV
θlab = 18.0°
T=2, ^{28}Al
g.s.^{10}B
g.s.^{14}N
3.945 ^{14}N
2.312 ^{14}N
0.031, g.s. ^{28}Al
2.143, ^{28}Al
0.717 ^{10}B
1.740 ^{10}B
0.229, ^{26}Al
Counts
50
100
150
200
300
400
500
600
700
Channel number
XBL6812-7508

Figure 12

Since these T=2 states had not been reported previously, a rough Coulomb energy calculation based on the mass excess of ^{28}Mg was used to predict excitation energies of 15.3 MeV in ^{28}Si and 6.1 MeV in ^{28}Al for these states. The peaks marked T=2 in Fig. 12 were found to be consistent with these predictions. Spectra were measured for seven angles, ranging from θ_{LAB} = 14.1 degrees to θ_{LAB} = 36.2 degrees.

In the upper portion of Fig. 13 are shown the angular distributions of triton and ^{3}He particles corresponding to the T=2 analogue states in ^{28}Si and ^{28}Al; the ^{3}He distribution has been multiplied by the momentum and isospin coupling coefficients as suggested by Eq. (IV-1), to facilitate comparison. Within the accuracy of the approximation used in the derivation of Eq. (IV-1), good agreement is obtained for the (p,t) and (p,^{3}He) cross section shapes and magnitudes, establishing these states as T=2 analogue states. Also shown in the figure are the characteristic L=0 and L=2 transitions to the ground and 1.779 MeV states in ^{28}Si. Simple comparison shows the analogue states to be L=0 transitions, which, since ^{30}Si is $J^{\pi} = 0^{+}$ permits an assignment of their J^{π} as 0^{+}, identifying them as analogues to the ^{28}Mg ground state. Further verification of the assigned L values was obtained from DWBA fits using the optical model parameters listed in Table 2. As was done previously, the fits, shown as solid curves in Fig. 13, were normalized to the experimental data. Because at some angles the T=2 state in ^{28}Al is degenerate with the ^{10}B* 0.717 MeV state, it was necessary to subtract this latter component; its strength was determined from the known cross section ratio of the ^{10}B ground state to the ^{10}B* 0.717-MeV

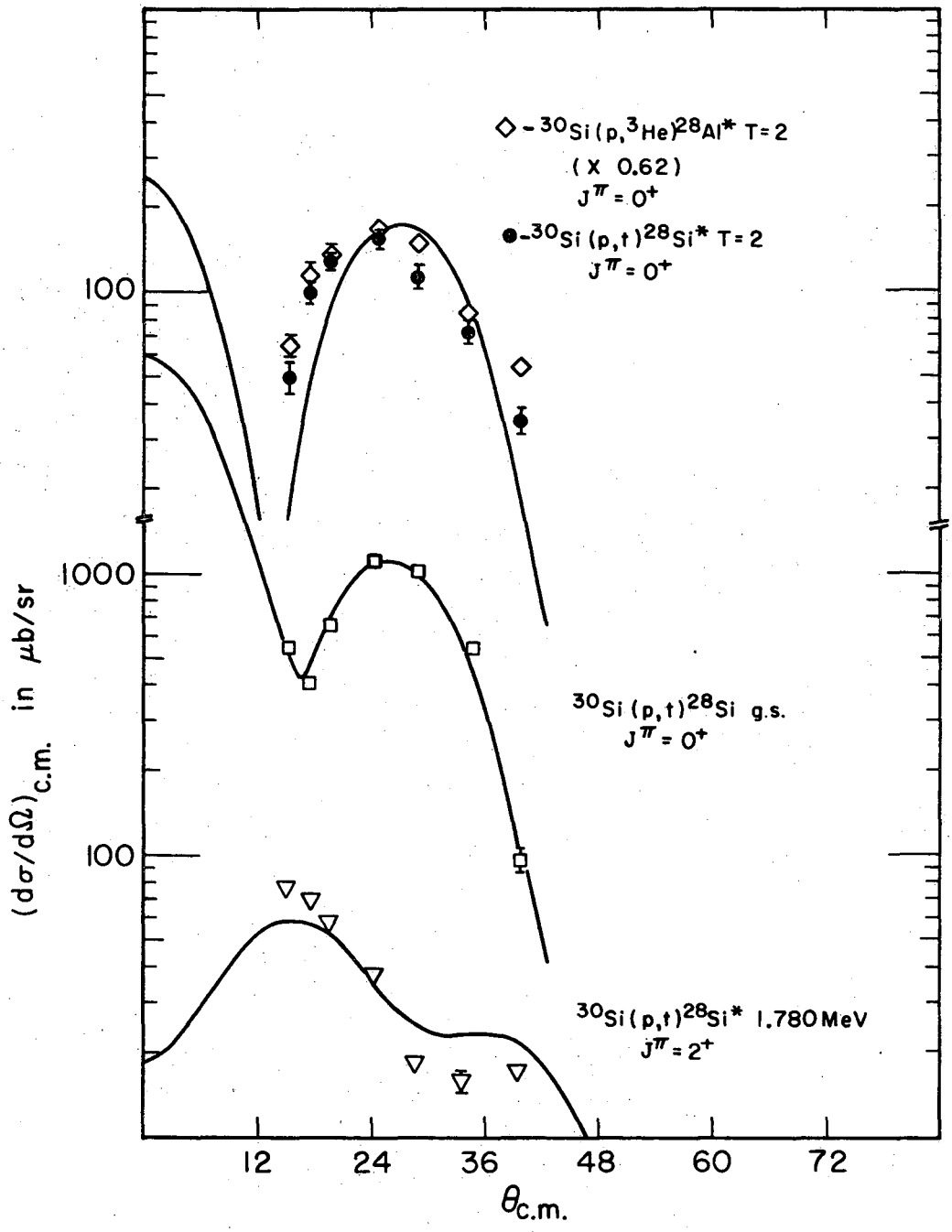
◇ - $^{30}Si(p,^{3}He)^{28}Al^{*}$ T=2
(X 0.62)
$J^{\pi} = 0^{+}$
● - $^{30}Si(p,t)^{28}Si^{*}$ T=2
$J^{\pi} = 0^{+}$
$^{30}Si(p,t)^{28}Si$ g.s.
$J^{\pi} = 0^{+}$
$^{30}Si(p,t)^{28}Si^{*}$ 1.780 MeV
$J^{\pi} = 2^{+}$
100
1000
100
$(d\sigma/d\Omega)_{c.m.}$ in μb/sr
12
24
36
48
60
72
$\theta_{c.m.}$
XBL 6812-7529

Figure 13

state, measured previously. The errors shown on the experimental points, however, still represent only the pure statistical error, as is the case for all data shown.

The states used as energy calibrations for the T=2 states in mass-28 are shown in Fig.12. Where interferences prevent the accurate determination of peak positions, the data were not used in the energy determinations, although cross section values were extracted as described above. The final excitation energies obtained for the analogue states are shown in Table 3.

Excitation energies of strong states in the region of excitation immediately above the lowest T=1 state were also extracted for both ^{28}Si and ^{28}Al. The energies observed for states in ^{28}Si were 10.675±0.030 MeV, and 10.903±0.030 MeV, which agree well with previously reported states[41] at 10.710±0.020 MeV and 10.909±0.010 MeV (see Fig. 14a). States observed in ^{28}Al were found to have excitations which corresponded within errors to the previously reported states at 1.372 MeV and 1.633 MeV. Possible J^{π} and T assignements are discussed later in Sec.V-B-3. Because the lower states in ^{28}Si are well known,[41] no attempt was made to determine accurate energies or angular distributions.

G. ^{34}S (p,t) ^{32}S and ^{34}S (p,^{3}He) ^{32}P; T=2 States

A self-supporting CdS target, approximately 100 μg/cm^2 thick, was used. The sulfur component of the target was 67.92% enriched in ^{34}S, the remaining isotopes being 31.55% ^{32}S, 0.44% ^{33}S, and 0.09% ^{36}S. This target was also found to contain small quantities of oxygen and carbon.

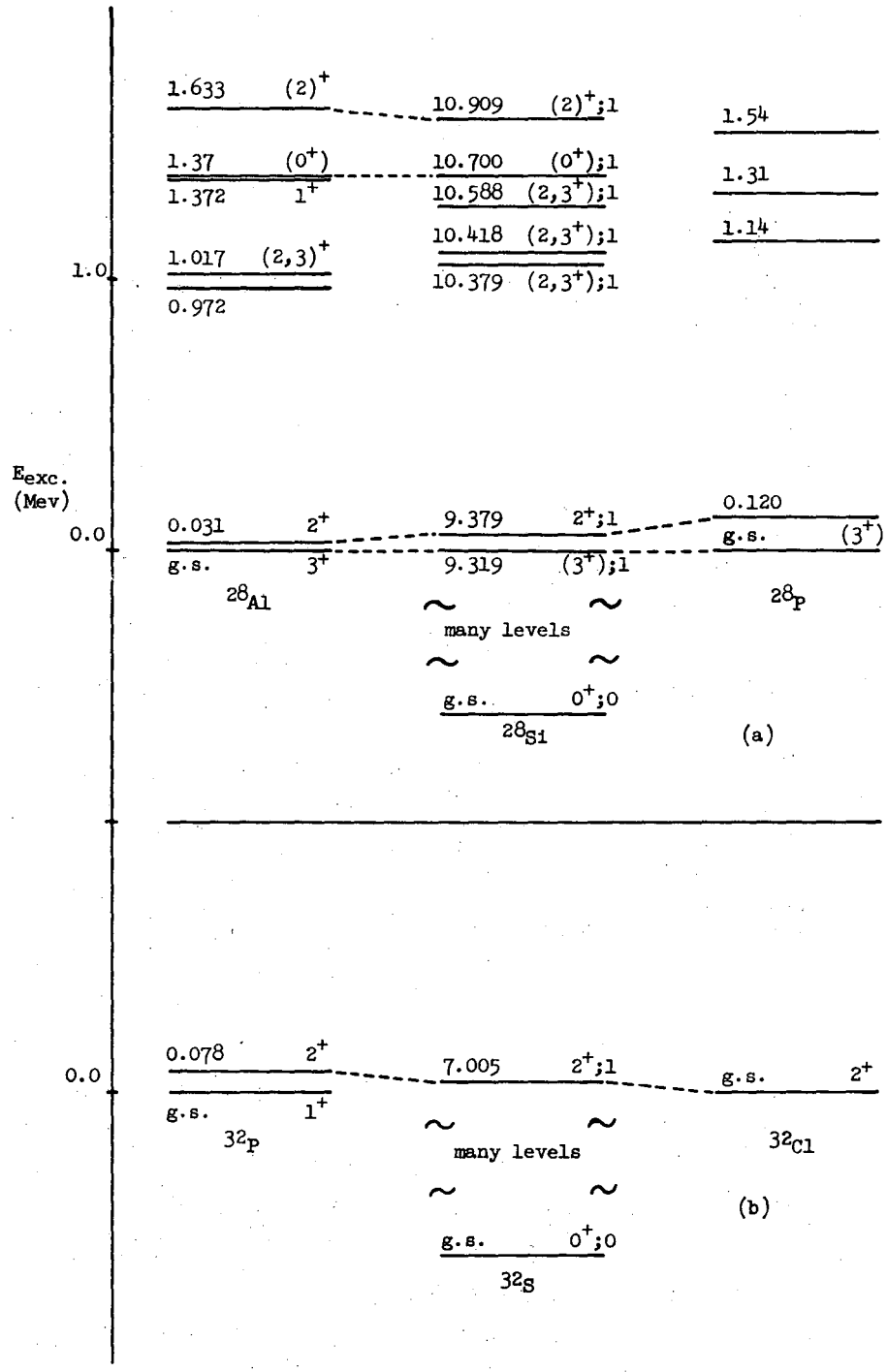
1.633 (2)+
1.37 (0+)
1.372 1+
1.017 (2,3)+
0.972
1.0
Eexc. (Mev)
0.0
0.031 2+
g.s. 3+
28Al
10.909 (2)+;1
10.700 (0+);1
10.588 (2,3+);1
10.418 (2,3+);1
10.379 (2,3+);1
9.379 2+;1
9.319 (3+);1
many levels
g.s. 0+;0
28Si
1.54
1.31
1.14
0.120
g.s. (3+)
28P
(a)
0.078 2+
g.s. 1+
32P
7.005 2+;1
many levels
g.s. 0+;0
32S
g.s. 2+
32Cl
(b)
XBL 6812-6458

Figure 14

Because no T=2 analogue states had been reported previously, a rough Coulomb energy calculation based on the mass-excess of ^{32}Si was used to predict approximate excitation energies for these states. The states shown in Fig. 15 marked as T=2 are consistent with these predicted values. A series of four angles ranging from θ_{LAB} = 20.5 degrees to θ_{LAB} = 31.5 degrees were measured; sample spectra obtained at θ_{LAB} = 22.3 degrees for 6380 microcoulombs are shown in Fig. 15. The thin targets available were capable of withstanding only very small beam intensities, resulting in very low counting rates. Consequently spectra were recorded only near angles where the L=0 angular distributions were a maximum. The ratio of the triton and ^{3}He cross sections to the T=2 analogue states were obtained, however, at all measured angles and found to have a value for $^{2k}t/3k3_{He}$ (=0.60) which agrees with that calculated by Eq. (IV-1). Since no systematic variation in cross section ratios was detected as a function of angle it is concluded that in the region measured, the angular distribution shapes are also identical. On the basis of this cross section data, the energy systematics of T=2 states in the (sd)-shell, and the Coulomb calculation energy prediction, these states are assigned as T=2 analogue states. Because of the enhancement of these transitions at θ_{LAB} = 22.3 degrees, it is likely that they are (L=0) transitions, forming 0^{+} states analogous to the T=2 ^{32}Si ground state.

The excitation energy obtained for the T=2 analogue state in ^{32}S is based primarily on the ^{10}C and ^{14}O ground states, although the ^{30}S ground state and ^{32}S 2.237-MeV states were also used; the excitation

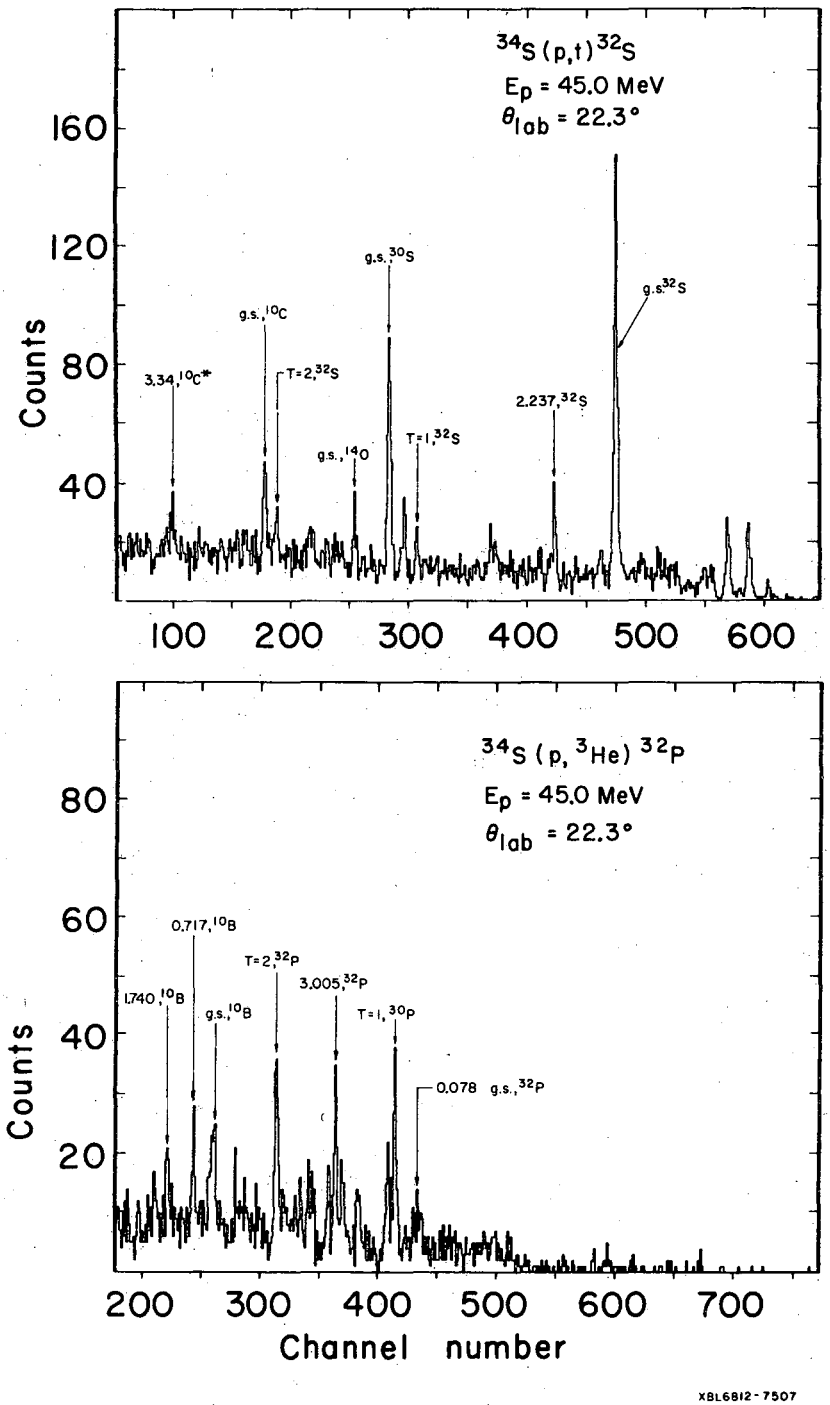
$^{34}S(p,t)^{32}S$
E_p = 45.0 MeV
θ_{lab} = 22.3°
Counts
160
120
80
40
100
200
300
400
500
600
g.s., ^{30}S
g.s. ^{32}S
g.s., ^{10}C
3.34, $^{10}C^*$
T=2, ^{32}S
g.s., ^{14}O
T=1, ^{32}S
2.237, ^{32}S
$^{34}S(p,{}^3He)^{32}P$
E_p = 45.0 MeV
θ_{lab} = 22.3°
Counts
80
60
40
20
0.717, ^{10}B
T=2, ^{32}P
3.005, ^{32}P
1.740, ^{10}B
g.s., ^{10}B
T=1, ^{30}P
0.078 g.s., ^{32}P
200
300
400
500
600
700
Channel number
XBL6812-7507

Figure 15

energy of the T=2 analogue state in ^{32}P is based on the ^{10}B ground and 0.717-MeV states, as well as the ^{30}P 0.678-MeV state, which is the T=1 analogue to the ^{30}S ground state. Final excitation energies obtained for the T=2 states are listed in Table 3.

Using the above calibrations, the energy determined for the lowest observed T=1 state in ^{32}S agreed well with a previous measurement of 7.005±0.005 MeV.[41]

A natural cadmium sulfide target was run at θ_{LAB} = 22.3 degrees in order to establish the states produced by the reactions $^{32}S(p,t)^{30}S$ and $^{32}S(p,^{3}He)^{30}P$ on the ^{32}S present in the ^{34}S enriched target. The only states observed with significant cross section were the ^{30}S ground state and its T=1 analogue in ^{30}P. These states were identified in the spectra obtained from the ^{34}S-enriched target and were used as calibrations.

H. ^{36}Ar (p,t) ^{34}Ar, $^{36}Ar(p,^{3}He)$ ^{34}Cl and ^{36}Ar (d,α) ^{34}Cl Reactions

Although the excitations of states in ^{34}Ar have recently been measured[42-44] up to about 4 MeV, there has been substantial disagreement in excitations reported, and no spin-parity assignments had been made. The $^{36}Ar(p,t)^{34}Ar$ reaction was used to establish J^{π} values and extend the range of excited states observed. The excitation energies of states in ^{34}Cl were better known[41] with spin-isospin assignments having recently been made up to an excitation of 3.5 MeV.[45] A comparison of the (p,t), $(p,^{3}He)$, and (d,α) reactions was used to establish the isospin of the states observed in ^{34}Cl.

The argon target used for these experiments was 99.6% enriched in ^{36}Ar. Triton and ^{3}He spectra were recorded over an angular range of θ_{LAB} =10.0 degrees to θ_{LAB} = 60.5 degrees; the α-particle spectra were taken over a range of θ_{LAB} = 14.1 degrees to θ_{LAB} = 50.7 degrees. The triton and ^{3}He spectra obtained at θ_{LAB} = 24.1 degrees for 3450 microcoulombs are shown in Fig. 16. A representative α-spectrum, recorded at θ_{LAB} = 22.3 degrees for 2200 microcoulombs is shown in the upper portion of Fig. 17. The excitation energies determined for the ^{34}Ar states observed by the (p,t) reaction were based on the known ^{34}Ar ground state Q-value, and the impurity ^{14}O ground state; the slope of the energy scale was established by the reactions $^{12}C(p,t)^{10}C$ and $^{16}O(p,t)^{14}O$, using a carbon dioxide target run immediately before and after the ^{36}Ar experiments. The values obtained are shown in square brackets in Fig. 16, and summarized in Table 5.

Although McMurray et al.[43] agree well with the other mass excess values reported for the ^{34}Ar ground state, their determination of excited states in ^{34}Ar appears to be erroneous. Because of the large inconsistencies noted, their values were not used in obtaining the average excitation summarized in Table 5. The values obtained for the excitations of states in ^{34}Ar utilizing the (p,t) reaction are found to agree well with previous determinations from the $^{32}S(^{3}He,n)^{34}Ar$ reaction, as reported by Hagen et al.[44] A comparison of levels reported for mass-34 is shown in Fig. 18.

The excitations of ^{34}Cl states produced by the reaction $^{36}Ar(p,^{3}He)^{34}Cl$ were determined using ^{34}Cl states of known excitation

Table 5. Summary of ^{36}Ar (p,t) ^{34}Ar Reaction

This Work			Previous Work			Average	
Excitation (MeV ± keV)	J^π	Intensity	Excitation (MeV ± keV)	J^π	Ref.	Excitation (MeV ± keV)	J^π
ground state	0^+	500μb/sr	g.s.	0^+	a,b,c	-	0^+
2.097 ± 20	2^+	100μb/sr	2.058 ± 35	(2^+)	a	2.092 ± 15	2^+
			2.190 ± 40*		b		
			2.10 ± 30		c		
3.303 ± 25	2^+	100μb/sr	3.59 ± 60*		b	3.302 ± 19	2^+
			3.30 ± 30		c		
3.899 ± 25	0^+	100μb/sr	3.90 ± 30		c	3.900 ± 19	0^+
			4.05 ± 30		c	4.05 ± 30	
			4.15 ± 30		c	4.15 ± 30	
4.56 ± 35	(3^-)	55μb/sr	not reported previously			4.56 ± 35	(3^-)
4.97 ± 40		40μb/sr				4.97 ± 40	
5.34 ± 40		~20μb/sr				5.34 ± 40	
6.10 ± 40		45μb/sr				6.10 ± 40	
6.86 ± 40		~20μb/sr				6.86 ± 40	
7.34 ± 45		45μb/sr				7.34 ± 45	
7.53 ± 45		30μb/sr				7.53 ± 45	
7.95 ± 50		30μb/sr				7.95 ± 50	

*These values were not used in obtaining the average value because they differ outside errors and are presumed erroneous.

(a) R. G. Miller and R. W. Kavanagh, Phys. Lett. 22, 461 (1966); Nucl. Phys. A94, 261 (1967).

(b) W. R. McMurray, P. Van der Merve, and I. J. Van Heerden, Nucl. Phys. A92, 401 (1967).

(c) M. Hagen, K. H. Maier, and R. Michaelsen, Phys. Lett. 26B, 432 (1968).

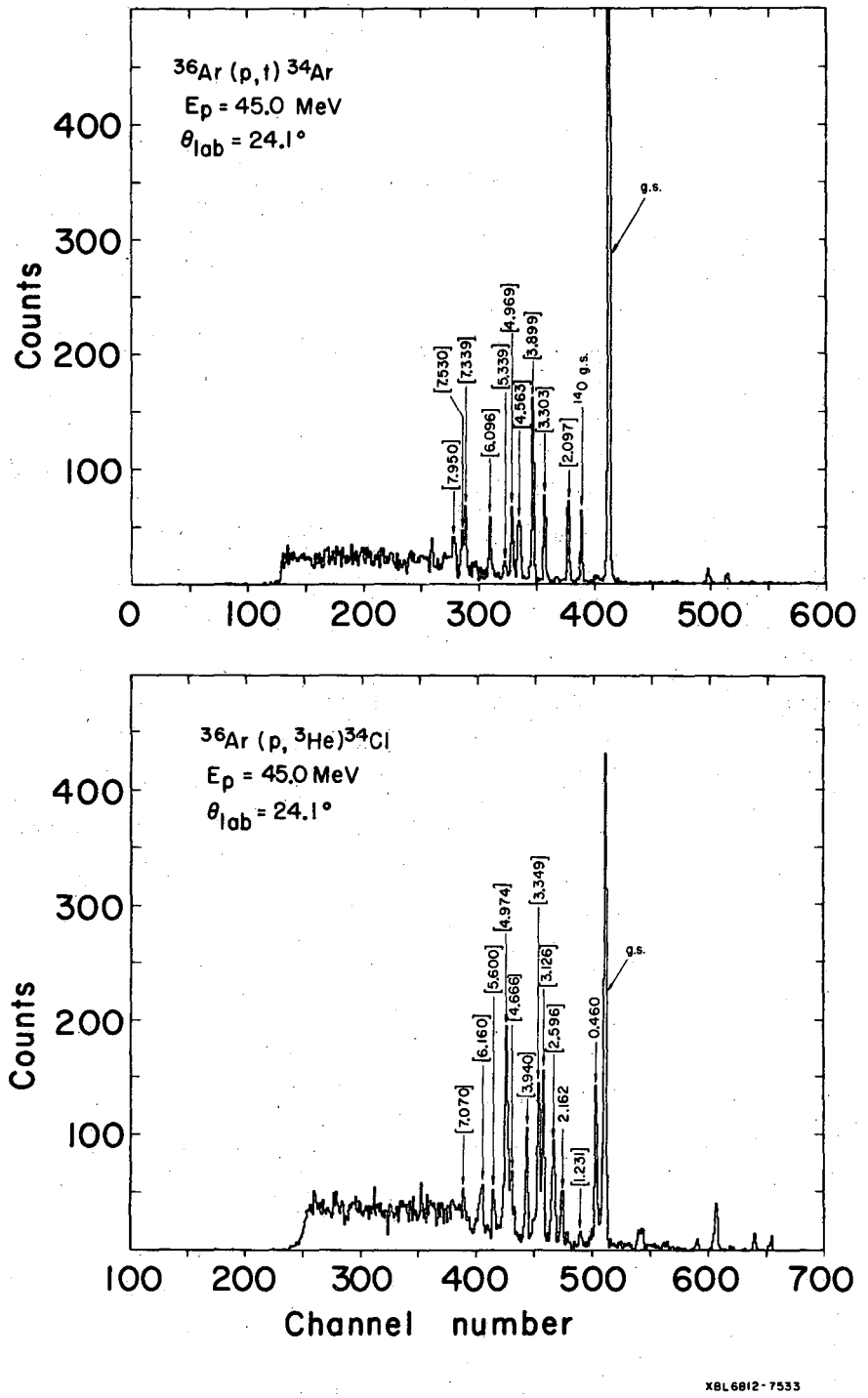
^{36}Ar (p,t) ^{34}Ar
Ep = 45.0 MeV
θ_{lab} = 24.1°
Counts
g.s.
[7.950]
[7.530]
[7.339]
[6.096]
[5.339]
[4.969]
[4.563]
[3.899]
[3.303]
[2.097]
^{40} g.s.
^{36}Ar (p, ^{3}He)^{34}Cl
Ep = 45.0 MeV
θ_{lab} = 24.1°
Counts
[7.070]
[6.160]
[5.600]
[4.974]
[4.666]
[3.940]
[3.349]
[3.126]
[2.596]
2.162
[1.231]
0.460
g.s.
Channel number
XBL6812-7533

Figure 16

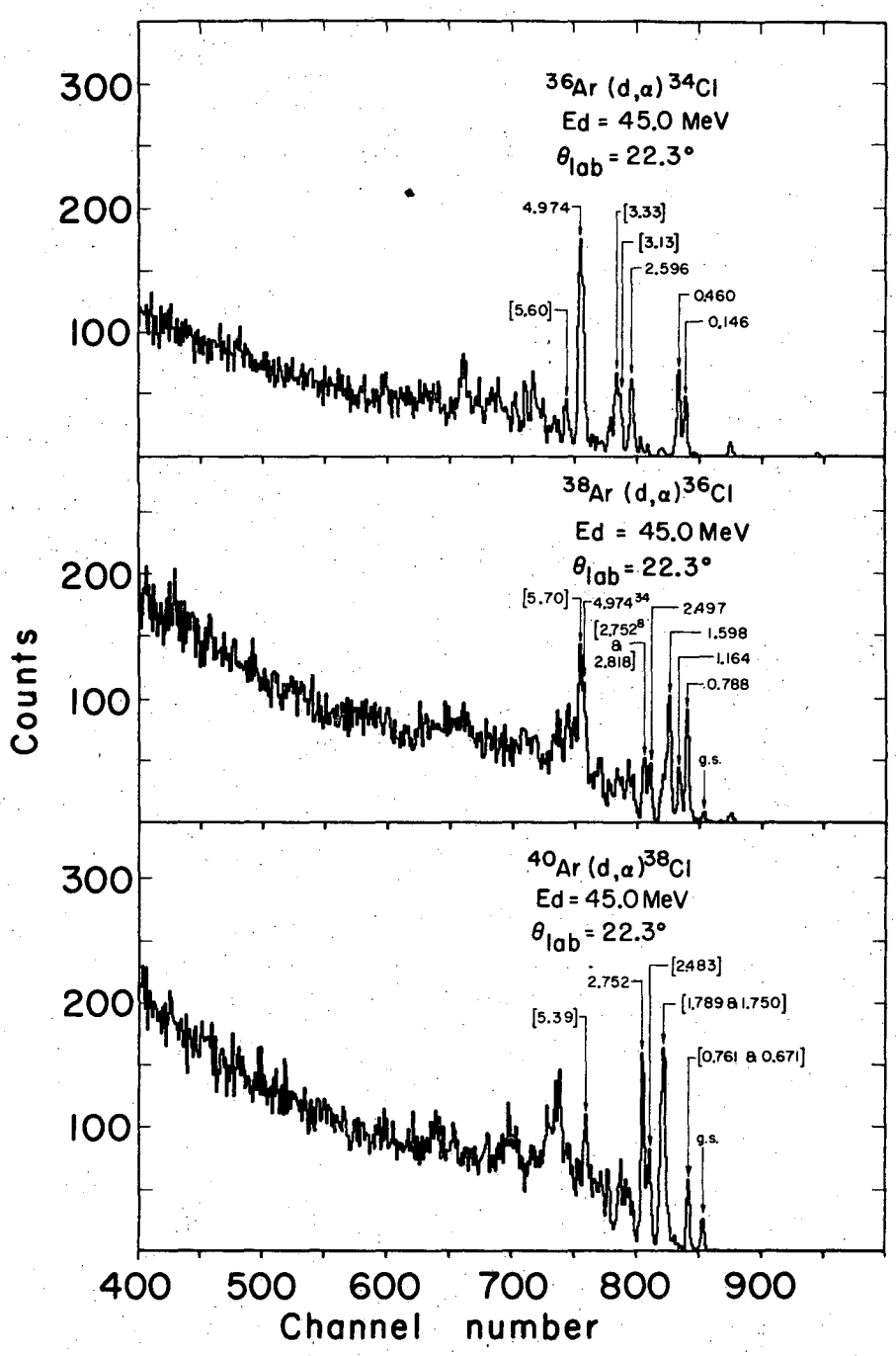
^{36}Ar (d,α) ^{34}Cl
Ed = 45.0 MeV
θ_{lab} = 22.3°
4.974
[3.33]
[3.13]
2.596
0.460
0.146
[5.60]
^{38}Ar (d,α) ^{36}Cl
Ed = 45.0 MeV
θ_{lab} = 22.3°
[5.70]
4.974 ^{34}
[2.752 ^{8} & 2.818]
2.497
1.598
1.164
0.788
g.s.
^{40}Ar (d,α) ^{38}Cl
Ed = 45.0 MeV
θ_{lab} = 22.3°
2.752
[2.483]
[1.789 & 1.750]
[0.761 & 0.671]
[5.39]
g.s.
Counts
300
200
100
400
500
600
700
800
900
Channel number
XBL6812-7506

Figure 17

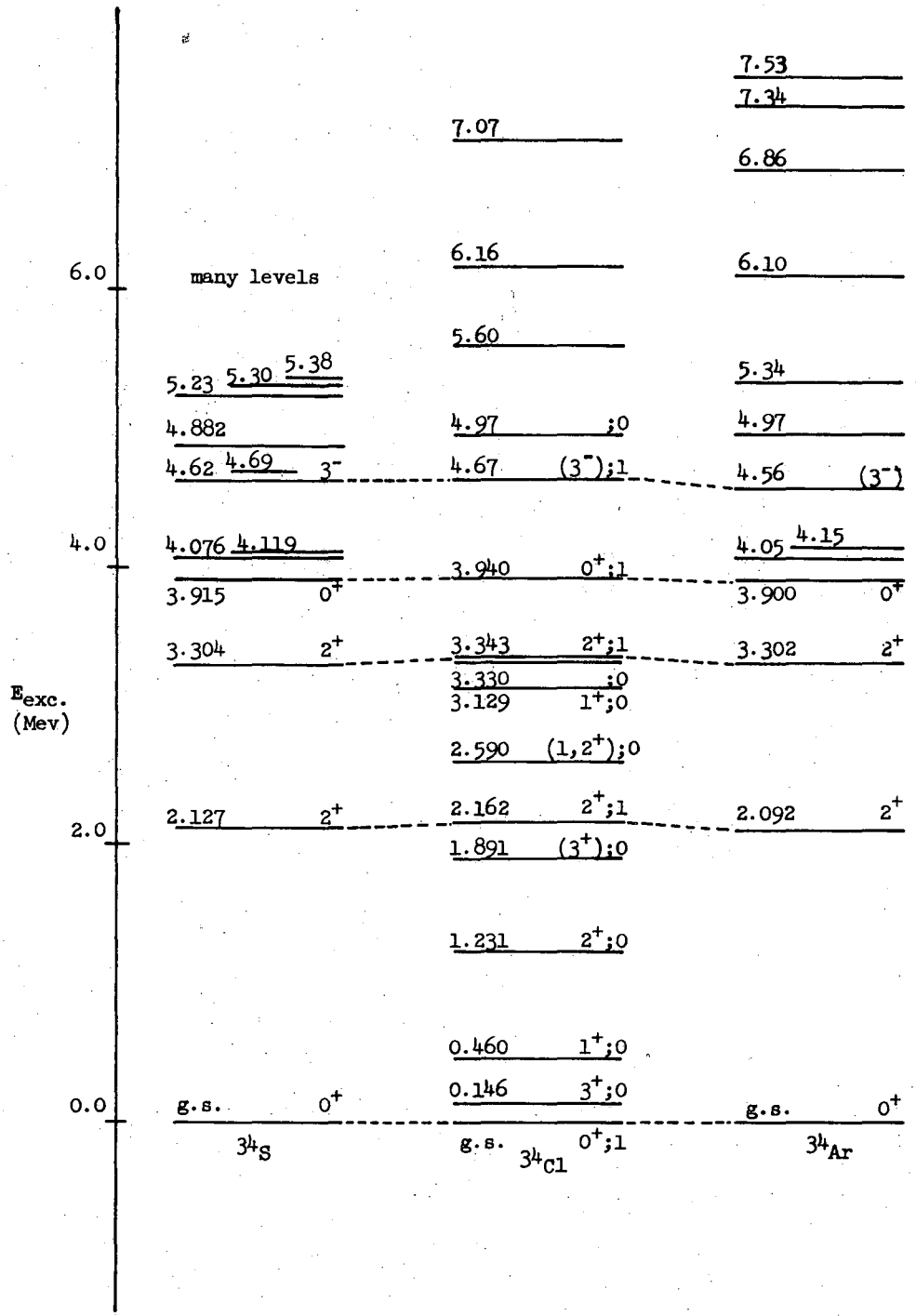
$E_{exc.}$ (Mev)
6.0
4.0
2.0
0.0
many levels
5.23 5.30 5.38
4.882
4.62 4.69 3⁻
4.076 4.119
3.915 0⁺
3.304 2⁺
2.127 2⁺
g.s. 0⁺
^{34}S
7.07
6.16
5.60
4.97 ;0
4.67 (3⁻);1
3.940 0⁺;1
3.343 2⁺;1
3.330 ;0
3.129 1⁺;0
2.590 (1,2⁺);0
2.162 2⁺;1
1.891 (3⁺);0
1.231 2⁺;0
0.460 1⁺;0
0.146 3⁺;0
g.s. 0⁺;1
^{34}Cl
7.53
7.34
6.86
6.10
5.34
4.97
4.56 (3⁻)
4.05 4.15
3.900 0⁺
3.302 2⁺
2.092 2⁺
g.s. 0⁺
^{34}Ar
XBL 6812-6456

Figure 18

up to 2.162 MeV. The excitations of ^{34}Cl states produced by ^{36}Ar(d,α)^{34}Cl were identified using the known ^{34}Cl T=0 states up to 2.162 MeV, and the 4.97 MeV state previously determined from the (p,^{3}He) reaction. A comparison of the results shows states identified as T=0 from a comparison of (p,t) and (p,^{3}He) were produced in the (d,α) reaction, confirming the earlier assignment[45] as summarized in Table 6. A single exception was noted in the case of the state at 3.349 MeV, however, and will be discussed below.

The angular distributions obtained for states identified as T=1 in mass-34 are shown in Fig. 19. The ^{3}He cross section data have been multiplied by a factor of $^{2k}t/k3_{He}$, as suggested by Eq. (IV-1). The dashed curves through the triton data serve to guide the eye; the identical curves have been drawn through the ^{3}He data to facilitate the comparison of distribution shapes. After correction for the above factor, the cross section magnitudes for both the triton and ^{3}He distributions are expected, within the accuracy of Eq. (IV-1), to be identical. Good agreement is obtained for all T=1 analogue states except the ^{34}Ar 3.303 MeV-^{34}Cl 3.343 MeV states; here the cross sections are observed to differ by a factor of 4. A further study of the states in ^{34}Cl by the reaction ^{36}Ar (d,α) ^{34}Cl revealed that a state, with an observed excitation of 3.33±0.035 MeV was populated in this reaction. Energy considerations and angular distribution shapes suggest the ^{34}Ar 3.303 MeV-^{34}Cl 3.343 MeV states are T=1 analogues. However, since the (d,α) reaction here populated only T=0 states, the population of a state at 3.33 MeV by this reaction suggests an unresolved doublet at this

Table 6. Summary of $^{36}Ar(p,^{3}He)^{34}Cl$ and $^{36}Ar(d,\alpha)^{34}Cl$ Reactions

This Work				Previous Work			Average	
		Intensity						
Excitation (MeV ± keV)	$J^{\pi};T$	$(p,^{3}He)$ (μb/sr)	(d,α) (μb/sr)	Excitation (MeV ± keV)	$J^{\pi};T$	Ref.	Excitation (MeV ± keV)	$J^{\pi};T$
g.s.	$0^{+};1$	260	-	g.s.	$0^{+};1$	c	-	$0^{+};1$
0.146(†)(a)	;0	-	100	0.1462 ± 0.3	$3^{+};0$	c,d	0.1462 ± 0.3	$3^{+};0$
0.460	;0	200	75	0.460 ± 14	$1^{+};0$	c,d	0.460 ± 14	$1^{+};0$
1.231	;0	25	-	1.231 ± 14	$2^{+};0$	c,d	1.231 ± 14	$2^{+};0$
1.891	;0	~20	-	1.891 ± 14	$(3^{+});0$	c,d	1.891 ± 14	$(3^{+});0$
2.162	$2^{+};1$	65	~40	2.162 ± 14	$2^{+};1$	c,d	2.162 ± 14	$2^{+};1$
2.596 ± 25	;0	80	140	2.587 ± 14	$(1,2^{+});0$	c,d	2.590 ± 13	$(1,2^{+});0$
3.126 ± 30	;0	100	-	3.130 ± 20	$1^{+};0$	c,d	3.129 ± 17	$1^{+};0$
3.33 ± 35(a)	;0	-	370	not reported		-	3.33 ± 35	(;0)
3.35 ± 35	$2^{+};1$	200(b)	-	3.340 ± 20	$2^{+};1$	c,d	3.34 ± 18	$2^{+};1$
3.94 ± 35	$0^{+};1$	60	-				3.94 ± 35	$0^{+};1$
4.67 ± 35	$(3^{-});1$	40	-	level density			4.67 ± 35	$(3^{-});1$
4.97 ± 35	;0	180	420	too large for			4.97 ± 35	;0
5.60 ± 40		40	95	meaningful			5.60 ± 40	
6.16 ± 40		70	-	comparison			6.16 ± 40	
7.07 ± 40		30	-				7.07 ± 40	

† Values listed without error bars were used to determine the energy scale.

(a) Excitations from (d,α) - all others from $(p,^{3}He)$.

(b) Includes any contribution to 3.33 MeV state also.

(c) P. M. Endt and C. Van der Leun, Nucl. Phys. A105, 1 (1967).

(d) J. Kouloumdjian, J. L'Ecuyer, and R. Fournier, Report #LYCEN-6830 (1967).

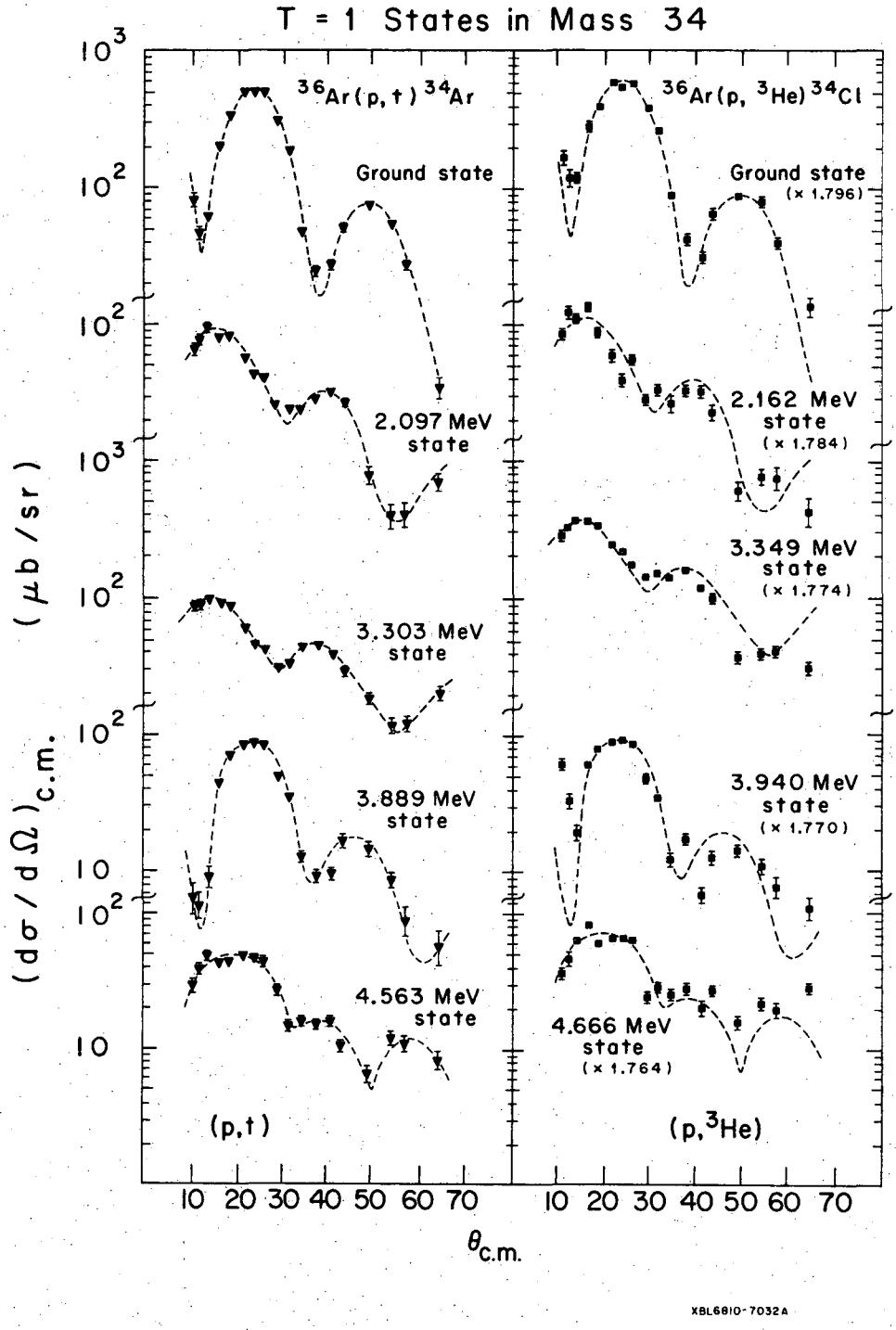
T = 1 States in Mass 34
^{36}Ar(p,t)^{34}Ar
Ground state
2.097 MeV state
3.303 MeV state
3.889 MeV state
4.563 MeV state
(p,t)
^{36}Ar(p, ^{3}He)^{34}Cl
Ground state (× 1.796)
2.162 MeV state (× 1.784)
3.349 MeV state (× 1.774)
3.940 MeV state (× 1.770)
4.666 MeV state (× 1.764)
(p,^{3}He)
(dσ/dΩ)c.m. (μb/sr)
θc.m.
XBL6810-7032A

Figure 19

energy (3.34±0.030 MeV), composed of a $J^{\pi} = 2^{+}$, T=1 member and a $J^{\pi} = (1,2,3^{+})$, T=0 member.

The angular distributions for states assigned a J^{π} by these experiments are compared with the known L=0 and L=2 distributions in mass 36 and 38 in Fig. 20. The dashed curves are DWBA fits using the parameters given in Table 2. The angular distributions obtained for the T=0 states in mass 34 are shown in Fig. 21. The curves drawn through these data serve only to guide the eye. Definite assignments of T were made up to ∿5 MeV, based on the comparison of energy and angular distribution data. Above this, however, statistics and complex distribution shapes precluded definite J^{π}; T assignments. The distributions obtained are, never-the-less, shown in Fig. 22.

I. $^{38}Ar\ (p,t)\ ^{36}Ar$, $^{38}Ar\ (p,^{3}He)\ ^{36}Cl$ and $^{38}Ar\ (d,\alpha)\ ^{36}Cl$ Reactions

Although the original purpose of studying the reactions $^{38}Ar(p,t)^{36}Ar$ and $^{38}Ar(p,^{3}He)^{36}Cl$ was to obtain values for the excitation of the previously unreported T=2 analogue states in mass-36, complete angular distributions were measured; further the reaction $^{38}Ar(d,\alpha)^{36}Cl$ was also studied in order to provide nuclear structure information about the levels observed. The target used for these experiments was argon gas, with an isotopic composition of 23.3% ^{36}Ar, 50.8% ^{38}Ar, and 25.9% ^{40}Ar, and a chemical composition of 99.9% argon. Because of the mixture of gases present in the target, the spectra were sufficiently complex that no advantage in calibration could be gained by adding methane. Instead, as was done previously in the ^{21}Ne case, accurately determined states in

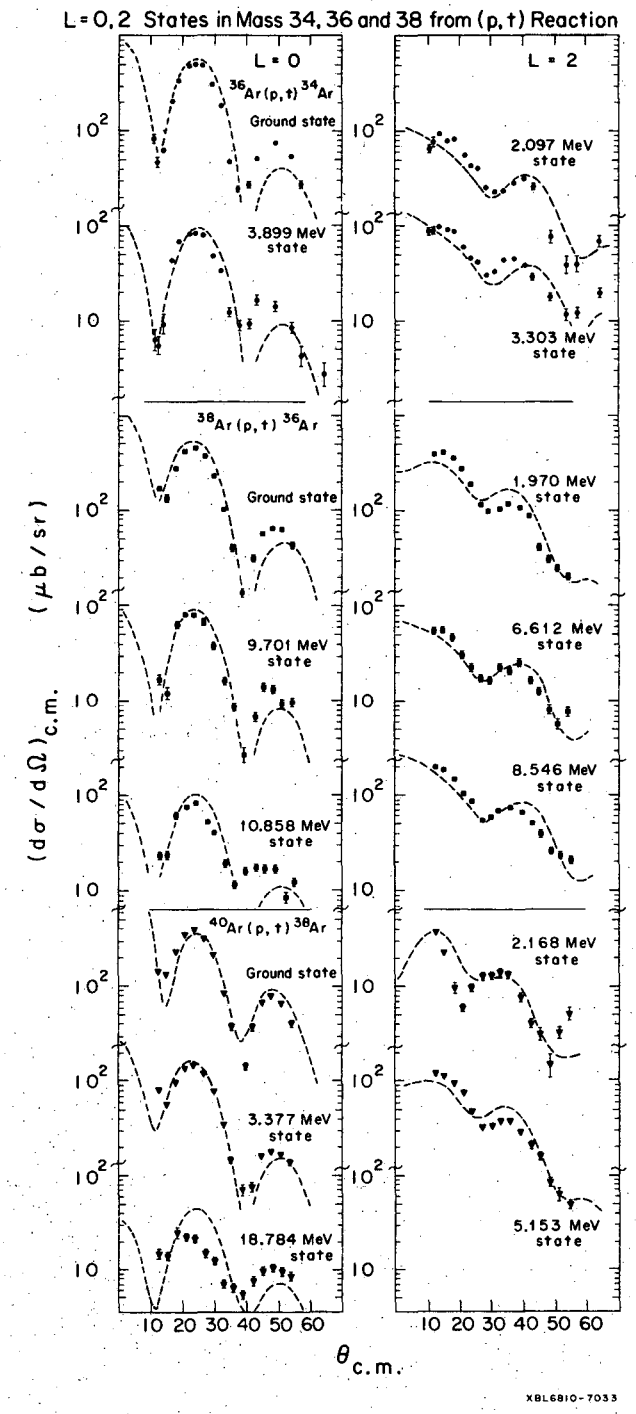
L = 0, 2 States in Mass 34, 36 and 38 from (p, t) Reaction
L = 0
L = 2
^{36}Ar(p, t)^{34}Ar
Ground state
3.899 MeV state
2.097 MeV state
3.303 MeV state
^{38}Ar(p, t)^{36}Ar
Ground state
9.701 MeV state
10.858 MeV state
1.970 MeV state
6.612 MeV state
8.546 MeV state
^{40}Ar(p, t)^{38}Ar
Ground state
3.377 MeV state
18.784 MeV state
2.168 MeV state
5.153 MeV state
$(d\sigma / d\Omega)_{c.m.}$ (μb / sr)
$\theta_{c.m.}$
10 20 30 40 50 60
XBL6810-7033

Figure 20

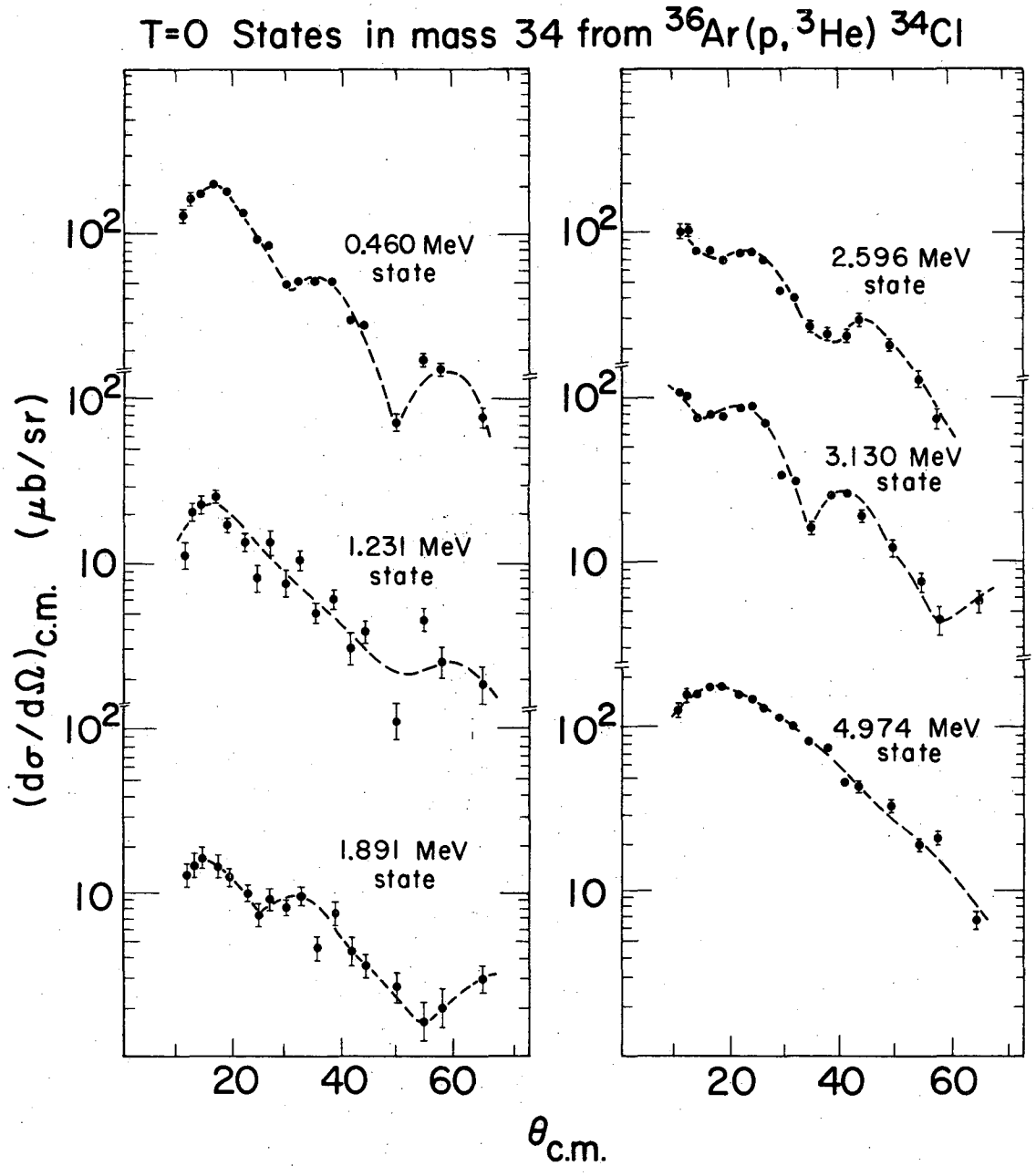
T=0 States in mass 34 from $^{36}Ar(p,^{3}He)\,^{34}Cl$
0.460 MeV state
1.231 MeV state
1.891 MeV state
2.596 MeV state
3.130 MeV state
4.974 MeV state
$(d\sigma/d\Omega)_{c.m.}$ (μb/sr)
$\theta_{c.m.}$
XBL6812-7532

Figure 21

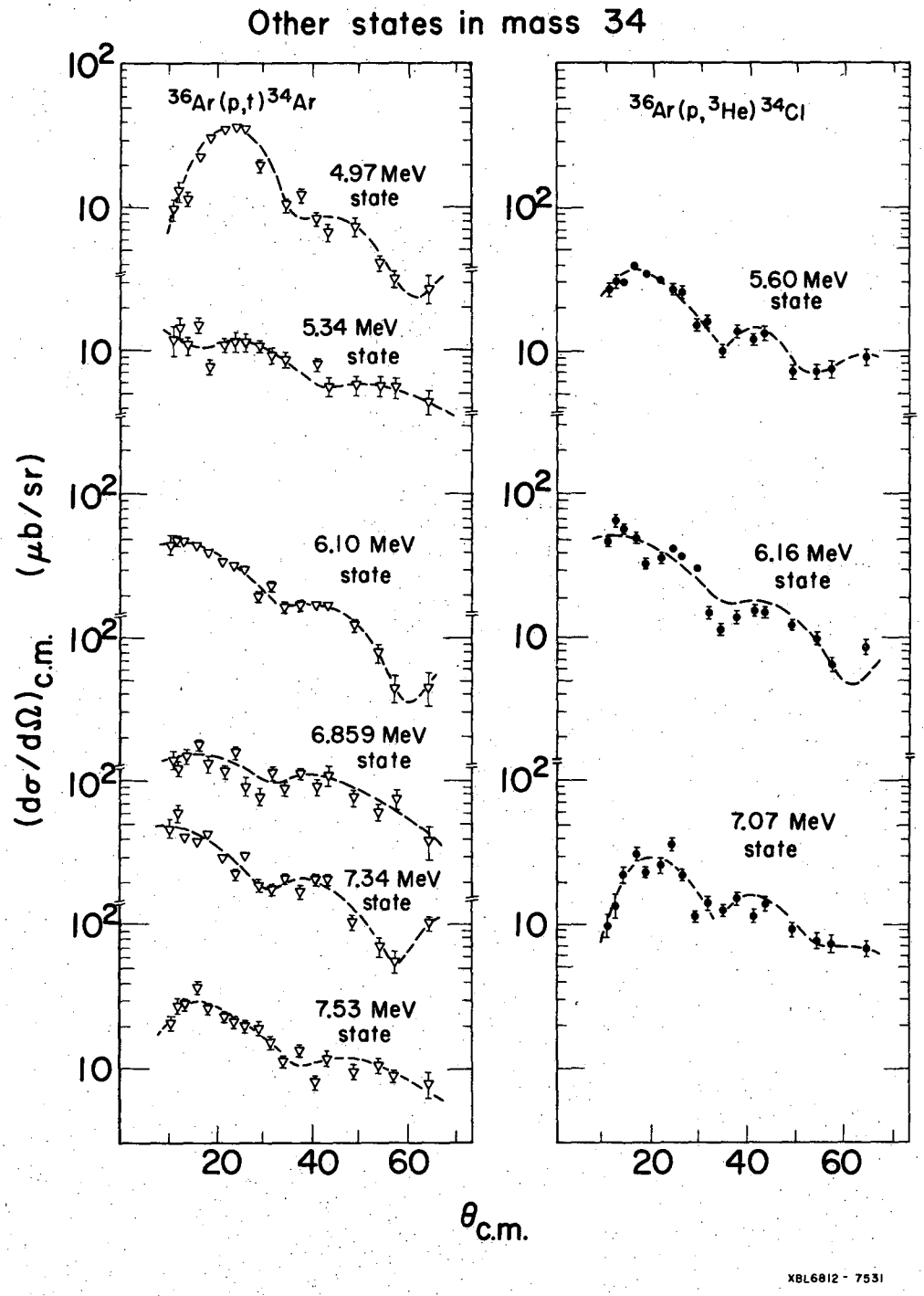
Other states in mass 34
^{36}Ar(p,t)^{34}Ar
4.97 MeV state
5.34 MeV state
6.10 MeV state
6.859 MeV state
7.34 MeV state
7.53 MeV state
^{36}Ar(p,^{3}He)^{34}Cl
5.60 MeV state
6.16 MeV state
7.07 MeV state
$(d\sigma/d\Omega)_{c.m.}$ (μb/sr)
$\theta_{c.m.}$
XBL6812 - 7531

Figure 22

mass-34 and mass-38 were used to determine the excitation energies of the unknown states in mass-36.

Spectra were obtained for the (p,t) and (p,^{3}He) reactions over an angular range from θ_{LAB} = 11.7 degrees to θ_{LAB} = 50.7 degrees; the sample spectra shown in Fig. 23 were obtained at θ_{LAB} = 22.3 degrees for 7562 microcoulombs. The (d,α) data were measured for angles ranging from θ_{LAB} = 14.1 degrees to θ_{LAB} = 50.7 degrees, with a representative spectrum, taken at θ_{LAB} = 22.3 degrees for 4000 microcoulombs, shown in the center portion of Fig. 17.

Rough Coulomb energy calculations based on the mass excess of ^{36}S indicated the T=2 analogue state in ^{36}Ar should be at an excitation of approximately 10.9 MeV, and its analogue in ^{36}Cl should be at an excitation of approximately 4.3 MeV. The peaks marked as T=2 states in Fig. 23 are consistent with these values. Using the known excited states in ^{34}Ar, ^{36}Ar, and ^{38}Ar as calibrations, accurate excitation energies were determined for the T=2 analogue state in ^{36}Ar, as well as two strongly populated (T=1) states at 8.456±0.025 MeV and 9.701±0.030 MeV. The levels observed from the (p,t) reaction are summarized in Table 7. The ^{36}Cl T=2 excitation is based on known excited state in ^{34}Cl, ^{36}Cl, and ^{38}Cl, including the previously calibrated T=3 state in ^{38}Cl (see Sec. IV-J). The T=2 analogue state excitations are summarized in Table 3, and a complete list of states observed in the (p,^{3}He) and (d,α) reactions is given in Table 8.

The angular distributions obtained for the T=1 and T=2 states in mass-36 are shown in Fig. 24. The dashed curves through the (p,t)

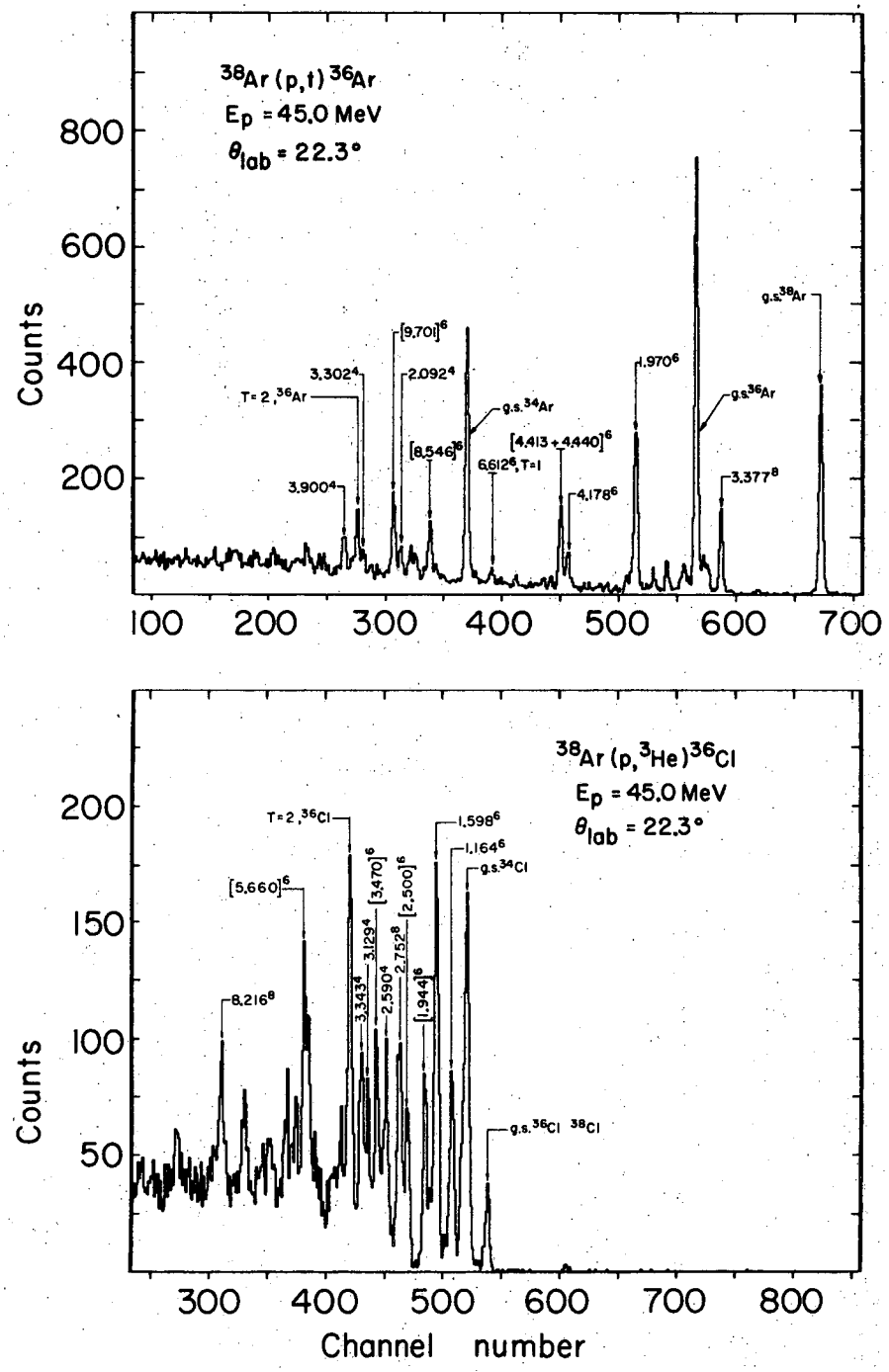
^{38}Ar (p,t) ^{36}Ar
E_p = 45.0 MeV
θ_{lab} = 22.3°
Counts
800
600
400
200
100
200
300
400
500
600
700
T=2, ^{36}Ar
3.302^4
3.900^4
[9.701]^6
2.092^4
g.s. ^{34}Ar
[8.546]^6
6.612^6, T=1
[4.413 + 4.440]^6
4.178^6
1.970^6
g.s. ^{38}Ar
g.s. ^{36}Ar
3.377^8
^{38}Ar (p, ^{3}He) ^{36}Cl
E_p = 45.0 MeV
θ_{lab} = 22.3°
Counts
200
150
100
50
300
400
500
600
700
800
Channel number
T=2, ^{36}Cl
[5.660]^6
8.216^8
3.343^4
3.129^4
[3.470]^6
2.590^4
2.752^8
[2.500]^6
[1.944]^6
1.598^6
1.164^6
g.s. ^{34}Cl
g.s. ^{36}Cl ^{38}Cl
XBL6912-7504

Figure 23

Table 7. Summary of $^{38}Ar(p,t)^{36}Ar$ Reaction

This Work			Previous Work[a]		Average	
Excitation (MeV ± keV)	$J^{\pi};T$	Intensity (μb/sr)	Excitation (MeV ± keV)	$J^{\pi};T$	Excitation (MeV ± keV)	$J^{\pi};T$
g.s.*	$0^+;0$	430	g.s.	$0^+;0$	-	$0^+;0$
1.970*	$2^+;0$	410	1.9701 ± 0.7	$2^+;0$	1.9701 ± 0.7	$2^+;0$
4.178*	$(3^-);0$	60	4.1779 ± 0.7	$3^-;0$	4.1779 ± 0.7	$3^-;0$
4.420 ± 20	;0	160	4.413 ± 5	$4^+;0$	4.413 ± 5	$4^+;0$
			4.4401 ± 1.2	$2^+;0$	4.4401 ± 1.2	$2^+;0$
6.612*	$2^+;1$	60	6.6119 ± 0.9	$(2^+);1$	6.6119 ± 0.9	$2^+;1$
8.546 ± 25	$2^+;1$	190	density of levels too high to make comparison		8.546 ± 25	$2^+;1$
9.701 ± 30	$0^+;1$	85			9.701 ± 30	$0^+;1$
10.858 ± 35	$0^+;2$	80			10.858 ± 35	$0^+;2$

[a] Only those previously known ^{36}Ar states corresponding to observed states are listed. Ref: P. M. Endt and C. Van der Leun, Nucl. Phys. A105, 1 (1967).

(*) These states were used as calibrations in addition to the impurity states discussed in the text, and were not determined in this work.

Table 8. Summary of $^{38}Ar(p,^{3}He)^{36}Cl$ and $^{38}Ar(d.\alpha)^{36}Cl$ Reactions

This Work				Previous Work[a]		Average	
Excitation (MeV ± keV)	$J^{\pi};T$	Intensity $(p,^{3}He)$ (μb/sr)	(d,α) (μb/sr)	Excitation (MeV ± keV)	$J^{\pi};T$	Excitation (MeV ± keV)	$J^{\pi};T$
g.s.*	$(2^{+});1$	~30[b]	<20[d]	g.s.	$0^{+};1$	g.s.	$0^{+};1$
0.788*		(c)	<180[d]	0.788 ± 2	$(3)^{+};1$	0.788 ± 2	$(3)^{+};1$
1.164*		<130[d]	(c)	1.164 ± 2	$(1)^{+};1$	1.164 ± 2	$(1)^{+};1$
1.598*		200	120	1.598 ± 3	$(1,2)^{+};1$	1.598 ± 3	$(1,2)^{+};1$
1.944 ± 25	$(2^{+});1$	~130[b]	80	1.949 ± 3	$2^{+};1$	1.949 ± 3	$2^{+};1$
2.500 ± 25		90	100	2.497 ± 5	$(1,2)^{+};1$	2.497 ± 5	$(1,2)^{+};1$
[3.12]†		35[b]	(c)	-	-	[3.12]	$0^{+};1$
3.470 ± 25		60	(c)	3.474 ± 5	$(\leq 3)^{-};1$	3.474 ± 5	$(\leq 3)^{-};1$
3.980 ± 35		90	(c)	3.970 ± 5	$(\leq 3)^{-};1$	3.970 ± 5	$(\leq 3)^{-};1$
4.295 ± 30	$0^{+};2$	130	(c)	not reported		4.295 ± 30	$0^{+};2$
5.657 ± 30		160[e]	500[e]	-		5.657 ± 30	

(*) These states were used as calibrations, and were not determined from this experiment.

(a) Only those previously known ^{36}Cl states corresponding to observed states listed. Ref: P. M. Endt and C. Van der Leun, Nucl. Phys. A105, 1 (1967).

Table 8. Continued

(b) These cross sections were obtained by subtracting cross-sections due to known impurities.

(c) These states were insufficiently strong to permit accurate cross-section determinations.

(d) These cross sections may contain other interfering states, but such contributions are expected to be small.

(e) These states may also contain contaminant contributions.

† Estimated energy - see text.

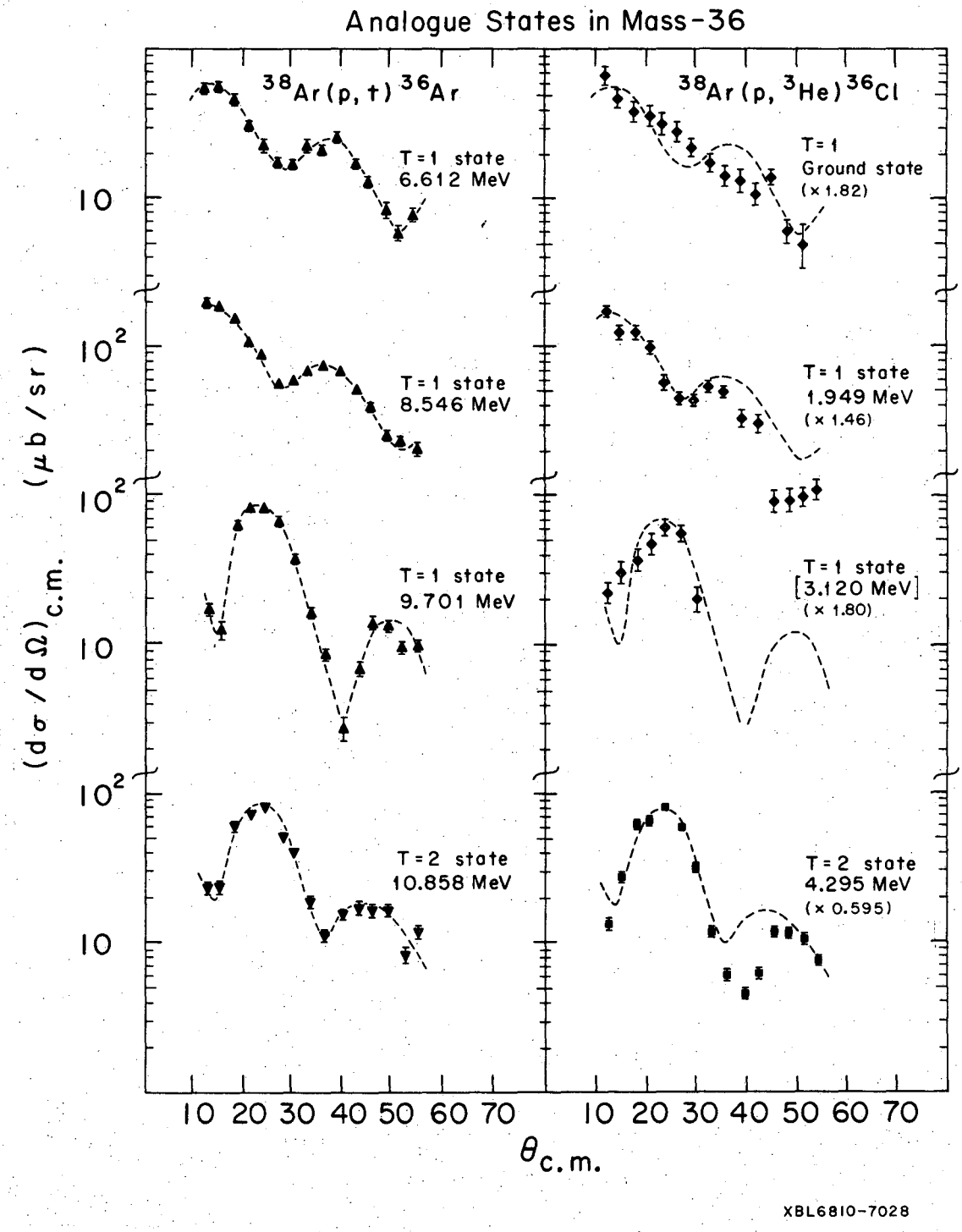
Analogue States in Mass-36
^{38}Ar(p, t) ^{36}Ar
^{38}Ar(p, ^{3}He) ^{36}Cl
T=1 state 6.612 MeV
T=1 Ground state (×1.82)
T=1 state 8.546 MeV
T=1 state 1.949 MeV (×1.46)
T=1 state 9.701 MeV
T=1 state [3.120 MeV] (×1.80)
T=2 state 10.858 MeV
T=2 state 4.295 MeV (×0.595)
$(d\sigma/d\Omega)_{c.m.}$ (μb/sr)
$\theta_{c.m.}$
10 20 30 40 50 60 70
XBL6810-7028

Figure 24

distributions serve to guide the eye; the same curves have been drawn through the $(p,{}^3He)$ distributions. The T=1 ^3He data have been multiplied by normalization factors which will be discussed in Sec.V-B-5. The T=2 data have been multiplied by $^{2k}t/3_{He}$ as suggested by Eq. (IV-1). In view of the fact that the distributions for all T=1 states in ^{36}Cl shown in Fig. 24 were obtained by subtracting impurity components in the angular distributions, good agreement in shape is observed. By comparison with previously identified states, the ^{36}Ar 6.612 MeV state is observed to be produced by an L=2 transition, determining its J^π as 2^+. From energy consideration and its known J^π, this state is identified as the lowest T=1 analogue to the ^{36}Cl ground state. Similarly, the angular distribution corresponding to the state at 8.546 MeV is observed to be characteristic of L=2, determining the J^π of this level as 2^+, and identifying it, on the basis of J^π and energy to be analogous to the ^{36}Cl 1.949-MeV state. The angular distribution of the ^{36}Ar 9.701 MeV state, however, is characteristic of L=0 transfer, and allows the assignment of $J^\pi = 0^+$ for this level. In ^{36}Cl, there are no known $J^\pi = 0^+$ levels,[41] but a rough Coulomb energy calculation based on the ^{36}Ar 9.701 MeV level predicts such a level at $\sim$3.12 MeV. A state of this energy would be degenerate with the ^{34}Cl 2.590 MeV state, and the angular distribution plotted for this [3.12 MeV] state is obtained by subtracting the component due to the ^{34}Cl 2.590 MeV state. The distribution shape is consistent with an L=0 transfer, suggesting an unresolved 0^+ state in ^{36}Cl at about 3.12 MeV. The T=2 analogue distributions are characteristically L=0, assigning the J^π as 0^+ for these states. This is in

agreement with the expected J^{π}, since the T_z=2 analogue state (^{36}S ground state) is known to have $J^{\pi} = 0^{+}$. The cross section ratio obtained is consistent with that expected from Eq. (IV-1). The angular distributions measured for low lying (T=0) states in ^{36}Ar obtained from the reaction ^{38}Ar (p,t) ^{36}Ar are shown in Fig. 25. The L=0 and 2 transitions to states in ^{36}Ar are summarized in Fig. 20.

J. ^{40}Ar (p,t) ^{38}Ar, ^{40}Ar (p,^{3}He) ^{38}Cl and ^{40}Ar(d,α) ^{38}Cl Reactions

Since the isospin of the ^{40}Ar ground state is T=2, the reactions ^{40}Ar(p,t)^{38}Ar and ^{40}Ar(p,^{3}He)^{38}Cl may be used to produce T=3 states in the T_z=+1 and T_z=+2 members of the mass 38 multiplet. To determine the excitation energies and cross sections of these T=3 analogue states, and additionally to provide a measure of excitations and intensities of all states produced by the (p,t) and (p,^{3}He) reactions for calibration purposes in ^{38}Ar discussed in Sec. IV-I, a natural argon target was used. Natural argon, which is 99.6% ^{40}Ar, was used both as a pure gas to provide angular distribution data, and in an argon-methane (80%-20% resp.) mixture to provide accurate excitations of states observed. The (d,α) reaction was also studied on this target and is found to confirm the high isospin assignment in addition to providing additional spectroscopic information, as will be discussed in Sec. V-B-6.

Triton and ^{3}He spectra were taken over an angular range of 39° from θ_{LAB} = 11.7 degrees to θ_{LAB} = 50.7 degrees for the pure target; accurate excitations were derived from several spectra obtained at θ_{LAB} = 26.8 degrees using the mixed target, where all states of interest

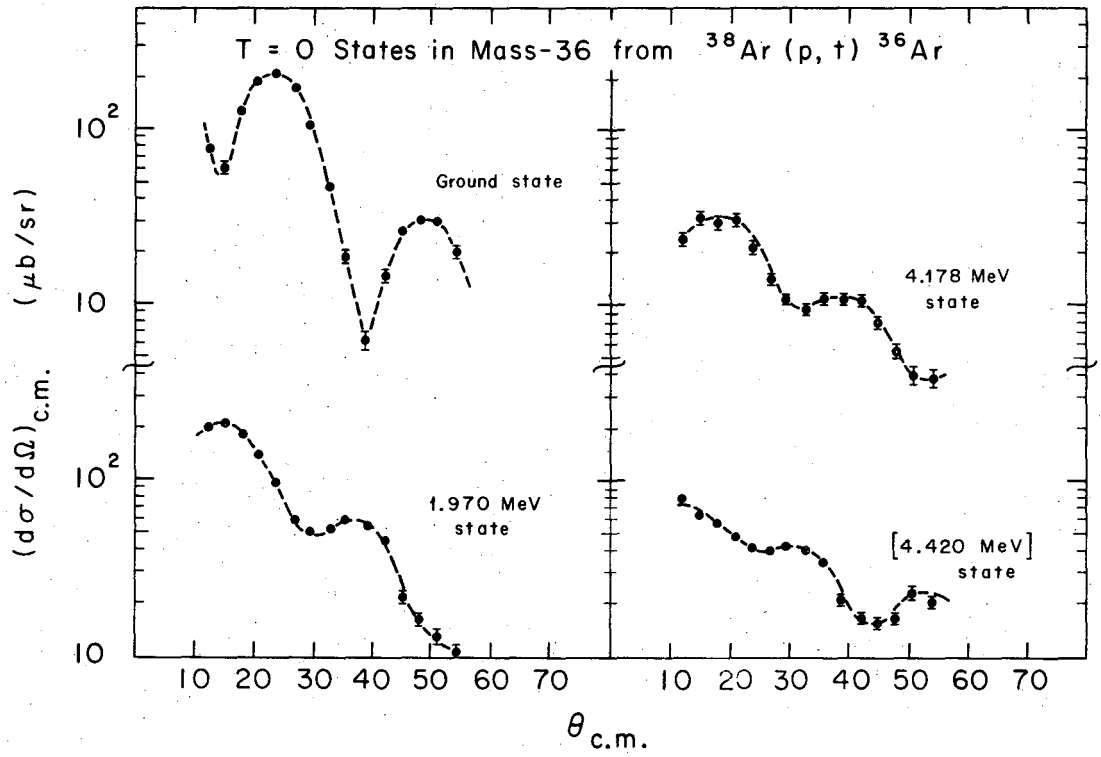
T = 0 States in Mass-36 from ^{38}Ar (p, t) ^{36}Ar
Ground state
1.970 MeV state
4.178 MeV state
[4.420 MeV] state
$(d\sigma/d\Omega)_{c.m.}$ (μb/sr)
$\theta_{c.m.}$
XBL6810-7026

Figure 25

were separated from the mass-10 calibration peaks. These energies are summarized in Tables 9 and 10. A sample pair of spectra, collected for 12,553 microcoulombs are shown in Fig. 26. The α-particle data were collected over angles ranging from θ_{LAB} = 14.1 degrees to θ_{LAB} = 50.7 degrees; a spectrum, taken at θ_{LAB} = 22.3 degrees for 5300 microcoulombs is shown in the lower portion of Fig. 17.

The angular distributions obtained for high-isospin analogue states in ^{38}Ar and ^{38}Cl are shown in Fig. 27. As in previous cases, the dashed line represents the same triton curve shape, drawn through both the triton and ^{3}He data. The ^{3}He angular distribution for the T=3 analogue state has been multiplied by $^{2k}t/^{5k}{}^{3}$He as suggested by Eq. (IV-1). The normalization factors of the other ^{3}He distributions depend on structure and will be discussed in Sec. V-B-6. The angular distributions of additional ^{38}Cl states, whose analogues were not observed with sufficient cross section to permit comparison, are shown in Fig. 28. T=1 states in ^{38}Ar have no analogues in ^{38}Cl (a T_z=2 nucleus) and their angular distributions are shown in Fig. 29.

Since no T=3 analogue states have been reported in T_z=1 light nuclei, this experiment represents a feasibility test of using the (p,t) and (p,^{3}He) reaction to populate such states. A rough Coulomb energy calculation, based on the mass excess of the ^{38}S ground state, assuming a uniformly charged sphere, predicted these states to lie at about 19.0 MeV in ^{38}Ar and at about 8.3 MeV in ^{38}Cl. The excitations determined for the states marked as T=3 in Fig. 26 are consistent with these predictions. The excitation of the T=3 analogue in ^{38}Ar was determined

Table 9. Summary of the $^{40}Ar(p,t)\ ^{38}Ar$ Reaction

This Work			Previous Work[a]		Average	
Excitation (MeV ± keV)	$J^\pi;T$	Intensity (μb/sr)	Excitation (MeV ± keV)	$J^\pi;T$	Excitation (MeV ± keV)	$J^\pi;T$
g.s.*	$0^+;1$	380	g.s.	$0^+;1$	g.s.	$0^+;1$
2.168*	$2^+;1$	14	2.16768 ± .14	$2^+;1$	2.16768 ± .14	$2^+;1$
3.377*	$0^+;1$	140	3.3768 ± .3	$0^+;1$	3.3768 ± .3	$0^+;1$
3.892 ± 30[†]	;1	220	3.8100 ± .2	$3^-;1$	3.8100 ± .2	$3^-;1$
			3.936 ± .5	$(2)^+;1$	3.936 ± .5	$(2)^+;1$
4.588 ± 25	;1	70	4.585 ± .5	$5^-;1$	4.585 ± .5	$5^-;1$
5.150 ± 25	;1	120	5.153 ± 10	$(1,2)^+;1$	5.153 ± 10	$(1,2)^+;1$
5.578 ± 35	;1	75	5.551 ± 10	$(1,2)^+;1$	5.551 ± 10	$(1,2)^+;1$
			5.591 ± 2.0	;1	5.591 ± 2.0	;1
6.253 ± 30	;1	45	density of states is		6.253 ± 30	;1
6.466 ± 45	;1	35	too high for		6.466 ± 45	;1
7.110 ± 45	;1	<20	comparison		7.110 ± 45	;1
7.653 ± 40	;1	~20			7.653 ± 40	;1
8.883 ± 40	;1	45			8.883 ± 40	;1

Table 9. Continued

This Work			Previous Work[a]		Average	
Excitation (MeV ± keV)	$J^{\pi};T$	Intensity (μb/sr)	Excitation (MeV ± keV)	$J^{\pi};T$	Excitation (MeV ± keV)	$J^{\pi};T$
11.300 ± 45		20	11.303	$5^{-};$	11.300 ± 45	
13.090 ± 40		35			13.090 ± 40	
13.332 ± 35	;(2)	60			13.332 ± 35	;(2)
13.700 ± 40	;(2)	40			13.700 ± 40	;(2)
18.784 ± 30	$0^{+};3$	25			18.784 ± 30	$0^{+};3$

[a] Only those previously known ^{38}Ar states corresponding to observed states are listed. Ref: P. M. Endt and C. Van der Leun, Nucl. Phys. A105, 1 (1967).

(*) These states were used as calibrations, and were not determined in this experiment.

(†) This value represents the average excitation of the unresolved states at 3.810 MeV. and 3.936 MeV. respectively.

Table 10. Summary of the $^{40}Ar(p,^{3}He)^{38}Cl$ and $^{40}Ar(d,\alpha)^{38}Cl$ Reactions;

This Work				Previous Work[a]		Average	
Excitation (MeV ± keV)	$J^{\pi};T$	Intensity $(p,^{3}He)$ (μb/sr)	Intensity (d,α) (μb/sr)	Excitation (MeV ± keV)	$J^{\pi};T$	Excitation (MeV ± keV)	$J^{\pi};T$
g.s.	;2	~25	~25	g.s.	$2^{-};2$	--	$2^{-};2$
0.691 ± 30	;2	12	35	0.671 ± 3	$5^{-};2$	0.671 ± 3	$5^{-};2$
				0.761 ± 3	$(3)^{-};2$	0.761 ± 3	$(3)^{-};2$
1.884 ± 45	;2	100	160	1.789 ± 7	$1^{+};2$	1.789 ± 7	$1^{+};2$
				1.986 ± 6	$^{-};2$	1.986 ± 6	$^{-};2$
2.483 ± 40		<15	60	2.461 ± 12	$(+);2$	2.463 ± 11.3	$(+);2$
2.756 ± 25		150	75	2.752 ± 12	$^{-};2$	2.753 ± 11	$^{-};2$
3.190 ± 35		25	--			3.190 ± 35	
3.490 ± 35		25	50			3.490 ± 35	
3.770 ± 35		35	65			3.770 ± 35	
4.345 ± 35		<20	--			4.345 ± 35	
5.38 ± 50		<20	90			5.38 ± 50	
6.63 ± 50		~20	--			6.63 ± 50	
8.216 ± 25	$0^{+};3$	70	--			8.216 ± 25	$0^{+};3$

[a] Only those previously known ^{38}Cl states corresponding to observed states are listed. Ref: P. M. Endt and C. Van der Leun, Nucl. Phys. A105, 1 (1967).

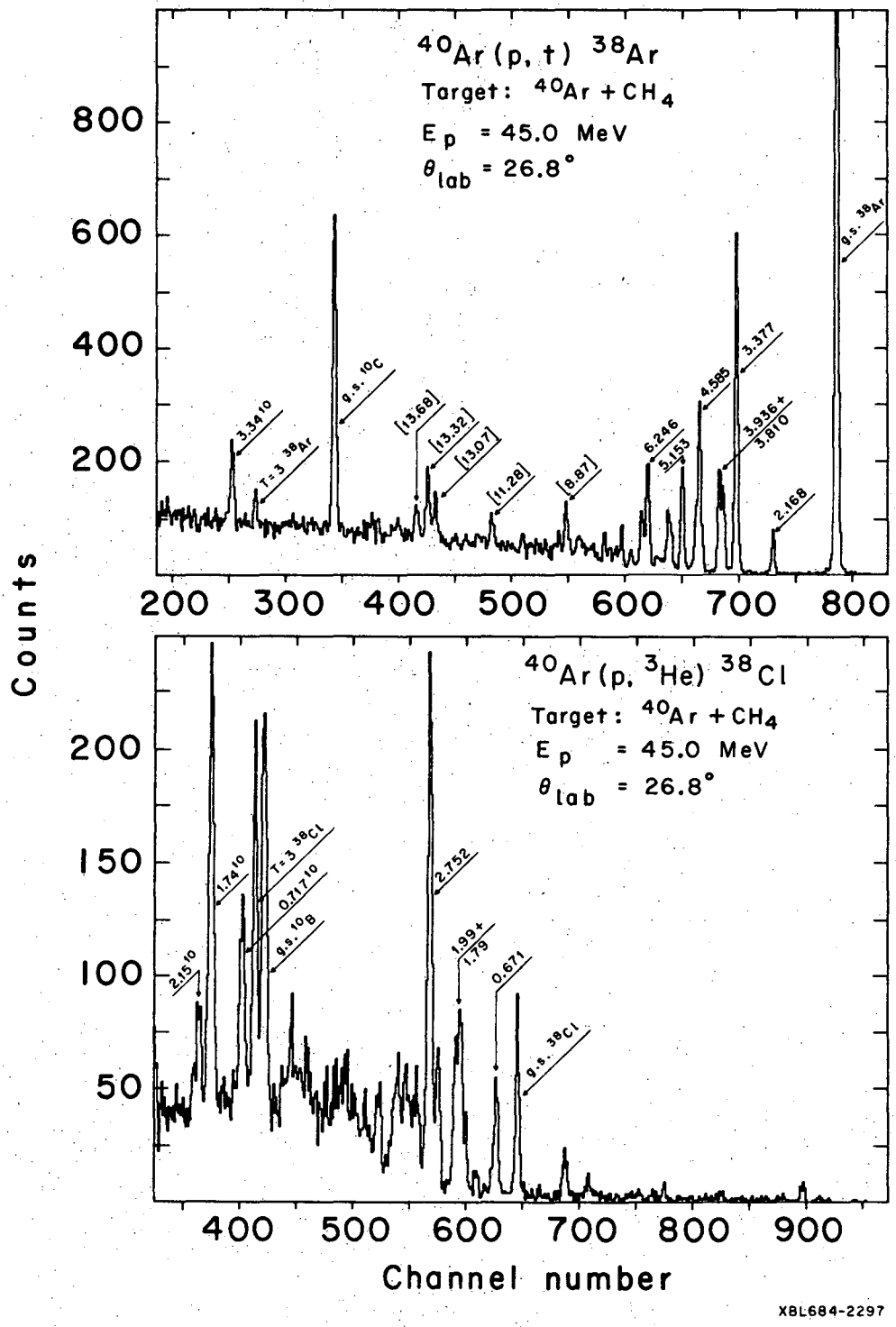
^{40}Ar (p, t) ^{38}Ar
Target: ^{40}Ar + CH_4
E_p = 45.0 MeV
θ_{lab} = 26.8°
3.34 ^{10}
T=3 ^{38}Ar
g.s. ^{10}C
[13.68]
[13.32]
[13.07]
[11.28]
[8.87]
6.246
5.153
4.585
3.377
3.936+
3.810
2.168
g.s. ^{38}Ar
^{40}Ar (p, ^{3}He) ^{38}Cl
Target: ^{40}Ar + CH_4
E_p = 45.0 MeV
θ_{lab} = 26.8°
2.15 ^{10}
1.74 ^{10}
T=3 ^{38}Cl
0.717 ^{10}
g.s. ^{10}B
2.752
1.99+
1.79
0.671
g.s. ^{38}Cl
Counts
Channel number
XBL684-2297

Figure 26

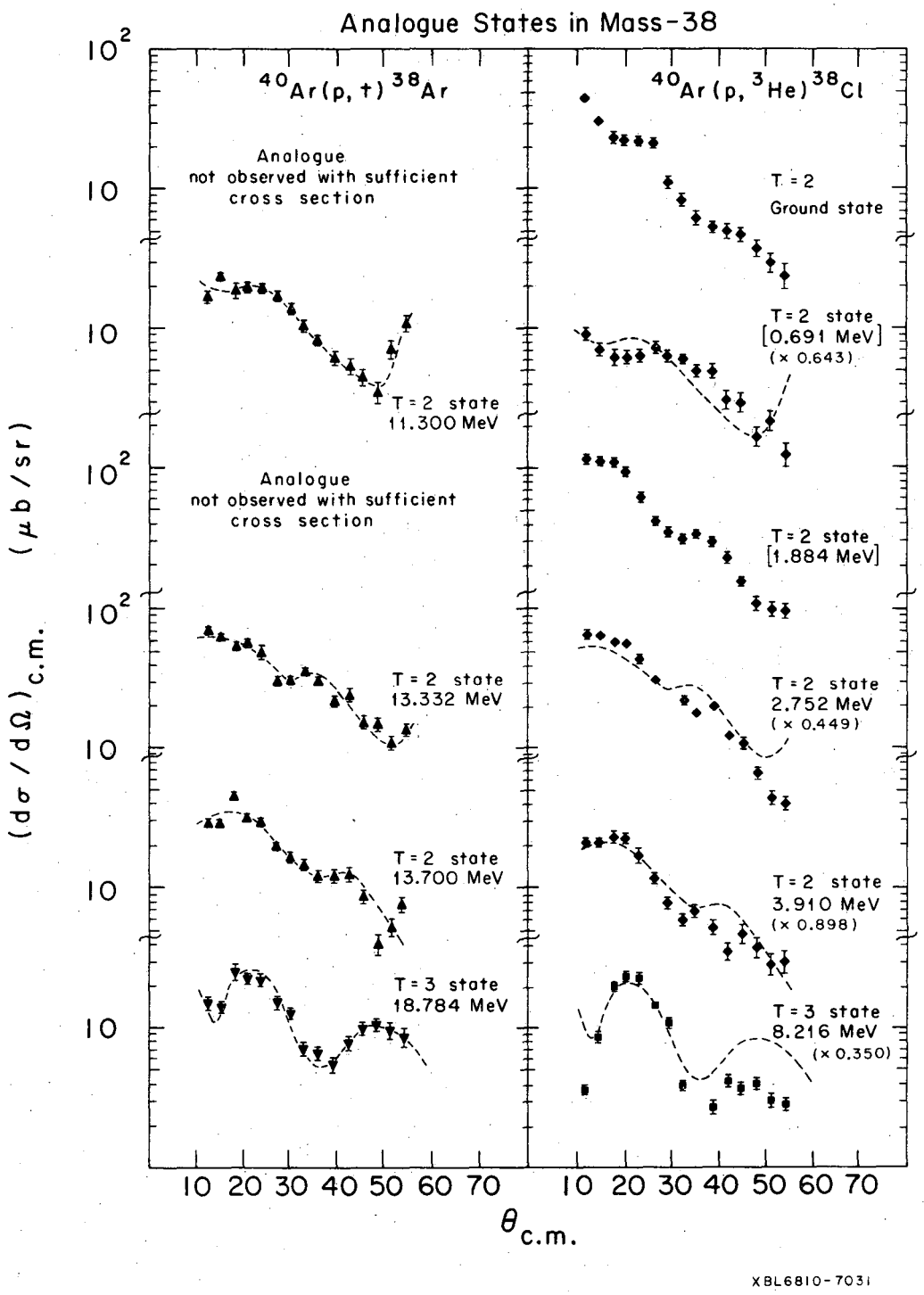
Analogue States in Mass-38
$^{40}Ar(p, t)^{38}Ar$
$^{40}Ar(p, {}^{3}He)^{38}Cl$
Analogue not observed with sufficient cross section
T = 2 state 11.300 MeV
Analogue not observed with sufficient cross section
T = 2 state 13.332 MeV
T = 2 state 13.700 MeV
T = 3 state 18.784 MeV
T = 2 Ground state
T = 2 state [0.691 MeV] (× 0.643)
T = 2 state [1.884 MeV]
T = 2 state 2.752 MeV (× 0.449)
T = 2 state 3.910 MeV (× 0.898)
T = 3 state 8.216 MeV (× 0.350)
$(d\sigma / d\Omega)_{c.m.}$ ($\mu b / sr$)
$\theta_{c.m.}$
10 20 30 40 50 60 70
XBL6810-7031

Figure 27

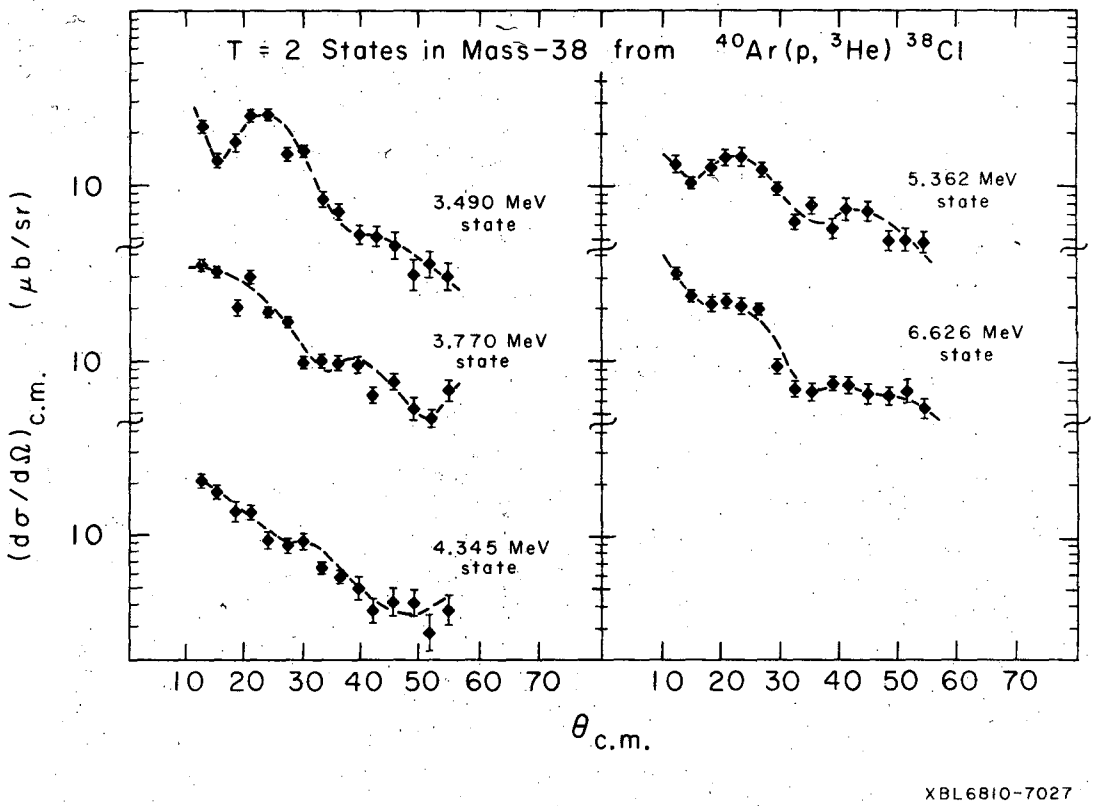
T = 2 States in Mass-38 from ^{40}Ar(p, ^{3}He) ^{38}Cl
3.490 MeV state
3.770 MeV state
4.345 MeV state
5.362 MeV state
6.626 MeV state
$(d\sigma/d\Omega)_{c.m.}$ (μb/sr)
$\theta_{c.m.}$
10 20 30 40 50 60 70
XBL6810-7027

Figure 28

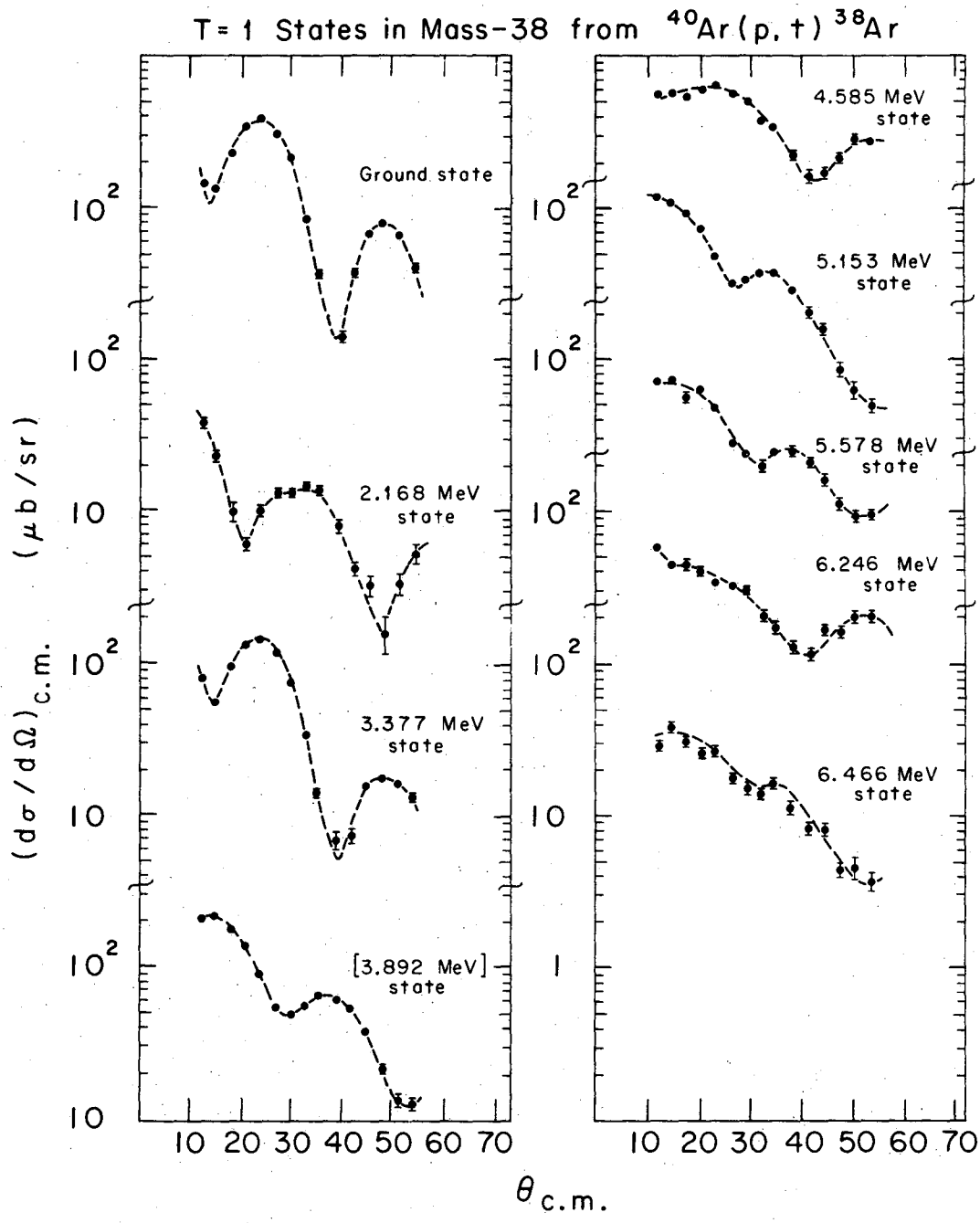
T = 1 States in Mass-38 from ^{40}Ar(p, t) ^{38}Ar
Ground state
2.168 MeV state
3.377 MeV state
[3.892 MeV] state
4.585 MeV state
5.153 MeV state
5.578 MeV state
6.246 MeV state
6.466 MeV state
$(d\sigma/d\Omega)_{c.m.}$ (μb/sr)
$\theta_{c.m.}$
XBL6810-7025

Figure 29

primarily from the ^{10}C ground and 3.34 MeV states; the excitations of intermediate T=2 states in the region of 11-14 MeV were determined using the above states and known[41] low-lying states in ^{38}Ar shown unbracketed in Fig. 26. The excitations of states in ^{38}Cl were determined using the known resolved[41] states at low excitation in ^{38}Cl and the ^{10}B states. The final excitations obtained for the T=3 states are summarized in Table 3. The excitations and cross section data for T=2 states are given in Tables 9 and 10.

From a comparison of the angular distributions for the T=3 states with known L=0 distributions previously obtained (see Fig. 20), it is evident that these states are found by L=0 transitions. Thus a value of $J^{\pi} = 0^{+}$ is assigned, confirming the states as analogues to ^{38}S. The observed relative magnitudes of the (p,t) and (p,^{3}He) distributions are found to agree very well with that expected from Eq. (IV-1), confirming the T=3 assignment to these states.

K. ^{42}Ca (p,t) ^{40}Ca and ^{42}Ca (p,^{3}He) ^{40}K; T=2 States

The target used to determine the excitation energies of T=2 analogue states in mass-40 was a self-supporting evaporated calcium foil, with a thickness of ∿400 μg/cm^2, and isotopic enrichment of ^{42}Ca of 94.42%; the remaining isotopic compositions were 4.96%, ^{40}Ca, 0.06% ^{43}Ca, 0.56% ^{44}Ca, < 0.05% ^{46}Ca, and < 0.05% ^{48}Ca. Impurity oxygen and carbon were also found to be present in substantial quantities, and the well known states in ^{10}C (^{10}B) and ^{14}O(^{14}N) produced by the (p,t) and (p,^{3}He) reactions proved to be useful calibrations for the excitation energies of the T=2 analogue states.

An approximate excitation for the T=2 states in mass-40 was obtained from a Coulomb calculation based on the mass excess of the ^{40}Ar ground state. The states identified as T=2 states in Fig. 30 are consistent with these values.

A series of four angles ranging from θ_{LAB} = 18.0 degrees to θ_{LAB} = 31.5 degrees were measured. A pair of spectra, obtained at θ_{LAB} = 26.8 degrees for 3554 microcoulombs is shown in Fig. 30. The angular distributions of the states identified as T=2 analogues show a characteristic L=0 shape, which assigns a J^{π} of 0^{+} to these states, and identifies the states as analogues to the ^{40}Ar ground state. The cross section ratio obtained for the triton and ^{3}He distributions is found to be 0.60±0.05 which is in excellent agreement with that expected from Eq. (IV-1) ($^{2k}t/3k3_{He}$ = 0.62).

The excitation energy obtained for the T=2 analogue state in ^{40}Ca is based on the low states[41] in ^{40}Ca shown in Fig. 30, in addition to the ^{10}C and ^{14}C ground states. No other strong states were observed in the triton spectra. The excitation of the T=2 analogue in ^{40}K was determined using known low-excited[41] states in ^{40}K, and the impurity ^{14}N and ^{10}B states shown in Fig. 30. The excitations of the T=2 states obtained are summarized in Table 3.

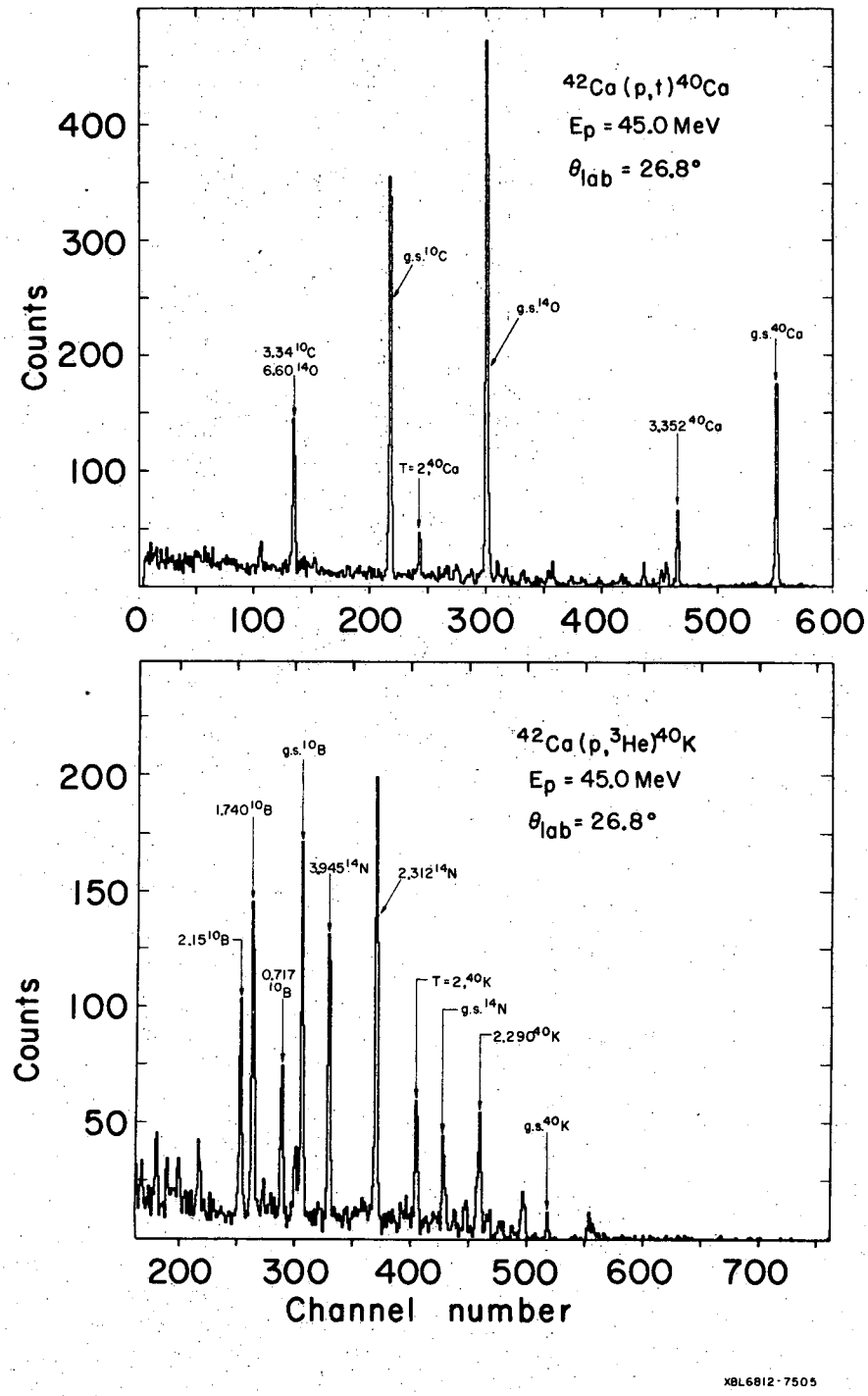
^{42}Ca (p,t)^{40}Ca
Ep = 45.0 MeV
θlab = 26.8°
g.s. ^{10}C
g.s. ^{14}O
g.s. ^{40}Ca
3.34 ^{10}C
6.60 ^{14}O
T=2, ^{40}Ca
3.352 ^{40}Ca
Counts
^{42}Ca (p, ^{3}He)^{40}K
Ep = 45.0 MeV
θlab = 26.8°
g.s. ^{10}B
1.740 ^{10}B
3.945 ^{14}N
2.312 ^{14}N
2.15 ^{10}B
0.717 ^{10}B
T=2, ^{40}K
g.s. ^{14}N
2.290 ^{40}K
g.s. ^{40}K
Counts
Channel number
XBL6812-7505

Figure 30

V. DISCUSSION OF RESULTS

A. Cross Section Ratios of States with $T_f = T_i + 1$

These states have been discussed individually in Sec. IV, and the overall results are summarized in Table 11. Wherever possible, the contributions to the cross section by interfering states have been removed prior to determining the experimental cross section ratios. Except in those cases where the interfering states are of unknown strength, good agreement is obtained between the experimental and calculated ratios. The cross section ratio expressions were derived assuming that $B^M_{NL}(k_i,k_f)$ and Ω_n occurring in the DWBA cross section expression were essentially identical for both the (p,t) and (p,^{3}He) reactions to analogue final states. The good agreement obtained with experiment appears to justify these assumptions.

B. Cross Section Ratios of States with $T_f = T_i$

The results obtained for states of $T_f=T_i$ character are discussed in detail below, and are summarized in Table 12. The cross section ratios of the (p,t) and (p,^{3}He) reactions have been used to distinguish states produced by a j^2 transfer from those produced by the transfer of more complicated configurations (i.e., j_1j_2 pickup). Since a specific configuration is required to determine a value for the theoretical ratio for j_1j_2 transfer the simplest shell model configurations consistent with the known character of the state were used for this purpose.

Table 11. Summary of experimental and calculated cross section ratios for states with $T_f=T_i+1$.

$J^\pi;T$	States	$R_x(t/^3He)$	$R_c(t/^3He)$[a]	Comments
$0^+;1$	^{18}Ne g.s. ^{18}F 1.081 MeV	1.45±0.15	1.88	^{18}F 1.081 MeV state is one of unresolved quartet, the remaining states are T=0.
$2^+;1$	^{18}Ne 1.887 MeV ^{18}F 3.060 MeV	1.62±0.20	1.86	^{18}F has unresolved T=0 state at 3.13 MeV.
$3/2^+;3/2$	^{19}Ne 7.620 MeV ^{19}F 7.660 MeV	1.05±0.10	0.93	These states are analogous to ^{19}O* 0.095 MeV first excited state.
$0^+;2$	^{20}Ne 16.732 MeV ^{20}F 6.513 MeV	0.70±0.09	0.62	The cross section data for this ratio was taken from Cerny et al.[b]
$5/2^+;3/2$	^{23}Mg 7.788 MeV ^{23}Na 7.900 MeV	0.85±0.09	0.92	These states are analogous to ^{23}Ne ground state.
$0^+;2$	^{24}Mg 15.426 MeV ^{24}Na 5.978 MeV	0.61±0.06	0.61	
$0^+;2$	^{28}Si 15.206 MeV ^{28}Al 5.983 MeV	0.54±0.10	0.60	^{28}Al T=2 cross section obtained by stripping ^{10}B 0.717 MeV state at θ_{LAB} = 15°-25°.
$0^+;2$	^{32}S 12.034 MeV ^{32}P 5.071 MeV	0.66±0.06	0.60	Thin targets and low beam intensity limited counting statistics.
$0^+;1$	^{34}Ar g.s ^{34}Cl g.s.	1.92±0.19	1.80	
$2^+;1$	^{34}Ar 2.092 MeV ^{34}Cl 2.162 MeV	1.54±0.20	1.78	

Table 11. (Continued)

$J^{\pi};T$	States	$R_x(t/^3He)$	$R_c(t/^3He)$[a]	Comments
$0^+;1$	^{34}Ar 3.303 MeV ^{34}Cl 3.343 MeV	0.50±0.05	1.77	$^{36}Ar(d,\alpha)^{34}Cl$ reveals previously unreported T=0 state at 3.33±0.035 MeV.
$0^+;1$	^{34}Ar 3.900 MeV ^{34}Cl 3.940 MeV	1.67±0.17	1.77	
$(3^-);1$	^{34}Ar 4.563 MeV ^{34}Cl 4.660 MeV	1.38±0.28	1.76	Small cross section-high density of states.
$0^+;2$	^{36}Ar 10.858 MeV ^{36}Cl 4.295 MeV	0.62±0.07	0.60	
$0^+;3$	^{38}Ar 18.784 MeV ^{38}Cl 8.216 MeV	0.36±0.04	0.35	
$0^+;2$	^{40}Ca 11.978 MeV ^{40}K 4.375 MeV	0.60±0.05	0.62	

(a) The calculated ratio is based on Eq. (IV-1).

(b) J. Cerny, R. H. Pehl, and G. T. Garvey, Phys. Letters 12, 234 (1964).

Table 12. Summary of experimental and calculated cross section ratios for states of $T_f=T_i$.

$J^\pi;T$	States	$R_x(t/^3He)$	Pickup	$R_c(t/^3He)$	Major Component of Final State Shell-Model Configuration
$2^+;1$	^{20}Ne 10.275 MeV ^{20}F g.s.	1.94±0.20	$(1d5/2)^2$	1.88	$[(1p1/2)^4_{00}(1d5/2)^4_{21}]_{21}$
$(3^-);1$	^{20}Ne 12.250 MeV ^{20}F 1.851 MeV	1.33±0.15	(1p1/2)(1d5/2)	1.30	$[(1p1/2)^3_{1/2\ 1/2}(1d5/2)^5_{5/2\ 1/2}]_{31}$
$4^+;1$	^{24}Mg 9.517 MeV ^{24}Na g.s.	2.52±0.30	$(1d5/2)^2$	1.86	$[(1p1/2)^4_{00}(1d5/2)^8_{41}]_{41}$
$(2^+);1$	^{24}Mg 10.072 MeV ^{24}Na 0.563 MeV	3.36±0.30	$(1d5/2)^2$	1.86	$[(1p1/2)^4_{00}(1d5/2)^8_{21}]_{21}$
;1	^{24}Mg 10.737 MeV ^{24}Na[1.35] MeV	1.28±0.25	j_1j_2	----	----------
;1	^{24}Mg 10.977 MeV ^{24}Na 1.508 MeV	0.11±0.10	j_1j_2	----	----------
$2^+;1$	^{28}Si 9.379 MeV ^{28}Al 0.031 MeV	1.15±0.10	(1d5/2)(2s1/2)	1.51	$[(1d5/2)^{11}_{5/2\ 1/2}(2s1/2)^1_{1/2\ 1/2}]_{21}$

Table 12 (Continued)

$J^{\pi};T$	States	$R_x(t/^3He)$	Pickup	$R_c(t/^3He)$	Major Component of Final State Shell-Model Configuration
$0^+;1$	^{28}Si 10.700 MeV ^{28}Al [1.37] MeV	1.86±0.20	$(1d5/2)^2$	1.84	$[(1d5/2)^{10}_{01}(2s1/2)^2_{01}]_{01}$
$(2^+);1$	^{28}Si 10.909 MeV ^{28}Al 1.633 MeV	1.81±0.20	$(1d5/2)^2$	1.83	$[(1d5/2)^{10}_{21}(2s1/2)^2_{01}]_{21}$
$2^+;1$	^{32}S 7.005 MeV ^{32}P 0.078 MeV	1.20±0.15	$(2s1/2)(1d5/2)$	1.22	$[(2s1/2)^3_{1/2\ 1/2}(1d3/2)^1_{3/2\ 1/2}]_{21}$
$2^+;1$	^{36}Ar 6.612 MeV ^{36}Cl g.s.	1.90±0.20	$(1d3/2)^2$	1.81	$[(2s1/2)^4_{00}(1d3/2)^4_{21}]_{21}$
$2^+;1$	^{36}Ar 8.546 MeV ^{36}Cl 1.949 MeV	1.46±0.20	$(2s1/2)(1d3/2)$	1.22	$[(2s1/2)^3_{1/2\ 1/2}(1d3/2)^5_{3/2\ 1/2}]_{21}$
$0^+;1$	^{36}Ar 9.701 MeV ^{36}Cl [3.12] MeV	2.43±0.70[a]	$(2s1/2)^2$	1.80	$[(2s1/2)^2_{01}(1d3/2)^6_{01}]_{01}$
$^-;2$	^{38}Ar 13.332 MeV ^{38}Cl 2.752 MeV	0.43±0.10	$(1d3/2)(1f7/2)$	0.45[b]	$[(1d3/2)^5_{3/2\ 3/2}(1f7/2)^1_{7/2\ 1/2}]_{32}$
$;2$	^{38}Ar 13.700 MeV ^{38}Cl 3.190 MeV	1.12±0.20	j^2	0.90	----------

Table 12 (continued)

The values in square brackets in this table denote approximate excitations of states suspected but as yet unconfirmed by other measurements.

(a) The errors on this ratio are somewhat larger than normal because the interfering state has a large cross section compared to the state of interest.

(b) Because the cross section ratio depends on configuration, this one was assumed to provide an order of magnitude expected. Other $j_1 j_2$ pickup configurations give about the same values (±0.20).

To obtain the cross section ratios for these comparisons, the best guide-the-eye line, drawn through the triton data was also drawn through the ^{3}He data; the experimental cross section ratio was taken as that multiplication factor required to produce the best fit. The first maxima in the distributions were most heavily weighted in determining the normalization factor except for these cases where no maximum was discernable. Here the normalization was weighted by the angles having the largest cross section measured with adequate statistics.

1. ^{20}Ne - ^{20}F T=1 States

The excitation energies of the states in ^{20}F shown in Fig. 31 were taken from de López et al.[46] and Chagnon.[47] The excitation of the lowest T=1 level in ^{20}Ne is based on measurements by Pearson[48] and MacFarlane.[49] Using this level as a calibration in addition to the ^{10}C levels, the excitations of the higher lying levels were determined from this work. The ^{20}Na states, taken from Endt[41] are also shown for comparison.

Two states observed in the reaction ^{22}Ne(p,t)^{20}Ne were identified as T=1 in character. The cross section data for other states in this region of excitation in ^{20}Ne were insufficient to provide additional J^{π};T assignments.

a. ^{20}Ne 10.275 MeV - ^{20}F ground states. These states are identified as T=1 analogue states from energy systematics and because both states are produced with identical angular momentum transfers in the mirror (p,t) and (p,^{3}He) reactions. The observed angular distributions[50] for these states are shown in the upper portion of Fig. 32, and are found

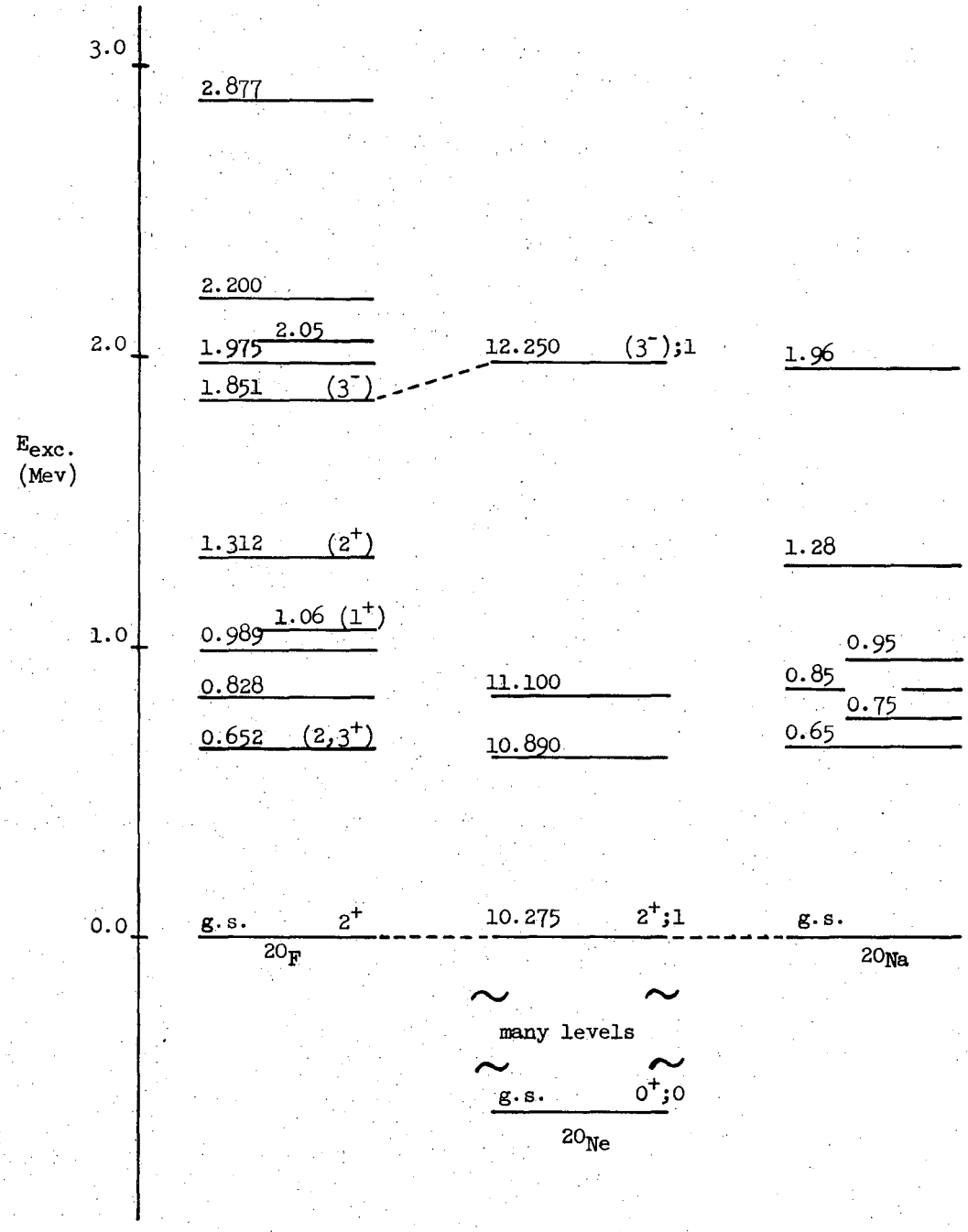
3.0
2.0
1.0
0.0
$E_{exc.}$ (Mev)
2.877
2.200
2.05
1.975
1.851 (3⁻)
1.312 (2⁺)
1.06 (1⁺)
0.989
0.828
0.652 (2,3⁺)
g.s. 2⁺
^{20}F
12.250 (3⁻);1
11.100
10.890
10.275 2⁺;1
many levels
g.s. 0⁺;0
^{20}Ne
1.96
1.28
0.95
0.85
0.75
0.65
g.s.
^{20}Na
XBL 6812-6457

Figure 31

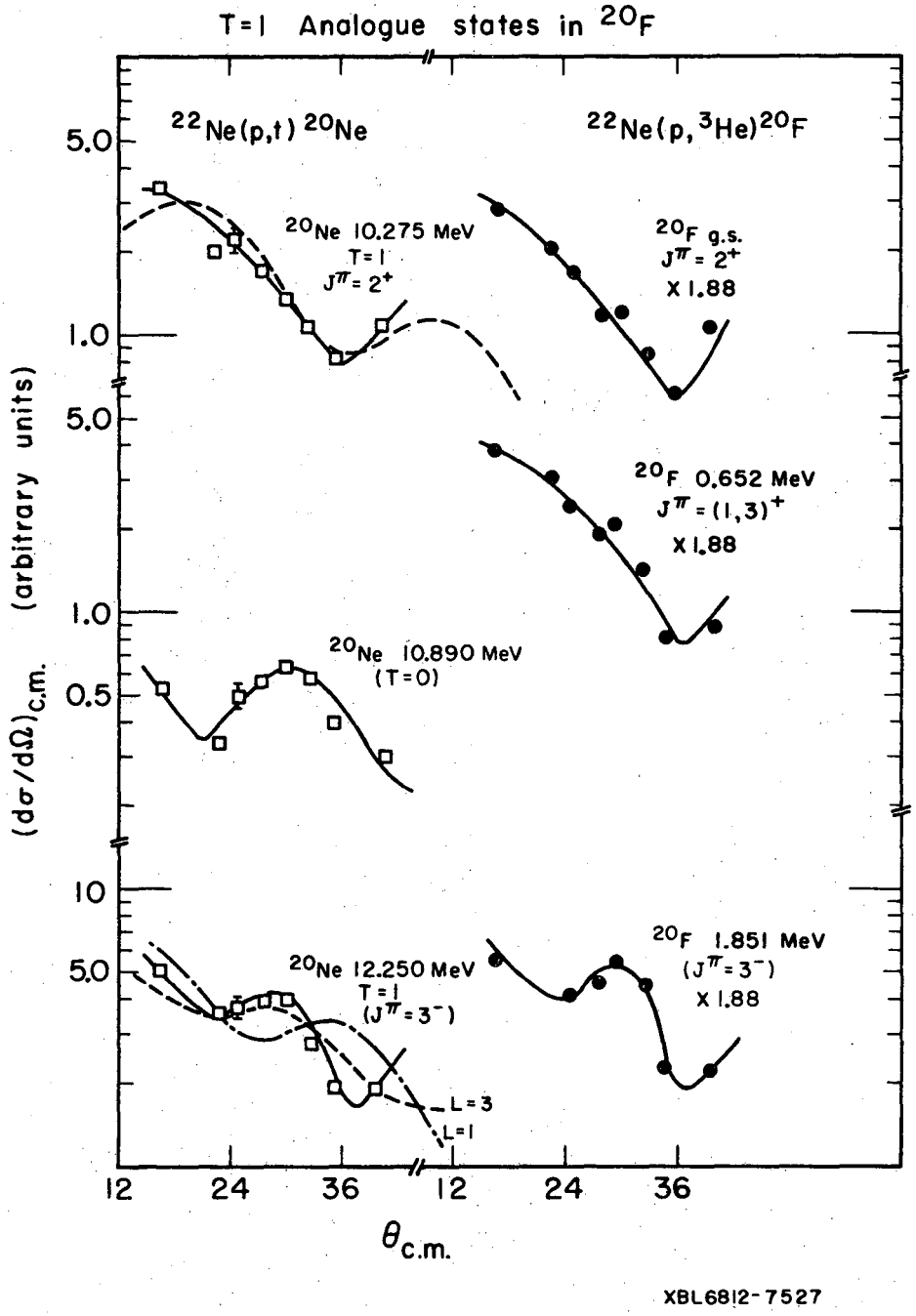
T=1 Analogue states in 20F
22Ne(p,t) 20Ne
22Ne(p, 3He)20F
20Ne 10.275 MeV
T=1
Jπ= 2+
20F g.s.
Jπ= 2+
X 1.88
20F 0.652 MeV
Jπ= (1,3)+
X 1.88
20Ne 10.890 MeV
(T=0)
20Ne 12.250 MeV
T=1
(Jπ=3-)
20F 1.851 MeV
(Jπ=3-)
X 1.88
L=3
L=1
5.0
1.0
5.0
1.0
0.5
10
5.0
(dσ/dΩ)c.m. (arbitrary units)
12
24
36
12
24
36
θc.m.
XBL6812-7527

Figure 32

to be consistent with an L=2 transfer. The solid curves in the figure represent the same guide-the-eye line through both the triton and ^{3}He data. The ^{3}He data have been multiplied by the calculated ratio for j^2 pickup (=1.88) to facilitate comparison. The dashed curve is a DWBA fit for a L=2 transfer using the parameters given in Table 2.

Despite some earlier uncertainty[46,47] in the spin-parity assignment of ^{20}F, its J^{π} has been confirmed by this experiment to be 2^{+}. Previous work, using the reaction $^{19}F(d,p)^{20}F$ to populate the ground state, has shown this stripping reaction proceeds with l_n=2, giving J^{π} of the final state as 1, 2, or 3^{+}. Since the (p,t) reaction on 0^{+} nuclei, restricted to populating natural parity states, can be used to populate the ^{20}Ne analogue to the ^{20}F g.s., this implies that both states have natural parity. Hence, the observed L=2 transitions assign a J^{π} of 2^{+} to the ^{20}Ne 10.275 MeV and ^{20}F ground states.

The observed cross section ratio for these states is found to be $R_x(t/^{3}He)$ = 1.94±0.20 which is an excellent agreement with the ratio calculated on the basis of j^2 pickup, as shown in Table 12. The cross section ratios calculated for a $j_1 j_2$ pickup, are typically ∿1.3, as also shown in Table 12.

The cross section ratio obtained for these states is consistent with the following simple shell-model pickup:

$$[(1p1/2)^{4}_{00}(1d5/2)^{6}_{01}]_{01} \rightarrow [(1p1/2)^{4}_{00}(1d5/2)^{4}_{21}]_{21}$$

If this latter configuration is indeed the principal component of the ^{20}F ground state, then this state should not be observed in the reaction

$^{22}Ne(d,\alpha)^{20}F$, because the pickup of $(d\ 5/2)^2$ particles cannot, as shown by Eq. (II-27), be coupled to even-spin natural parity states. Hence, the transition from the 0^+ ^{22}Ne ground state to the 2^+ ^{20}F ground state is forbidden.

Experimentally, the ^{20}F ground state produced by the (d,α) reaction using 40 MeV incident deuterons, is observed with an intensity of only 8% of the strongest state in the spectrum.[50] Such a small cross section may be readily explained by small admixtures of other configurations to the wave functions of the initial ^{22}Ne and final ^{20}F states.

b. <u>^{20}Ne 12.250 MeV - ^{20}F 1.851 MeV states</u>. Energy systematics and angular distribution data suggest that the ^{20}Ne 12.250-MeV and the ^{20}F 1.851-MeV state are analogue T=1 states. As shown in the lower portion of Fig. 32, the triton and ^3He distributions are distinctive and virtually identical in shape for both states; the solid curves are the same guide-the-eye line through both distributions. The broken curves are DWBA fits for the L values indicated using the parameters given in Table 2. A comparison with the distinctive L=0 and L=2 shapes observed previously (see Fig. 20) shows these distributions to be totally different. No J^π has been previously reported for either state, but present experiments suggest a $J^\pi=(3^-)$ to be consistent with all data obtained.

The experimental cross section ratio obtained for these states is $R_x(t/^3He) = 1.33\pm0.15$ which is inconsistent with a ratio of 1.88, calculated assuming j^2 pickup. However, the calculated ratio for a j_1j_2 pickup of the sort $[(1p1/2)^4_{00}(1d5/2)^6_{01}]_{01} \rightarrow [(1p1/2)^3_{1/2\ 1/2}(1d5/2)^5_{5/2\ 1/2}]_{31}$ is found to be $R_c=1.30$, which agrees very well with the experimental value

obtained. From simple shell-model considerations, such a configuration would be likely for the lowest $j_1 j_2$ pickup in these nuclei. Although the configuration can also be recoupled to give a state of $J^\pi=2^-$, such a state cannot be produced by the (p,t) reaction on ^{22}Ne and hence the probable spin-parity of the observed states is restricted to 3^- for these configurations. Figure 32 shows the cross section data to be consistent with the DWBA calculation for L=3. The calculated L=1 distribution is also shown for comparison.

The ^{20}F 1.851 MeV state is observed to be the strongest state populated in the reaction ^{22}Ne(d,α)^{20}F, and hence must have a primary configuration of either $(1d5/2)^2$ coupled to a final $J^\pi=1$, 3 or 5^+, or (p1/2)(d5/2), (the $J^\pi=0$, 2 or 4^+ are not allowed by Eq. (II-27)). Any configuration coupled to 1,3 or 5^+ is ruled out because their analogues would not be observed in the (p,t) reaction. Hence it appears this state is a natural parity state of (p1/2,d5/2) character with a $J^\pi=(3^-)$.

Further verification of this configuration suggested for the ^{20}Ne 12.250 MeV and ^{20}F 1.851 MeV states is obtained from the ^{19}F(d,p)^{20}F reaction. A state with this configuration would not be expected to be produced by this stripping reaction, because the ^{19}F ground state wave function does not have much p-hole state admixture, as would be required to produce this state in ^{20}F by the (d,p) reaction. The work by de López[46] and Chagnon[47] confirms that this state is indeed very weakly produced.

An additional $j_1 j_2$ pickup, of the type $[(1p1/2)^4_{00}(1d5/2)^6_{01}]_{01}$ $\rightarrow [(1p1/2)^3_{1/2\ 1/2}(1d5/2)^5_{5/2\ 3/2}]_{31}$ gives a calculated ratio of R_c=0.68.

Because the observed ratio disagrees strongly with this ratio, any significant admixtures of this configuration are unlikely.

c. Other T=1 states in mass 20. Additional states have been observed in ^{20}Ne at excitations of 10.890 MeV and 11.100 which may be T=1 in character. From energy considerations, it is expected that the ^{20}Ne 10.890 MeV state is analogous to the ^{20}F 0.652 MeV state. The angular distributions observed for the triton and ^{3}He particles corresponding to these states are not the same in shape (see Fig. 32), suggesting the states are not formed by the same angular momentum transfer, and hence are not analogues. Because the T=1 analogue in ^{20}Ne to the ^{20}F 0.652 is not observed in the (p,t) reaction, this would suggest a $J^{\pi}=1,3^{+}$ for this state, based on these and the (d,p) results.

Similarly, a T=1 state in ^{20}Ne at an excitation of 11.100 MeV is expected to be analgous to a state in ^{20}F at an excitation of $\sim$0.8 MeV. Due to the number of states in this region, no state in the ^{3}He spectrum was observed with sufficient cross section and separation from the neighbouring strong states to permit comparison.

2. ^{24}Mg - ^{24}Na T=1 States

The excitation energies given for the ^{24}Na states shown in Fig. 33 were taken from Endt and Van Der Leun[41] except for that of 1.508±0.010 state which has been recently reported by Jahr et al.[51] The excitation energies shown for ^{24}Mg were also taken from Endt, except for the states reported at 10.740±0.035 MeV and 10.977±0.040 MeV which are determined from this work. A $(J^{\pi};T)=(3^{-};1)$ has been assigned to the latter state and its analogue in ^{24}Na as being consistent with all experimental data.

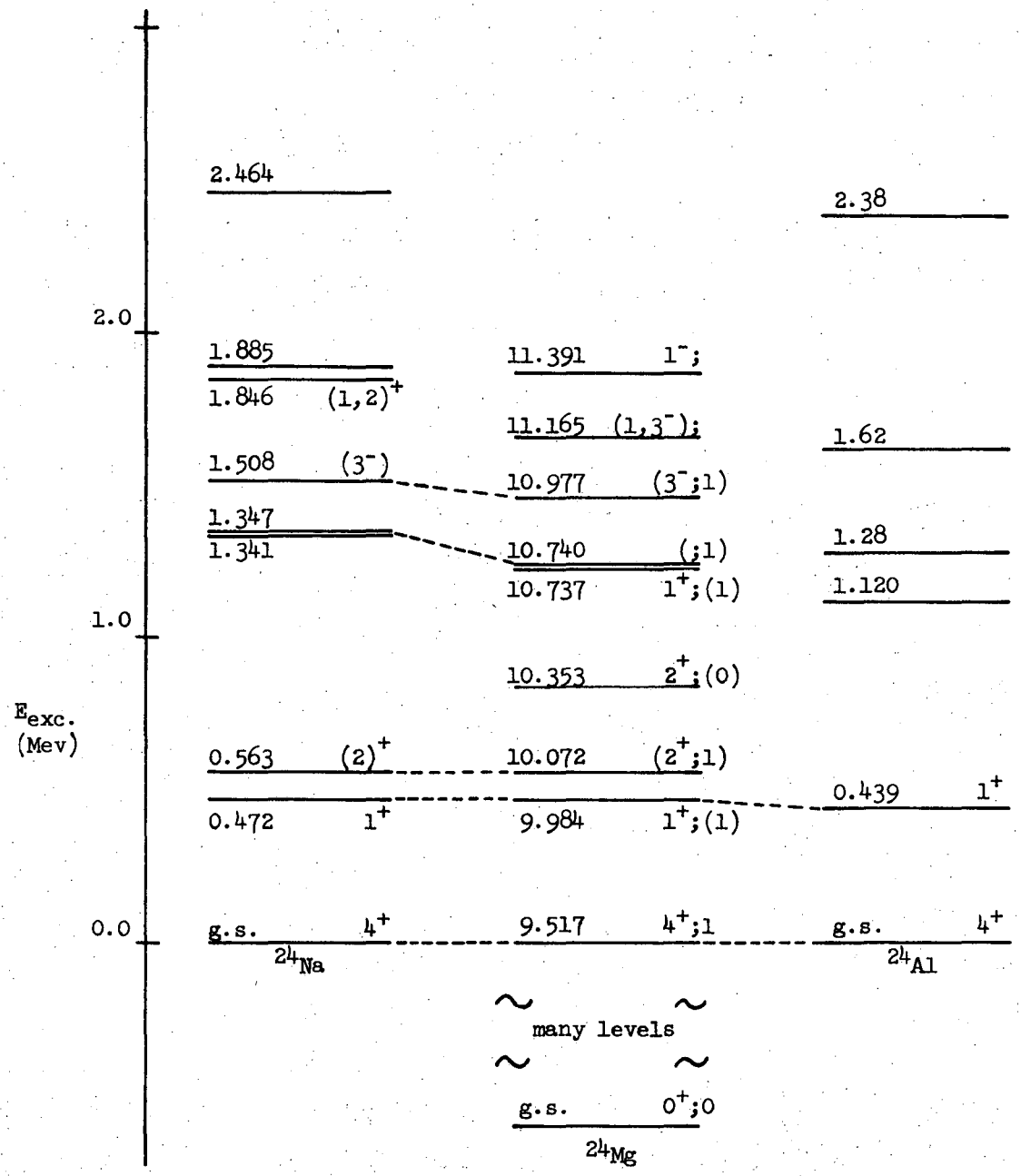

XBL 6812-6455

Figure 33

The present work also observes states at excitations of 10.337±0.035 MeV and 11.375±0.040 MeV, which are to be compared with the previously reported states at 10.353±0.020 and 11.391±0.004 MeV. Because of the greater accuracy of the latter excitations, these have been used in the figure. The states reported by Endt[41] for ^{24}Al have also been included for comparison.

The cross section ratios were obtained in the manner described previously. Due to the better counting statistics available at $\theta_{cm} \sim 24°$, these data were weighted more strongly than the other points obtained in the distributions. Because the angular distributions of states in ^{24}Mg produced by the (p,t) reaction had been extensively studied,[29] only sufficient distributions were obtained for the (p,^{3}He) reaction[50] to indicate the analogue nature of the states observed.

a. <u>^{24}Mg 9.517 MeV - ^{24}Na ground states</u>. The excitation energies and angular distribution data determined for these states identify them as the previously reported[41] lowest T=1 analogue states in mass 24. The observed distributions are similar, and are consistent with the previously assigned $J^{\pi}=4^{+}$.

The experimental cross section ratio for these states is found to be $R_x(t/3_{He}) = 2.52\pm0.30$ which is higher than the calculated ratio for j^2 pickup, $R_c=1.86$. Since the calculated ratio for $j_1 j_2$ pickup can never exceed the j^2 ratio, and is generally much smaller (see Table 12), for simple shell model configurations, this results is consistent only with a j^2 pickup.

A possible explanation of the enhanced cross section observed for the ^{24}Mg 9.517 MeV state by the (p,t) reaction is the inclusion of unresolved T=0 states. Endt[41] has reported two states, one at 9.456±0.012 MeV of unknown J^{π} and another at 9.52 (no reported error) MeV with a $J^{\pi}=(6^{+})$, which would be unresolved in this work. However, the peaks observed in this work are sharp and symmetric. Since ^{24}Mg is known to be a deformed nucleus, high J states are populated with relatively large cross sections. Consequently the 9.52 MeV $(J^{\pi};T)=((6^{+});0)$ state which is virtually degenerate with the lowest T=1 state could make a significant contribution to the cross section, and give rise to this abnormally large ratio.

b. <u>^{24}Mg 10.072 MeV - ^{24}Na 0.563 MeV states</u>. From previous work[41] and energy systematics these states have been identified as T=1 analogue states. Present energy determinations and similar angular distributions confirm the earlier assignments of $(J^{\pi};T)=(2^{+};1)$ for the ^{24}Mg 10.072 MeV and ^{24}Na 0.563 MeV states.

Since the (p,t) reaction on 0^{+} targets cannot populate unnatural parity states, the 9.984 MeV state in ^{24}Mg, with a $(J^{\pi};T)=(1^{+};(1))$ would not be produced by this reaction. However, its analogue, the ^{24}Na 0.472 MeV state can be produced by the (p,^{3}He) reaction, both by L=0 and L=2 angular momentum transfer. With an experimental resolution of ∿150 keV, this state should be unresolved from the ^{24}Na 2^{+} state, and would contribute to that cross section. Consequently the experimental ratio is expected to fall somewhat below the calculated value.

For these 2^+ states (^{24}Mg 10.072 MeV and ^{24}Na 0.563 MeV) a j^2 pickup gives a calculated ratio of R_c=1.86. The experimental cross section ratio is found to be $R_x(t/3_{He})$=3.36±0.30 which is higher than expected.

The enhanced triton cross section is possibly due to the inclusion of unresolved T=0 states, which may be produced with significant cross section in the deformed ^{24}Mg nucleus. Two states, with excitation energies reported[41] to be 10.025±0.015 MeV and 10.161±0.015 MeV, are sufficiently close to be unresolved from the 10.072 MeV state. They should, however, significantly broaden the observed peak if they are produced. The observed peak corresponding to the 10.072 MeV state is symmetric and shows no greater FWHM than other peaks observed at this energy. Earlier angular distribution data from Cosper et al.[29] do suggest though, that this state is complex.

c. <u>^{24}Mg 10.74 MeV - ^{24}Na 1.34 MeV states</u>. From energy systematics, (see Fig. 33) it appears that the 10.737 MeV 1^+;(1) state in ^{24}Mg is analogous to one of the two states in ^{24}Na located at an excitation of about 1.34 MeV. Since both the states in ^{24}Na must have analogues in ^{24}Mg a second T=1 state near the ^{24}Mg 10.737 MeV state is predicted.

In the reaction ^{26}Mg(p,t)^{24}Mg, the state observed at an excitation of 10.740±0.035 MeV is found to have a cross section 30% larger than the lowest T=1 state. Since the (p,t) reaction does not populate unnatural parity states, this state cannot be the previously reported 1^+;(1) state at 10.737 MeV. It is assumed this state is analogous to

the second state in ^{24}Na at 1.34 MeV. The angular distribution obtained using a 46 MeV proton beam by Cosper et al.[29] for the 10.74 MeV state suggests an L=1 or L=2 angular momentum transfer.

The cross section ratio obtained for the ^{24}Mg 10.74 state and the component of the ^{24}Mg 1.34 MeV state extracted from the unresolved multiplet at θ_{LAB} = 22.3° gives an experimental cross section of $R_x(t/3_{He})$=1.28±0.35 suggesting these states are probably not formed by pure j^2 pickup. Since no J^π information is known about these states, it is not possible to suggest a likely configuration. A comparison of the experimental ratio obtained here with the j_1j_2 ratios calculated in Table 12 shows them to be consistent.

d. ^{24}Mg 10.977 MeV - ^{24}Na 1.508 MeV states. The existence of a state in ^{24}Na at an excitation of 1.508 MeV by Jahr et al.[51] is confirmed by these experiments. Because this state is not clearly resolved from the 1.34 MeV doublet no accurate energy determination could be made from this work. From energy systematics, however, this state appears to be an analogue to a ^{24}Mg state observed at an excitation of 10.977±0.040 MeV.

The observed cross section ratio for these states is found to be $R_x(t/3_{He})$=0.11±0.10 indicating a complex pickup of configurations, certainly including strongly mixed j_1j_2 pickup.

Previous work suggests $J\leq 4$ for the ^{24}Na 1.508 MeV state, based on its lack of strength in the reactions ^{24}Ne(β^-)^{24}Na [41] and ^{23}Na(d,p)^{24}Na.[52,53] The similarity of behavior noted for this state based on the assumption of a j_1j_2 pickup, with that of the ^{20}F 1.851 MeV state discussed

previously, suggests that the lack of strength of this state in the (d,p) reaction can be accounted for by a p-hole configuration. Hence, the possible configuration of the final state may be a mixture of the following:

$$[(1p1/2)^4_{00}(1d5/2)^{10}_{01}]_{01} \rightarrow [(1p1/2)^3_{1/2\ 1/2}(1d5/2)^9_{5/2\ 1/2}]_{31} \quad R_c=1.30$$

$$\rightarrow [(1p1/2)^3_{1/2\ 1/2}(1d5/2)^9_{5/2\ 3/2}]_{31} \quad R_c=0.68$$

(Since these states must be natural parity states, and the parity must be odd from (p1/2)(d5/2) pickup, only $J^\pi=3^-$ is allowed.) This $J^\pi=3^-$ is also consistent with the observed β^- decay data, since $\Delta J=3;\Delta^\pi=-$ is strongly forbidden.

The observed cross section ratio is significantly lower than that calculated for either suggested configuration. This means that neither is dominant, and substantial cancellation of transition amplitudes is possible.

3. ^{28}Si - ^{28}Al T=1 States

The excitation energies shown in Fig. 14a for the T=1 states in mass-28 are taken from Endt and Van der Leun,[41] except for the state in ^{28}Si at 10.700 MeV, which represents an average of the previously reported value[41] of 10.710±0.020 MeV and the value of 10.676±0.030 MeV obtained in the present experiments. The spin-parity values reported for excited T=1 states in ^{28}Si are determined by the characteristic L=0 and L=2 angular momentum transfers shown in Fig. 34. (Compare the observed shapes with those shown in Fig. 20.) Based on the spin assignments in

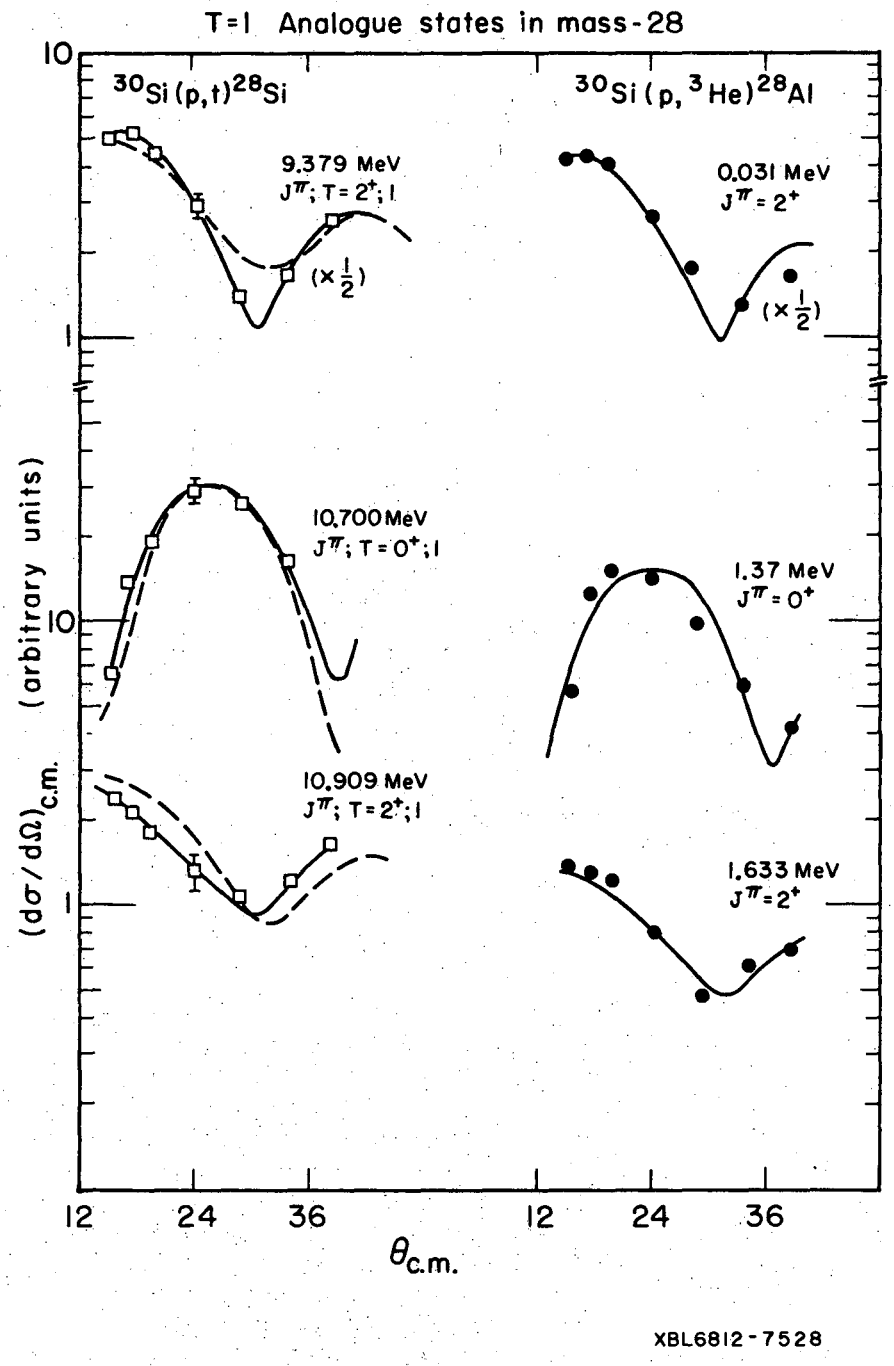
T=1 Analogue states in mass-28
^{30}Si (p,t)^{28}Si
^{30}Si (p, ^{3}He)^{28}Al
9.379 MeV
J$^{\pi}$; T= 2^{+}; 1
(× 1/2)
0.031 MeV
J$^{\pi}$ = 2^{+}
(× 1/2)
10.700 MeV
J$^{\pi}$; T = 0^{+}; 1
1.37 MeV
J$^{\pi}$ = 0^{+}
10.909 MeV
J$^{\pi}$; T = 2^{+}; 1
1.633 MeV
J$^{\pi}$ = 2^{+}
10
1
10
1
(dσ/dΩ)c.m. (arbitrary units)
12
24
36
12
24
36
θc.m.
XBL6812-7528

Figure 34

^{28}Si, and the analogue character of the 10.909 MeV ^{28}Si and 1.633 MeV ^{28}Al states, it is possible to tentatively assign a $J^{\pi}=(2^{+})$ to the latter state.

The experimental cross section ratio was determined as described previously. The solid curves through the (p,t) data serve to guide the eye; the identical curves have been drawn through the (p,^{3}He) distributions to facilitate comparison. The statistical errors on the experimental cross section points are indicated in Fig. 34. The dashed curves represent DWBA fits, using pure configurations and single L transfers. The parameters used for the fits are summarized in Table 2.

a. <u>^{28}Si 9.379 MeV - ^{28}Al 0.031 MeV states</u>. The angular distribution observed for the T=1 state at 9.379 MeV in ^{28}Si is found to exhibit a characteristic L=2 shape, confirming the earlier tentative assignment of 2^{+} for this state.[41] The distribution observed for ^{3}He particles corresponding to the 0.031 MeV state in ^{28}Al was found to be identical in shape to the 9.379 MeV state in ^{28}Si (see Fig. 34). From the identity of their angular distributions, and from energy systematics, these states were assigned as T=1 analogues in mass 28.

The experimental cross section ratio obtained for these states is $R_{x}(t/3_{He})=1.15\pm0.10$. Because the 2^{+} 0.031 MeV state in ^{28}Al is unresolved from the 3^{+} ground state, the latter will also contribute to the observed ^{3}He cross section. Since the 3^{+} analogue in ^{28}Si cannot be produced in first order by the (p,t) reaction, the observed ratio is expected to be somewhat lower than calculated. Detailed wave functions for these states are not available, hence it is not possible to estimate the relative strengths for the 2^{+} and 3^{+} states in ^{28}Al.

The experimental precision in the energy determinations of these experiments is found to be ~30 keV. As a result, it was not possible to use the "effective excitation" obtained, as a measure of the relative strengths of these states. Also, both states are produced primarily by an L=2 angular momentum transfer, and hence the angular distribution shape would be insensitive to the amounts of each state present.

From simple shell model considerations, the transition can probably be represented as occurring primarily as follows:

$$[(1d5/2)^{12}_{00}(2s1/2)^{2}_{01}]_{01} \rightarrow [(1d5/2)^{11}_{5/2\ 1/2}(2s1/2)^{1}_{1/2\ 1/2}]_{21}$$

The theoretical cross section calculated for such a configuration is R_c=1.51, as compared to a ratio of R_c=1.84 calculated for a j^2 configuration.

The experimental result appears indicative of a $j_1 j_2$ pickup, but because no estimate of the magnitude of the cross section of the 3^+ ground state in ^{28}Al is available, no definite assignment can be made.

b. <u>^{28}Si 10.700 MeV - ^{28}Al 1.35 MeV state</u>. A state, with a characteristic L=0 angular distribution has been observed in ^{28}Si, at an excitation energy of 10.700±0.030 MeV. If this state is a T=1 state, one would expect from energy systematics, to find its analogue in ^{28}Al at an excitation of about 1.35 MeV. Such a state is in fact observed by the (p,^{3}He) reaction, at an excitation of 1.35±0.040 MeV, and is produced by an L=0 transfer. Although these data are consistent with a previously reported 1^+ state at an excitation of 1.372±0.005 MeV in ^{28}Al, this state

state cannot be the analogue to the ^{28}Si 10.700 since the J^{π} of the latter has been identified as 0^{+} by the (p,t) reaction. The J^{π} of the ^{28}Al 1.372 MeV state has been assigned from the β-decay of the ^{28}Mg 0^{+} ground state, and this state has been observed in a variety of neutron stripping reactions on ^{27}Al, such as ^{27}Al(d,p)^{28}Al. Hence, it appears unlikely that the J^{π} assignment of the 1.372 MeV state in ^{28}Al is in error; a more probable explanation is the existence of an additional state in ^{28}Al, with a J^{π} of 0^{+} at an excitation of 1.350±0.040 MeV.

The experimental cross section ratio obtained, assuming a T=1 character for these states, is found to be

$$R_x(t/^3He) = 1.86\pm0.20$$

which is consistent with a theoretical ratio of R_c=1.84; calculated for a j^2 pickup.

The observed $J^{\pi}(=0^{+})$ and the low excitation may be explained by a transition of the type

$$[(1d5/2)^{12}_{00}(2s1/2)^{2}_{01}]_{01} \rightarrow [(1d5/2)^{10}_{01}(2s1/2)^{2}_{01}]_{01}$$

This configuration is consistent with the fact that the ^{28}Al 1.35 MeV state has not been observed in neutron stripping reactions, since it would be produced only by a core excitation in addition to the pickup of a neutron.

Experiments using the reaction $^{30}Si(d,\alpha)^{28}Al$ have been performed[54] at a deuteron energy of 9.5 MeV, but no evidence of another state has been observed. This is additional confirmation of the configuration suggested above, since the J=0 transfer is forbidden in the (d,α) reaction.

c. ^{28}Si 10.909 MeV - ^{28}Al 1.633 MeV states. The angular distributions observed for these states were identical in shape, and exhibited a characteristic L=2 structure, as shown in the lower portion of Fig. 34. From this and energy systematics, these states were tentatively assigned as T=1 analogue states. Based on the angular distribution shapes, the J^π of the 10.909 MeV state in ^{28}Si can be assigned as 2^+. If these states are indeed analogues, a $J^\pi=2^+$ can also be assigned to the 1.633 MeV state in ^{28}Al.

The experimental cross section ratio obtained is

$$R_x(t/^3He) = 1.81\pm0.20$$

which agrees well with the ratio $R_c=1.83$ calculated assuming a j^2 transfer.

Based on simple shell model considerations, and the known J^π of the states, the transfer can be explained by a pickup of the sort:

$$[(1d5/2)^{12}_{00}(2s1/2)^2_{01}]_{01} \rightarrow [(1d5/2)^{10}_{21}(2s1/2)^2_{01}]_{21}$$

The ^{28}Al 1.633 MeV state is observed in the (d,α) reaction, but because of the low E_d(=9.5 MeV) used, no information about its structure can be obtained from the intensity of this state relative to other states produced by the reaction.

4. ^{32}S - ^{32}P T=1 States

The energy level data shown in Fig. 14b for the T=1 states in mass 32 are taken from Endt and Van der Leun.[41] Because the thin targets used in these experiments were capable of withstanding only small beam intensities, only those angles near the peak of the L=0 distributions were measured. Consequently, the data are insufficient to extract angular distributions. To obtain the cross section ratio for the T=1 states, the ratio of counts observed for several individual runs were averaged; the final result was corrected for J_θ (Jacobian).

In this experiment, only the ^{32}S 7.005 MeV $(2^+;1)$ state and its analogue in ^{32}P were observed with sufficient cross section to permit comparison. Although no angular distributions are available from these experiments, previous work[41] has shown these states to be T=1 analogues.

The position of the 1^+ state analogous to the ^{32}P ground state is unknown in the other members of this multiplet. It should not, however, interfere in the case of ^{32}S, since it is an unnatural parity state and would not be produced by the (p,t) reaction on ^{34}S. In the ^{32}P case, the 1^+ state is not completely resolved from the 2^+ excited state, but a peak asymmetry was observed and corrected for.

From the wave functions as calculated by Glaudemans et al.,[55] the following initial and final configurations (neglecting small components) are obtained:

$^{34}S_{g.s.}$ $\psi(0^+) = -0.842\ s^4_{00}d^2_{01} + 0.352\ s^2_{01}d^4_{00} - 0.339\ s^2_{01}d^4_{02}$

$^{32}P_{g.s.}$ $\psi(1^+) = -0.758\ s^3_{1/2\ 1/2}d^1_{3/2\ 1/2} + 0.374\ s^2_{10}d^2_{01} + 0.330\ s^2_{01}d^2_{10}$

$+0.330\ s^1_{1/2\ 1/2}d^3_{3/2\ 3/2}$

0.78 MeV $\psi(2^+) = -0.854\ s^3_{1/2\ 1/2}d^1_{3/2\ 1/2} + 0.330\ s^1_{1/2\ 1/2}d^3_{3/2\ 1/2}$

An inspection of these wave functions reveals that the major component of both the 2^+ and 1^+ states in ^{32}P is produced by (2s1/2)(1d3/2) pickup. Consequently both states will be produced primarily by an L=2 transition. Based on this assumption, the DWBA prediction for the relative strengths of the 2^+:1^+ are calculated to be 4.4:1.

The observed cross section ratio, correcting for peak asymmetry, is found to be $R_x(t/^3He)=1.20\pm0.15$ which is consistent with the calculated ratio, $R_c=1.22$, based on the j_1j_2 transition:

$$[(2s1/2)^4_{00}(1d3/2)^2_{01}]_{01} \rightarrow [(2s1/2)^3_{1/2\ 1/2}(1d3/2)^1_{3/2\ 1/2}]_{21}$$

The ratio calculated for j^2 transitions is $R_c=1.82$, and is inconsistent with the experimental data.

The experimental cross section ratio obtained using the whole ^3He peak (1^+ and 2^+ states) gives a value of $R_x(t/^3He)= 1.00\pm0.12$. Correcting this ratio based on the relative 2^+:1^+ strengths of 4.4:1 as

calculated above, gives a final result of $R_x(t/3_{He}(corr))=1.23\pm0.15$. This is in excellent agreement with the result obtained by correcting the ^3He cross section for observed peak asymmetry.

The experimental ratio obtained agrees very well with theoretical predictions. The availability of wave functions in this case has provided confirmation of the effectiveness of the cross section ratio to indicate the type of transition observed, and hence possible major components of the configuration of the final states produced.

5. $^{36}Ar - ^{36}Cl$ T=1 States

The energies of the excited states in ^{36}Cl and the lowest T=1 state in ^{36}Ar, as shown in Fig. 35 are taken from Endt and Van der Leun.[41] The higher T=1 states in ^{36}Ar are determined from this work. The state in ^{36}Cl at 3.12 was not observed sufficiently resolved from target impurities to permit a determination of its excitation; the value given is obtained from a rough Coulomb energy calculation, based on the excitation of the ^{36}Ar 9.701 MeV state.

The target used for these experiments contained only 50.8% ^{38}Ar, the remaining isotopic composition being 23.3% ^{36}Ar and 26.9% ^{40}Ar. Consequently the density of states observed at higher excitation was large, particularly in the $(p,^3He)$ reaction where all target components have similar Q-values and produce odd-odd final nuclei.

As a result of this mixed target, the cross sections of states in ^{36}Cl were obtained by subtracting the known impurity components, and the experimental errors are somewhat larger than the pure counting statistic errors shown in Fig. 24. The experimental cross section ratio was obtained as previously described.

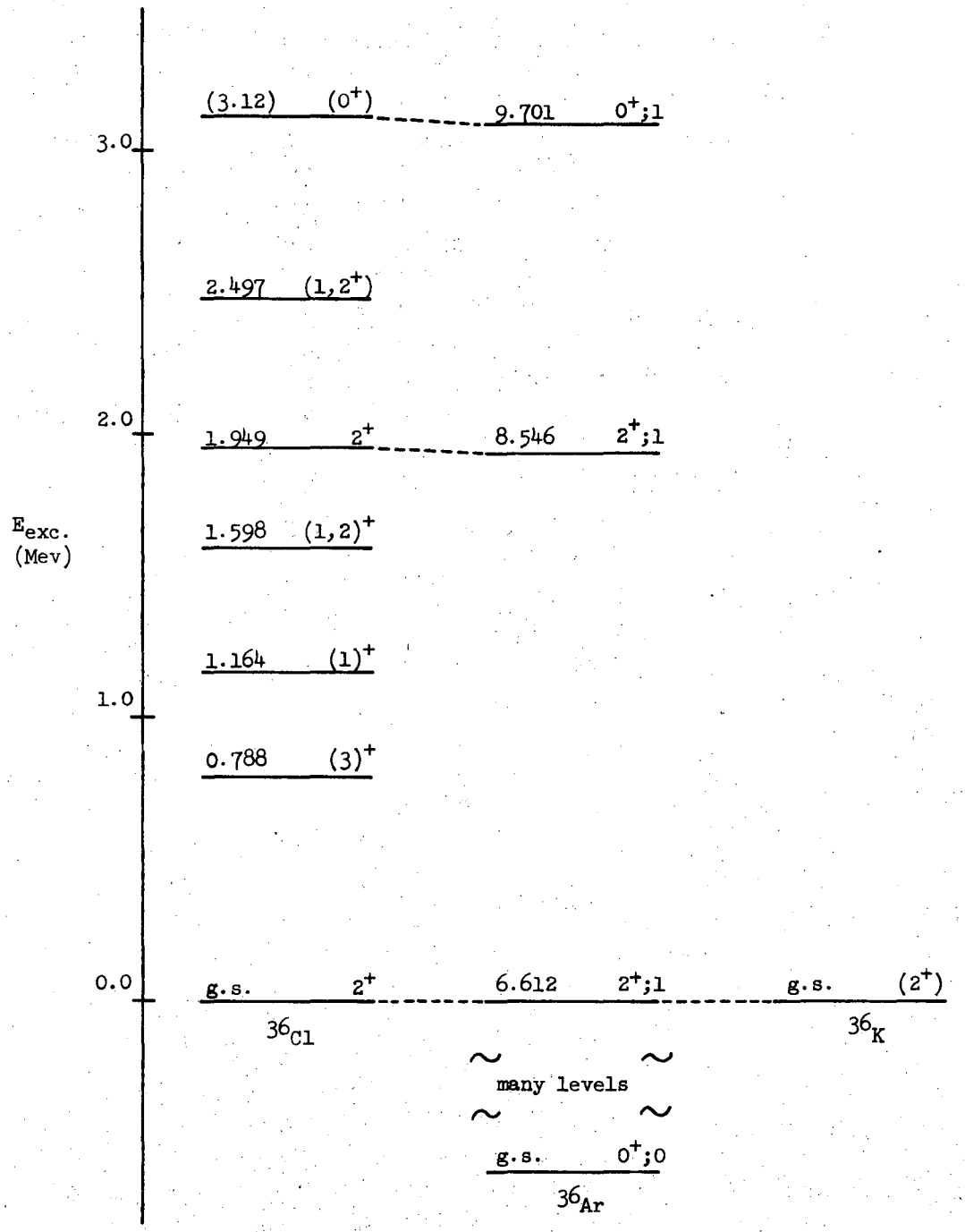
(3.12) (0+)
9.701 0+;1
3.0
2.497 (1,2+)
2.0
1.949 2+
8.546 2+;1
Eexc.
(Mev)
1.598 (1,2)+
1.164 (1)+
1.0
0.788 (3)+
0.0
g.s. 2+
6.612 2+;1
g.s. (2+)
36Cl
36K
many levels
g.s. 0+;0
36Ar
XBL 6812-6459

Figure 35

a. ^{36}Ar 6.612 MeV - ^{36}Cl ground states. The spin-parity of the lowest T=1 state in ^{36}Ar had been tentatively assigned as (2^+). The angular distribution obtained from the (p,t) reaction corresponding to this state is characteristic of an L=2 transfer, and hence confirms the above assignment. The angular distribution observed for the ^{36}Cl ground state is, within statistics, essentially the same, as shown in Fig. 24, and confirms the analogue character of these levels.

Glaudemans et al.[55] have calculated the following wave functions for the ^{38}Ar target and the ^{36}Ar 6.612 MeV-^{36}Cl 0.000 MeV final states:

$$^{38}\text{Ar}_{\text{g.s.}} \quad \psi(0^+) = -0.973\ s_{00}^4 d_{01}^6 - 0.230\ s_{01}^2 d_{00}^8$$

$$^{36}\text{Ar}/^{36}\text{Cl(T=1)} \quad \psi(2^+) = -0.930\ s_{00}^4 d_{21}^4 - 0.274\ s_{01}^2 d_{21}^6$$

An examination of these wave functions shows that the dominant mode of this transition will be j^2 pickup. This pickup predicts a calculated value for the cross section ratio of R_c=1.82. The experimentally observed cross section ratio corrected for any contribution from the degenerate $^{38}\text{Cl}_{\text{g.s.}}$ is $R_x(t/^3\text{He})$=1.90±0.20 which is in excellent agreement with the predicted j^2 ratio.

Further evidence for the j^2 character of the pickup leading to the lowest T=1 state in mass-36 is obtained from a comparison of the relative magnitudes of states observed by the reaction ^{38}Ar(d,α)^{36}Cl. Since the pickup in this reaction is primarily S=1, T=0, even spin-natural parity states with a j^2 configuration would not be produced

since they require T=1 pickup. The intensity observed for the ^{36}Cl ground state in the (d,α) reaction was found to be approximately 8% of that observed for the strongest state in the spectrum.

Although the ^{38}Cl ground state produced by the (d,α) reaction on the impurity ^{40}Ar is unresolved from the ^{36}Cl ground state in these experiments, the observed cross section for the former state is sufficiently small, as determined using a pure ^{40}Ar target, that any contributions can be ignored for these comparisons.

b. ^{36}Ar 8.546 MeV - ^{36}Cl 1.949 MeV states. The angular distributions obtained corresponding to the ^{36}Ar 8.546 MeV and ^{36}Cl 1.949 MeV states are shown in Fig. 24. On the basis of the characteristic L=2 distribution obtained for the ^{36}Ar 8.546 MeV state, a $J^{\pi}=2^{+}$ is assigned. The angular distribution obtained for the 1.949 MeV state is identical in shape, confirming the earlier 2^{+} assignment.[41] Based on this fact, and excitation energy systematics, these states are determined to be analogues.

The experimental cross section ratio, using the value obtained for the ^{36}Cl state after correcting for the known contribution of the ^{38}Cl 1.88 MeV unresolved multiplet of states gives $R_x(t/3_{He})=1.46\pm0.20$ which indicates the transition is not a j^2 pickup.

The wave-function of this final state has been calculated by Glaudemans et al.[55] as follows, neglecting small components:

$$^{36}\text{Ar}/^{36}\text{Cl}(T=1)\ \psi(2^{+}) = 0.820\ s^{3}_{1/2\ 1/2}d^{5}_{3/2\ 1/2} + 0.454\ s^{3}_{1/2\ 1/2}d^{5}_{3/2\ 3/2}$$

This transition would proceed primarily by $j_1 j_2$ pickup of the type

$$[(2s1/2)^4_{00}(1d3/2)^6_{01}]_{01} \rightarrow [(2s1/2)^3_{1/2\ 1/2}(1d3/2)^5_{3/2\ 1/2}]_{21}$$

which predicts a cross section ratio of R_c=1.21. This value is essentially in agreement with the experimental ratio given above. The small discrepancy noted is attributable to the admixture of other configurations in the initial and final states.

From the $^{38}Ar(d,\alpha)^{36}Cl$ experiment, the intensity of 1.949 MeV state in ^{36}Cl is observed to be approximately 3 times larger than that of the ground state. This result is consistent with a pickup which is predominantly $j_1 j_2$ in character.

c. <u>^{36}Ar 9.701 MeV - ^{36}Cl 3.12 MeV states</u>. A characteristic L=0 transition of moderate strength was observed leading to a state in ^{36}Ar at an excitation of 9.701±0.030 MeV [see Fig. 24]; a $J^\pi=0^+$ is assigned to this state. From the systematics of (p,t) reaction on other targets in the 2s-1d shell, it appears unlikely that a T=0 state at such a high excitation would have such a large cross section.

Using a Coulomb energy calculation, based on the observed excitation of the ^{36}Ar state, the energy predicted for the ^{36}Cl analogue state is found to be 3.12 MeV. Because of target impurities, this state was found to be degenerate with the ^{34}Cl 2.596 MeV state produced by the reaction $^{36}Ar(p,^3He)^{34}Cl$. Subtracting the contribution of the ^{34}Cl state, the angular distribution shown in Fig. 24 was obtained. The errors shown in the figure are counting statistical errors only, but a comparison with

the shape observed for the ^{36}Ar 9.701 MeV state reveals the shapes to be identical (within statistics).

Glaudemans et al.[55] have calculated the wavefunction for a 0^+ state in ^{36}Cl at an excitation of 3.30 MeV (neglecting small components) to be:

$$^{36}\text{Ar}/^{36}\text{Cl}(T=1)\psi(0^+) = 0.217\ s^3_{1/2\ 1/2} d^5_{1/2\ 1/2} + 0.976\ s^2_{01} d^6_{01}$$

A comparison of this wave function with that calculated for $^{38}\text{Ar}_{g.s.}$ reveals these states are simply related through a j^2 pickup from the major component of the target configuration.

The experimental cross section ratio observed for the ^{36}Ar 9.701 MeV and ^{36}Cl (3.12) MeV states is $R_x(t/^3\text{He}) = 2.43 \pm 0.70$ which agrees well with the theoretical j^2 ratio of $R_c = 1.80$.

The (3.12) MeV state is not observed with sufficient cross section in the ^{38}Ar (d,α) ^{36}Cl reaction to permit an accurate determination. This weak population is consistent with the previously assigned j^2 character of the state.

6. ^{38}Ar - ^{38}Cl T=2 States

The excitation energies of the states shown in Fig. 36 for ^{38}Cl up to 2.752 MeV are taken from Endt and Van der Leun;[41] the higher excited states were determined by this work. Also determined here are the excited ^{38}Ar states which are produced at excitations above that expected for the ^{38}Ar state analogous to the ^{38}Cl ground state. (This T=2 state in ^{38}Ar is an unnatural parity state, and hence would not be produced by

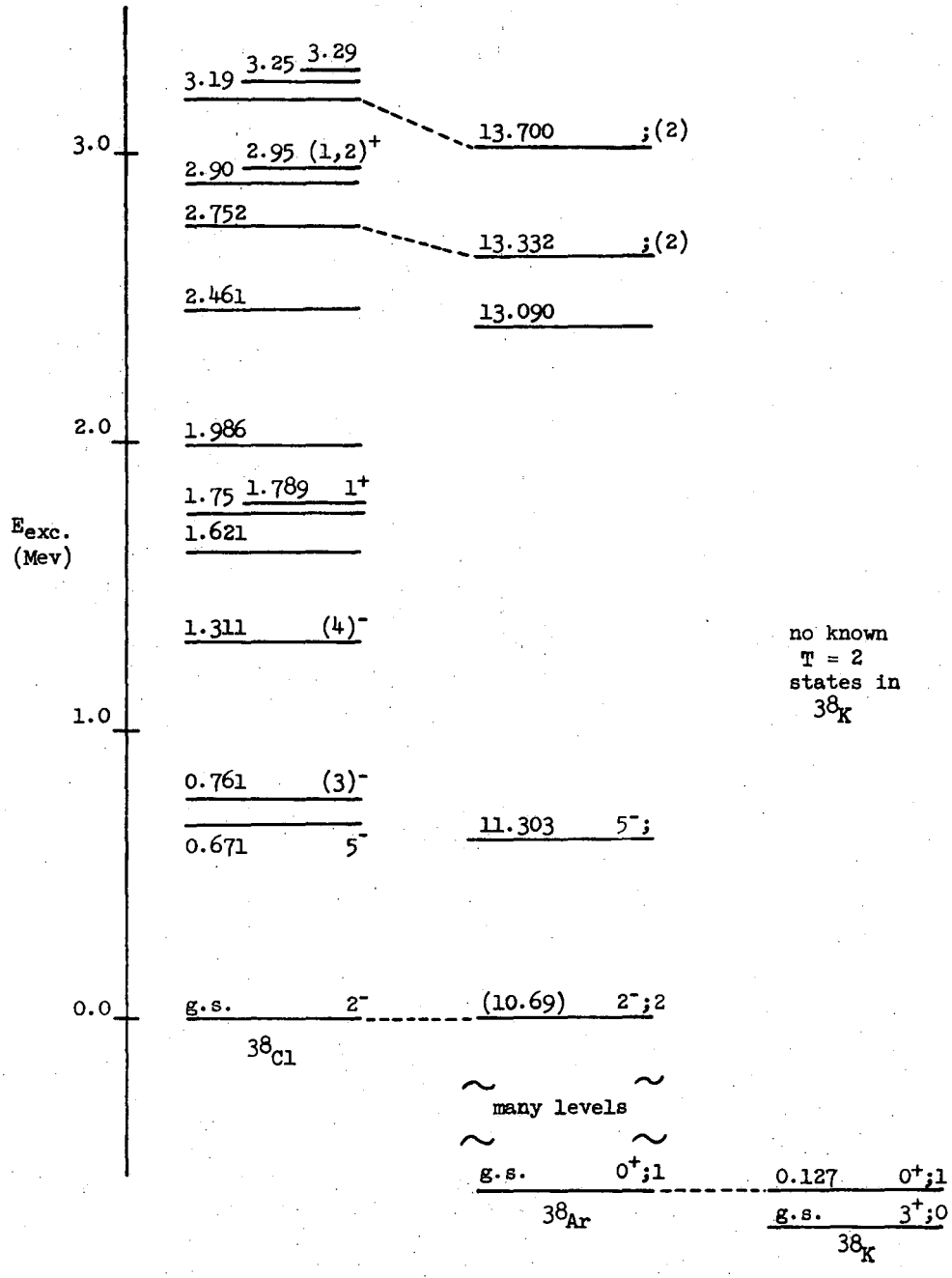
3.19
3.25
3.29
13.700 ;(2)
3.0
2.90
2.95 (1,2)+
2.752
13.332 ;(2)
2.461
13.090
2.0
1.986
1.75
1.789 1+
1.621
Eexc.
(Mev)
1.311 (4)-
no known
T = 2
states in
38K
1.0
0.761 (3)-
11.303 5-;
0.671 5-
0.0
g.s. 2-
(10.69) 2-;2
38Cl
many levels
g.s. 0+;1
0.127 0+;1
38Ar
g.s. 3+;0
38K
XBL 6812-6460

Figure 36

the (p,t) reaction on ^{40}Ar, - its expected position is obtained from a rough Coulomb calculation based on the mass excess of $^{38}Cl_{g.s.}$). The state in ^{38}Ar observed by this work at 11.300±0.045 MeV is, within error, in agreement with either (or both) of the two previously reported $J^{\pi}=5^{-}$ states at 11.303 and 11.308 MeV,[41,56] which have been produced by the reaction $^{37}Cl(p,\gamma)^{38}Ar$.

The experimental cross section ratios were obtained as described previously. Since the calculated cross section ratio depends on a factor of $2/T_f$, the comparison of these ratios to determine configurations becomes less sensitive as T increases. In addition, the high excitations of the ^{38}Ar T=2 states places them on a relatively large background when produced by the (p,t) reaction. Consequently only those states with exceptionally large cross sections can be accurately compared.

a. <u>^{38}Ar 11.300 MeV - ^{38}Cl 0.691 MeV states</u>. With an experimental resolution of ∿130 keV FWHM it was not possible to clearly resolve the $J^{\pi}=5^{-}$ and (3^{-}) states reported at 0.671 and 0.761 MeV respectively in ^{38}Cl. But since both are negative natural parity states, both their analogues in ^{38}Ar should be produced, and all must be produced by $j_1 j_2$ pickup from a ^{40}Ar target.

Assuming simple shell model configurations for the transitions:

$$[(1d3/2)^{6}_{01}(1f7/2)^{2}_{01}]_{02} \rightarrow \begin{cases} [(1d3/2)^{5}_{3/2}\ 3/2\,(1f7/2)^{1}_{7/2}\ 1/2]_{52} \\ [(1d3/2)^{5}_{3/2}\ 3/2\,(1f7/2)^{1}_{7/2}\ 1/2]_{32} \end{cases}$$

The calculated cross section ratio is $R_c(5^-)=0.643$ and $R_c(3^-)=0.452$. Hence the experimental ratio is expected to lie between these values.

From energy systematics, these states are potential analogues. The experimentally observed angular distributions however, are shown in Fig. 27 to be dissimilar in shape. Hence it appears that other states are contributing to the ^{38}Ar state observed, in addition to the analogues of the ^{38}Cl 5^- and 3^- states. This complex structure is consistent with there being two 5^- states near this excitation, as previously reported.[41,56] Consequently, no comparison can be made for the ^{38}Ar 11.300 MeV and ^{38}Cl 0.691 MeV states.

b. ^{38}Ar 13.332 MeV - ^{38}Cl 2.752 MeV states. The angular distributions observed for the ^{38}Ar 13.332 MeV and ^{38}Cl 2.752 MeV states are found, within statistics to exhibit essentially the same shapes (see Fig. 27). From this, and from energy systematics, these states are tentatively assigned as T=2 analogues.

Although identical, the angular distributions are insufficiently distinctive to permit a spin assignment from these data. Since the spins of these states are unknown, it is not possible to suggest any configurations, however, the known negative parity of the ^{38}Cl 2.752 MeV state[41] means these states must be formed by $j_1 j_2$ pickup. Calculations shown in the preceeding section show R_c is in the range of $0.6 \rightarrow 0.4$ for simple configurations, but is equal to ~ 0.9 for j^2 pickup.

The experimental cross section ratio observed for these states is $R_x(t/^3He)=0.43\pm0.10$ which is consistent only with $j_1 j_2$ pickup.

Additional evidence for the $j_1 j_2$ character of these states is obtained from the reaction $^{40}Ar(d,\alpha)^{38}Cl$. The ^{38}Cl 2.752 MeV is observed to be a very strongly excited state in the spectrum. For reasons discussed previously, this is consistent with a $j_1 j_2$ character of this state.

c. ^{38}Ar 13.700 MeV - ^{38}Cl 3.190 MeV states. The next states observed in mass-38 which, based on similar angular distributions and energy systematics could be tentatively assigned as T=2 analogue states, were observed in ^{38}Ar and ^{38}Cl at excitations of 13.700 MeV and 3.190 MeV respectively. The distribution shapes of these states are illustrated in Fig. 27.

Again, the angular distributions of the states are not sufficiently characteristic to permit a spin assignment from this work. The experimental cross section ratio for these states if found to be $R_x(t/^3He)=1.12\pm0.20$ which is inconsistent with the $j_1 j_2$ ratios calculated in the previous sections. The calculated ratio for j^2 is, of course, independent of configuration, and is found to be $R_c=0.90$. Since the pickup is j^2 in nature, a positive parity can be assigned because j^2 pickup on even-even targets can produce only positive parity final states.

The j^2 configuration of these states is consistent with the $^{40}Ar(d,\alpha)^{38}Cl$ data, which shows the ^{38}Cl 3.190 MeV state to be populated with an intensity of $\sim$10% of that of the ^{38}Cl 2.752 MeV state discussed in the preceeding section.

C. Coulomb Displacement Energies of Analogue States

1. Calculation of Coulomb Energy Displacements

The potential which describes the Coulomb interaction between nucleons can be expressed in terms of three operators in isospin space, a scalar, a vector and a tensor.[8,57] Using first order perturbation theory, the general expression for the Coulomb energy of a state with A nucleons can be derived from this potential. The result obtained for a state with isospin quantum numbers T and T_z is

$$E_c(A,T,T_z) = E^{(0)}(A,T)+T_zE^{(1)}(A,T)+[3T_z^2-T(T+1)]E^{(2)}(A,T) \qquad (V-1)$$

where $E^{(0)}$, $E^{(1)}$, and $E^{(2)}$ are the isoscalar, isovector and isotensor coefficients. These coefficients, which depend only on A and T are related to the coefficients (a,b,c) of the isobaric multiplet mass equation (IMME):[58]

$$M(A,T,T_z) = a(A,T) + b(A,T)T_z + c(A,T)T_z^2 \qquad (V-2)$$

The IMME has been used successfully to relate the masses of members of an isobaric multiplet, and, with the possible exception of the mass 9 T=3/2 multiplet, no deviations from its predictions have been observed experimentally.[59] Since any charge dependent effect arising from two body forces which can be treated as a simple perturbation also gives rise to only quadratic terms in T_z,[60] the coefficients of the IMME will include not only the effect of the Coulomb force, but also other small effects such as those which might result from the charge dependence.

of nuclear forces. However, the comparison with calculations which include the known charge dependent (Coulomb) effects would yield a magnitude for any additional nuclear charge dependence.

For the purpose of such a comparison, the Coulomb displacement energies can be used. In terms of those quantities defined by Eq. (V-1), the Coulomb displacement energy between neighbouring isobars is given by

$$\Delta E_c(A,T,T_z - 1|T_z) = E_c(A,T,T_z) - E_c(A,T,T_z - 1)$$
$$= E_c^{(1)}(A,T) - 3(2T_z - 1)\, E^{(2)}(A,T) \qquad \text{(V-3)}$$

This quantity is given experimentally by

$$\Delta E_c(A,T,T_z - 1|T_z) = m\,(A,T,T_z - 1) - m\,(A,T,T_z) + \Delta m \qquad \text{(V-4)}$$

where Δm is the neutron-hydrogen mass difference (=0.7824 MeV). Any differences between the calculations using Eq. (V-3) and the experimental quantities given by Eq. (V-4) can be interpreted as arising from non-Coulomb charge-dependent forces. In this work, however, Eq. (V-3) is parameterized according to calculations based on two different coupling schemes. The five parameters used are determined from a fit to the data throughout the entire shell; only the final values obtained for the parameters are used for comparison.

a. Low-seniority limit of the jj-coupling scheme. Using shell model states of configuration j^n and seniority ≤ 2 Hecht[8] has derived theoretical expressions for $E^{(1)}$ and $E^{(2)}$; the representation used is such that each state is defined by the quantum numbers v,t(reduced isospin), J and T. The expressions are given in terms of two-body Coulomb-energy matrix elements

$$V_j' = \left\langle j^2 J' \left| \frac{e^2}{3r_{ij}} \right| j^2 J' \right\rangle \qquad \text{(V-5)}$$

The interaction of the nucleons in the j-shell with those in the core is given by

$$a_c = \sum_{J', j_c} \frac{(2J'+1)}{(2j+1)} \left\langle (jj_c)J' \left| \frac{e^2}{3r_{ij}} \right| (jj_c)J' \right\rangle \qquad \text{(V-6)}$$

In this formulation, there are three parameters to be evaluated, or treated as free; they are a_c, V, and $\bar{V}_2$, where $\bar{V}_2$ is the average seniority = 2 matrix element as defined by

$$\bar{V}_2 = \frac{1}{(2j-1)(j+1)} \sum_{J' \text{ even} > 0} (2J'+1)V_{J'}, \qquad \text{(V-7)}$$

As described below, these expressions have been generalized in the manner described by Jänecke[59] to take into account additional non-Coulomb charge dependent effects and the variation of nuclear radius with mass number. This results in an increase of the number of free parameters to five and should permit direct comparison with experiment.

To illustrate the method used, an isobaric multiplet with configuration j^n and seniority 0 is considered. From Table 1 of Ref. 8,[61] the following expressions are obtained:

$$\left.\begin{aligned} E^{(1)} &= 3a_c + 3b(n-1) + 12c(j+1) && \text{(a)} \\ E^{(2)} &= b + c + \frac{c[(n-2j-1)^2 - (2j+4)^2]}{(2T-1)(2T+3)} && \text{(b)} \end{aligned}\right\} \qquad \text{(V-8)}$$

where a_c has been defined in Eq. (V-6) and

$$b = \frac{2(j+1)\cdot\bar{V}_2 - V_0}{2(2j+1)} \qquad \text{and} \qquad c = \frac{V_0 - \bar{V}_2}{4\cdot(2j+1)} \qquad \text{(V-9)}$$

Using these expressions and Eq. (V-3), a formula for the Coulomb displacement energy depending on a_c, b, and c could be derived. However, the additional charge dependent effects are expected to have a significant effect upon the parameter c. In particular, the electromagnetic spin-orbit interaction[62] between nucleons is expected to increase this parameter up to 40%, and its increase in the tensor coefficient should exceed that in the vector coefficient by a factor $1.7(=(g_p-g_n)/g_p)$. Hence the quantity c in Eq. (V-8) is replaced by two parameters, $c^{(1)}$ in Eq. (V-8a), and $c^{(2)}$ in Eq. (V-8b). It should be noted that the parameters $c^{(1)}$ and $c^{(2)}$ will also contain the charge-dependent effects of the nuclear force.

Also considered in the parameterization was the variation of charge radius with mass number, since this affects the values of matrix elements in Eqs. (V-5 and V-6). The radius variation used in this work was

$$R = R_0[1 + \frac{1}{3} \cdot \lambda \cdot \frac{n}{N}] \equiv R_0\, f(\lambda) \qquad \text{(V-10)}$$

where n is the number of active nucleons (=A-N); N is the number of nucleons in the core (=4 for (1p)-shell and =16 for (1d5/2)-shell) and R_0 is the charge radius of the core. Equation (V-10) is the first term of a binomial expansion and, for λ=1 this variation of R corresponds approximately to $A^{1/3}$. In this work λ has been treated as a free parameter.

Having modified Eq. (V-8) in this manner, Eq. (V-3) can be used to give a final expression for the Coulomb displacement energy:

$$\Delta E_c(A,T,T_z\text{-}1|T_z) = [\alpha+\beta(\frac{n}{2} - T_z) + A_1\gamma^{(1)} + A_2\gamma^{(2)}][f(\lambda)]^{-1} \qquad \text{(V-11)}$$

where

$$\alpha = 3a_c + 12c^{(1)}(j_1 + 1)$$

$$\beta = 6b$$

$$\gamma^{(i)} = 3c^{(i)} \qquad i = 1,2$$

The general formulae[63] for j^n configurations with $\nu \leq 2$ are given in Table 13; they were all calculated using expressions for $E^{(1)}$ and $E^{(2)}$ given in Table 1 of Ref. 8. Note that the expressions for ν=2 cases have been simplified using the fact that, to a good approximation[59] $V_{J'}=\bar{V}_2$ for all J'(even) $\geq$ 2. For the particular example chosen (ν=0) the coefficient A_1=0 and the expression for A_2 is given by the first line of Table 13.

Table 13. Coefficients in the expansion of the Coulomb displacement energy; $\Delta E_c(A,T,T_z-1|T_z) = [\alpha + (\frac{n}{2} - T_z)\beta + A_1\gamma^{(1)} + A_2\gamma^{(2)}][f(\lambda)]^{-1}$, where A_1 and A_2 are listed for configurations j^n in the seniority scheme.

v	t	J	A_1	A_2
0	0	0	0	$-(2T_z-1)\left[1 + \frac{(2j+4)^2-(n-2j-1)^2}{(2T-1)(2T+3)}\right]$
1	1/2	j	$\frac{(n-2j-1)-(-)^{n/2-T}(2T+1)(2j+3)}{2T(T+1)}$	$-(2T_z-1)\left[1 + \frac{(2j+3)^2-(n-2j-1)^2}{4T(T+1)}\right]$
2	0	odd	0	$-(2T_z-1)\left[1 + \frac{(2j+2)^2-(n-2j-1)^2}{(2T-1)(2T+3)}\right]$
2	1	even,>0	$\frac{2(n-2j-1)}{T(T+1)}$	$-(2T_z-1)\left[1 + \frac{(2j+1)(2j+3)-(n-2j-1)^2}{T(T+1)} - \frac{3(2j+2)^2-3(n-2j-1)^2}{(2T-1)(2T+3)}\right]$

b. The Wigner supermultiplet scheme. Hecht[8] has pointed out that approximation similar to those made in the seniority scheme should also be valid for other coupling schemes, and he has derived general algebraic expressions for $E^{(1)}$ and $E^{(2)}$ assuming certain configurations in the Wigner supermultiplet scheme.[64] States in this coupling scheme are characterized by the quantum numbers L, S, T and $[\tilde{f}]$ where $[\tilde{f}]$ is the partition which characterized a particular irreducible representation[65,66] of U_4 symmetry. The form of $[\tilde{f}]$ is given by $[\tilde{f}]=[x_1,x_2,x_3,x_4]$ where $\sum_{i=1}^{4} x_i=n$, the number of nucleons in the major oscillator shell and $x_i \geq x_k$ when $i < k$.

The supermultiplet quantum numbers of the ground states have been predicted by Jahn[65] for nuclei through the (p)- and (d)-shells. Using these results and the formulae in Ref. 8, general expressions for the Coulomb displacement energies applying to most ground state supermultiplets throughout the shell have been derived. The following example will illustrate the method used: consider states for which $(\frac{n}{2} - T)$ and A are both even (i.e., analogues to ground states of even-even nuclei). These states must be $^1S_0$, and Table 2 of Ref. 65 indicates that all such states in the (p)- and (d)-shells are characterized by partitions of the type [x+y, x+y, x, x]; for example, the d^6 state with T=1 is [42]≡[2211]. The expressions for $E^{(1)}$ and $E^{(2)}$ given in Table 1 of Ref. 8 are for partitions of this type, and the general expression for the Coulomb displacement energy was obtained in the same manner as described for the seniority scheme. The resulting expression has the identical form as Eq. (V-11), viz:

$$\Delta E_c(A,T,T_z - 1|T_z) = [\alpha+\beta(\tfrac{n}{2} - T_z) + A_1\gamma^{(1)}+A_2\gamma^{(2)}][f(\lambda)]^{-1} \qquad (V\text{-}12)$$

but in this case,

$$\alpha = 3a_c' + 18c^{(1)'}$$

$$\beta = 6b'$$

$$\gamma^{(i)} = 3c^{(i)'} \qquad i = 1,2$$

Note that a_c', b', and $c^{(i)'}$ are primed values, and appear in the notation of Ref. 8. The general formulae for A_1 and A_2 for most ground state configurations are given in Table 14; the only cases where these formulae are inadequate are for those multiplets based on the ground states of odd-odd nuclei with $T > 1$. For the example being considered, the value for A_1=0 and for A_2 is given by the first line in Table 14.

A comparison of the formulae listed in Tables 13 and 14 shows a number of striking similarities, in spite of the different character of the coupling schemes used in their derivation. This, in view of the similarity of the general expressions [Eqs. (V-11 and V-12)] for the Coulomb displacement energies, suggests that these expressions might also apply in some more realistic intermediate coupling scheme.

2. Coulomb Displacement Energies-Comparison with Experiment

The experimentally determined Coulomb displacement energies throughout the total (1p)- and the (1d5/2)-shells, including those determined from this work are summarized in Tables 15 and 16. The values quoted represent the weighted averages of all the data given in the references, and are intended to be complete up to September 1968.

Table 14. Coefficients in the expansion of the Coulomb displacement energy, $\Delta E_c(A,T,T_z-1|T_z) = [\alpha + (\frac{n}{2} - T_z)\beta + A_1\gamma^{(1)} + A_2\gamma^{(2)}][f(\lambda)]^{-1}$ where A_1 and A_2 are listed for various ground state configurations in the (P-) and (d-) shells using the supermultiplet scheme. The Wigner supermultiplet quantum numbers are denoted by $[\tilde{f}]$.

$[\tilde{f}]$	S	J	$\frac{n}{2}$ -T	x	A_1	A_2
$[x+y,x+y,x,x]^a$	0	0	even	$\frac{n-2T}{4}$	0	$(2T_z-1)\left[1-\frac{2T+5}{2T-1}\right]$
$[x+y,x+y,x+1,x]$	1/2	3/2,5/2	odd	$\frac{n-2T-2}{4}$	$-(-)^{\frac{n}{2}-T}\frac{3}{T}$	$(2T_z-1)\left[1+\frac{3-(2T+3)(2T+5)}{4T(T+1)}\right]$
$[x+y,x+y-1,x,x]$	1/2	3/2,5/2	even	$\frac{n-2T}{4}$		
$[x+2,x+1,x+1,x]^b$	0,1	2,3,4	odd	$\frac{n-4}{4}$	0	$(2T_z-1)\left[6-4S(S+1)\right]$

(a) $T > 0$

(b) Only applies to ground states when $T = 1$

Table 15. Experimental and calculated Coulomb displacement energies for (1p) shell data using the supermultiplet scheme.

A	T	T_z	J^π	Experimental $\Delta E_c(A,T,T_z-1\|T_z)$ (keV)	Ref.	All $J^\pi=\frac{3}{2}^-$, and even A data ΔE_c(calc.) (keV)	$\delta(\Delta E_c)$* (keV)	All $(J^\pi;T)=(\frac{3}{2}^-;\frac{3}{2})$ data ΔE_c(calc.) (keV)	$\delta(\Delta E_c)$* (keV)
5	1/2	1/2	3/2-	1007.4±41.6†	(a)	760.0	-247.4		
7	1/2	1/2	3/2-	1644.0±1.5	(a)	1655.7	11.7		
9	1/2	1/2	3/2-	1850.5±1.6	(a)	1888.4	37.9		
11	1/2	1/2	3/2-	2763.1±1.2	(b)	2666.9	-96.2		
13	1/2	1/2	3/2-	2830.0±10.0	(c,d)	2842.7	12.7		
15	1/2	1/2	3/2-	3397.9±5.6	(c,e)	3528.0	130.1		
6	1	1	0^+	834.6±5.7	(a)	836.2	1.6		
10	1	1	0^+	1967.6±3.0	(a)	1935.2	-32.4		
14	1	1	0^+	2839.2±1.2	(c,d)	2867.9	28.7		
6	1	0	0^+	1508.0±6.5	(a)	1599.4	91.4		
10	1	0	0^+	2692.7±2.7	(a,f)	2636.0	-56.7		
14	1	0	0^+	3613.0±1.3	(d,g)	3515.7	-97.3		
7	3/2	3/2	3/2-	859.7±50.0	(h,i)	787.6	-72.1	866.3	6.6
9	3/2	3/2	3/2-	1559.9±21.0	(a,i)	1448.6	-111.3	1574.1	14.2
13	3/2	3/2	3/2-	2452.4±5.1	(c,i)	2436.9	-15.5	2453.5	1.1
7	3/2	1/2	3/2-	1370.0±50.0	(i)	1451.1	81.1	1402.7	32.7
9	3/2	1/2	3/2-	2114.5±7.3	(i)	2084.4	-30.1	2101.9	-12.6
13	3/2	1/2	3/2-	2962.0±5.1	(i)	3023.6	61.6	2965.0	3.0
7	3/2	-1/2	3/2-	1947.5±105.0	(i,j)	2114.6	167.1	1939.1	-8.4
9	3/2	-1/2	3/2-	2623.8±7.2	(i,k)	2720.2	96.4	2629.8	6.0
13	3/2	-1/2	3/2-	3481.2±70.0	(i,l)	3610.3	129.1	3476.5	-4.7
12	2	1	0^+	2242.2±122.0	(i)	2457.4	215.2		
8	1	1	$2^{+\ddagger}$	3541.7±2.1	(a)	3549.0	7.3		
12	1	1	$1^{+\ddagger}$	5536.6±5.3	(b,c)	5513.0	-23.6		
				χ^2/degree of freedom =		609.5/18=33.9		2.16/3=0.72	

Table 15 (Continued)

References to Table 15.

* $\delta(\Delta E_c) = \Delta E_c(\text{calc.}) - \Delta E_c(\text{exp.})$

† These are the experimental errors on the values listed. The errors used in the calculation have 10 keV added in quadrature.

‡ These values are double Coulomb energies, which do not depend on S, and hence are included here.

(a) T. Lauritzen and F. Ajzenberg-Selove, Nucl. Phys. 78, 1 (1966).

(b) F. Ajzenberg-Selove and T. Lauritzen, Nucl. Phys. A114, 1 (1968).

(c) C. Maples, G. W. Goth, and J. Cerny, Nucl. Data 2, 429 (1966).

(d) F. Ajzenberg-Selove and T. Lauritzen, Nucl. Phys. 11, 1 (1958).

(e) E. K. Warburton, J. W. Olness, and D. E. Alburger, Phys. Rev. 140, B1202 (1965).

(f) H. Brunnader, J. C. Hardy, and J. Cerny, Phys. Rev. 174, 1247 (1968).

(g) J. M. Freeman, J. G. Jenkins, D. C. Robinson, G. Murray, W. E. Burcham, Phys. Letters 27B, 156 (1968).

(h) R. H. Stokes and P. G. Young, Phys. Rev. Letters 18, 611 (1967).

(i) J. Cerny, Ann. Rev. of Nucl. Sci. 18, 27 (1968).

(j) R. L. McGrath, J. Cerny, and E. Norbeck, Phys. Rev. Letters 19, 1442 (1967).

(k) C. A. Barnes, E. G. Adelberger, D. C. Hensley, and A. B. McDonald, Inter. Nucl. Phys. Conf., 261, R. L. Becker, C. D. Goodman, P. H. Stelson, and A. Zucker, eds., (Academic Press, New York,1967)pp. 1121.

(l) J. Cerny, R. H. Pehl, G. Butler, D. G. Fleming, C. Maples, and C. Détraz, Phys. Letters 20, 35 (1966).

Table 16. Experimental and calculated Coulomb displacement energies for (1d5/2) shell data.

A	T	T_z	J^π	Experimental $\Delta E_c(A,T,T_z-1\|T_z)$ (keV)	Seniority Calculations ΔE_c (keV)	Seniority Calculations $\delta(\Delta E_c)$** (keV)	Supermultiplet Calculations ΔE_c (keV)	Supermultiplet Calculations $\delta(\Delta E_c)$** (keV)
17	1/2	+1/2	5/2+	3542.0±1.0[a]	3542.2	0.2	3542.8	0.6
19	1/2	+1/2	5/2+*	4060.8±2.0[b,c]	4104.3	43.5†	4103.2	42.4†
21	1/2	+1/2	5/2+*	4315.3±8.3[b,d]	4316.6	1.3	4314.8	-0.5
23	1/2	+1/2	5/2+*	4850.5±4.7[b]	4861.1	10.6	4860.0	9.5
25	1/2	+1/2	5/2+	5062.5±1.1[e]	5062.6	0.1	5062.2	-0.3
27	1/2	+1/2	5/2+	5592.5±3.2[b]	5590.3	-2.2	5592.8	0.3
18	1	+1	0^+	3478.9±1.0[a,f]	3549.4	70.5†	3510.4	31.5†
20	1	+1	2+	4027.8±8.4[b,g]	4024.9	-2.9	--	--
22	1	+1	0+	4282.1±2.8[b,h]	4279.0	-3.1	4280.0	-2.1
24	1	+1	4+	4783.5±4.6[b,i]	4790.2	6.7	--	--
26	1	+1	0+	5014.8±4.2[b]	5021.1	6.3	5025.0	10.2
18	1	0	0+	4187.6±4.8[a,f]	4142.8	-44.8†	4137.6	-50.0†
20	1	0	2+	4420.9±30.8[b,g]	4386.3	-34.6	--	--
22	1	0	0+	4931.6±20.2[b,h]	4901.2	-30.4	4897.0	-34.6
24	1	0	4+	5148.7±7.7[b,i]	5144.9	-3.8	--	--
26	1	0	0+	5623.2±11.6[b]	5592.8	-30.4	5632.1	8.9
19	3/2	+3/2	3/2+	3528.3±35.9[j,k]	3524.6	-3.7	3501.8	-26.5
21	3/2	+3/2	5/2+	3954.4±9.2[l]	3964.7	10.3	3944.9	-9.5
23	3/2	+3/2	5/2+	4302.7±21.3[j,m]	4268.8	-33.9	4268.4	-34.3
25	3/2	+3/2	5/2+	4743.4±15.8[n]	4707.1	-36.3	4698.2	-45.2

Continued

Table 16. Experimental and calculated Coulomb displacement energies for (1d5/2) shell data.

A	T	T_z	J^π	Experimental $\Delta E_c(A,T,T_z-1\|T_z)$ (keV)	Seniority Calculations ΔE_c (keV)	Seniority Calculations $\delta(\Delta E_c)^{**}$ (keV)	Supermultiplet Calculations ΔE_c (keV)	Supermultiplet Calculations $\delta(\Delta E_c)^{**}$ (keV)
19	3/2	+1/2	3/2+	3980.4±43.0[j,k]	3997.3	16.9	3989.0	8.6
21	3/2	+1/2	5/2+	4440.4±9.2[l]	4439.6	-0.8	4428.1	-12.4
23	3/2	+1/2	5/2+	4726.0±32.7[j,m]	4739.3	13.3	4747.7	21.7
25	3/2	+1/2	5/2+	5161.4±15.3[n]	5166.7	5.3	5173.6	12.2
20	2	+2	0+	3484.4±33.9[a,j]	3516.0	31.6	3481.7	-2.7
24	2	+2	0+	4292.4±29.7[a,j,q]	4259.9	-33.1	4245.5	-46.9
20	2	+1	0+	3971.4±33.0[a,j,p]	3986.4	15.00	3966.8	-4.6
24	2	+1	0+	4724.4±28.4[r]	4721.0	-3.4	4722.8	-1.6
20	1	+1	2+	8448.7±31.9[‡,b]	--	--	8418.8	-29.9
24	1	+1	4+	9932.2±9.0[‡,b]	--	--	9923.0	-9.2

* These states are not ground states but the lowest excited $5/2^+$ states.

** $\delta(\Delta E_c) = \Delta E_c(\text{calc.}) - \Delta E_c(\text{exp.})$

† These values were not used in the χ^2 fit.

‡ These values are double Coulomb displacement energies.

Continued

Table 16. Continued.

[a] C. C. Maples, G. W. Goth, and J. Cerny, Nucl. Data A2, 429 (1966).

[b] P. M. Endt and C. Van der Leun, Nucl Phys. A105, 1 (1967).

[c] F. Ajzenberg-Selove and T. Lauritzen, Nucl. Phys. 11, 1 (1959); J. W. Olness, A. R. Poletti and E. K. Warburton, Phys. Rev. 161, 1131 (1967).

[d] T. Lauritzen and F. Ajzenberg-Selove, Nucl. Data Sheets, May (1962).

[e] C. Van der Leun, private communication (1968) giving the mass excesses of ^{25}Al and ^{25}Mg as -8.9145±0.0021 MeV and -13.1947±0.0018 MeV respectively.

[f] A. E. Blaugrund, D. H. Youngblood, G. C. Morrison, and R. E. Segel, to be published; E. K. Warburton, J. W. Olness, and A. R. Poletti, Phys. Rev. 155, 1164 (1967).

[g] R. D. McFarlane and A. Siivola, Nucl. Phys. 59, 168 (1964); J. D. Pearson and R. H. Spear, Nucl. Phys. 54, 434 (1964).

[h] A. Gallman, G. Frick, E. K. Warburton, D. E. Alberger, and S. Hechtl, Phys. Rev. 163, 1190 (1967).

[i] A. J. Armini, J. W. Sunier, and J. R. Richardson, Phys. Rev. 165, 1194 (1967).

[j] This work.

[k] J. L. Wiza, and R. Middleton, Phys. Rev. 143, 676 (1965); F. A. El Bedewi, M. A. Fawzi, and N. S. Rigk, Proc. Int'l. Conf. on Nucl. Phys. (Paris, 1964); R. Moreh, and A. A. Jaffe, Proc. Phys. Soc. (London) 84, 330 (1964).

[l] H. Brunnader, J. C. Hardy, and J. Cerny, to be published; D. C. Hensley, Phys. Lett. 27B, 644 (1968); A. B. McDonald and E. G. Adelberger, Phys. Lett. 26B, 380 (1968).

[m] S. Mubarakmand and B. E. F. Macefield, Nucl. Phys. A98, 97 (1967) and private communication from B. E. F. Macefield; J. Dubois, Nucl. Phys. A104, 657 (1967).

Continued

Table 16. Continued.

[n]J. C. Hardy and D. J. Skyrme in Isotopic Spin in Nucl. Phys., (J. D. Fox and D. Rohson, ed. Academic Press, N. Y. and London) (1966) pp. 701; D. Denhard, and J. L. Yntema, Phys. Rev. 160, 964 (1967); G. C. Morrison, D. H. Youngblood, R. C. Bearse and R. E. Segel, to be published. These values have been appropriately corrected for the changes noted in Ref. e.

[p]E. Adelberger, and A. B. McDonald, Phys. Lett. 24B, 270 (1967); H. M. Kuan, D. W. Heikkinen, K. A. Snover, F. Riess, and S. S. Hanna, Phys. Lett. 25B, 217 (1967); R. Block, R. E. Pixley, and P. Trüol, Phys. Lett. 25B, 215 (1967).

[q]F. G. Kingston, R. J. Griffiths, A. R. Johnston, W. R. Gibson, and E. A. McClatchie, Phys. Lett. 22, 458 (1966).

[r]E. Adelberger, and A. B. McDonald, Phys. Lett. 24B, 270 (1967); F. Riess, W. J. O'Connell, D. W. Heikkinen, H. M. Kuan, and S. S. Hanna, Phys. Rev. Lett. 19, 367 (1967).

The errors given for each Coulomb displacement energy are the experimental uncertainties. The tables only include those multiplets for which, in terms of the simple shell-model, all active nucleons can be considered to be entirely within the same [(1p) or (1d5/2)] shell. In addition, for each value of A and T, only multiplets built on the ground states of $T=T_z$ members are considered; an exception arises for those odd A nuclei whose spins and parities are not $3/2^-$ for the (1p) shell case, and $5/2^+$ for the (1d 5/2) shell; here the lowest $3/2^-$ ($5/2^+$) states were used. In the T=3/2 multiplets for A=11 and 19 the $3/2^-$ ($5/2^+$) states are not known for all members. As a result, in mass 11, the T=3/2 states were not included in the analysis of the (1p) shell, and in mass 19, the $(J^\pi;T)=(3/2^+;3/2)$ states were used instead in the analysis of the (1d5/2) shell. In all subsequent fitting, these two mass 19 T=3/2 displacement energies were both included and removed; at no time was the overall fit changed by their inclusion. The last two items in each table are double Coulomb displacement energies which are denoted by $\Delta E_c(A,T,T_z-2|T_z)$.

In Eq. (V-11) for the seniority scheme, and Eq. (V-12) for the supermultiplet scheme, the Coulomb displacement energy is given in terms of five parameters: α, β, $\gamma^{(1)}$, $\gamma^{(2)}$ and λ. These equations have been fitted to the data presented in Tables 15 and 16 by treating all five parameters as free, and minimizing the function χ^2, where χ^2 is defined by:

$$\chi^2 = \sum_{i=1}^{M} \left\{ \frac{\Delta E_c(\text{calc})_i - \Delta E_c(\text{exp.})_i}{\sigma(\text{exp.})i} \right\}^2 \qquad \text{(V-13)}$$

M is the total number of experimental values fit and $\sigma(\text{exp})$ is the experimental error. If the averaged experimental errors in Tables 15 and 16 represent a good approximation to the true standard deviations, then the chi-square test can be applied to the final χ^2_{min} obtained by minimizing Eq. (V-13). If all the single displacement energies for the (1d5/2) shell (Table 16) are used, M=28, and the number of degrees of freedom of the assumed chi-square distribution is (28-5-1)=22. Under these conditions for an acceptable fit, χ^2_{min} should lie between 11 and 37. Since the method of determining experimental errors is inconsistent between different authors, it seems likely that these errors are, at best, only an indication of the true standard deviations. Consequently, the chi-square test should, in this work, be interpreted somewhat loosely.

a. Fitting of seniority and supermultiplet schemes to the (1d5/2)-shell. The variation of χ^2 as a function of λ for this shell is shown in Fig. 37 for three cases in both the seniority and supermultiplet schemes. Each point on the graph corresponds to the minimization of χ^2 as a function of α, β, $\gamma^{(1)}$ and $\gamma^{(2)}$ for a particular choice of λ. The three cases considered are:

(I) For the seniority scheme, all single displacement energies listed in Table 16 were used. For the supermultiplet scheme all single displacement energies were used except those for the T=1 multiplets of A=20 and 24. As indicated by the fourth line in Table 14, such multiplets can have either S=0 or 1, and the calculated displacement energies depend on this choice. However, when T_z=1, the double Coulomb displacement energy is independent of S, and consequently the four single displacement energies

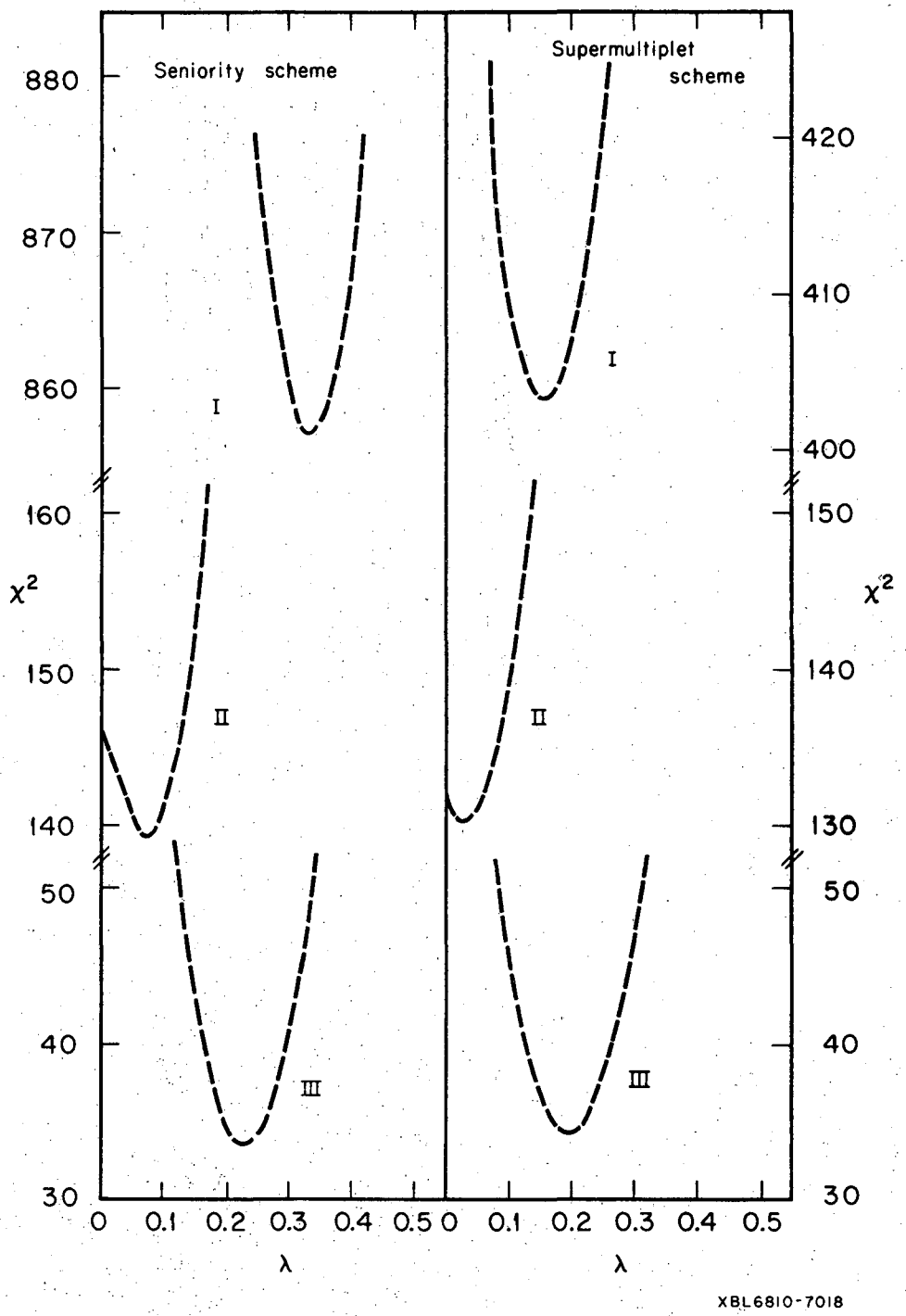
Seniority scheme
Supermultiplet scheme
880
870
860
160
150
140
50
40
30
420
410
400
150
140
130
50
40
30
I
II
III
χ^2
0 0.1 0.2 0.3 0.4 0.5
λ
XBL6810-7018

Figure 37

were replaced by the two double values appearing at the end of the table.

(II) The same values were used as in (I) except the two energies for A=18, T=1 were removed.

(III) The same values were used as in (II) except the single energy for A=19, T=1/2 was removed.

The removal of additional data did not improve the observed χ^2 per degree of freedom.

It is evident from Fig. 37 that both (I) and (II) give totally unacceptable χ^2_{min}. For case (III), the seniority and supermultiplet calculations involve, respectively, 19 and 17 degrees of freedom for which the range of acceptability of χ^2 is 8 to 34 and 7 to 31. In view of the reservations about χ^2 noted earlier, case (III) is deemed to be an acceptable fit for both schemes.

The values of the parameters for the minimum χ^2 for case (III) in the (1d5/2)-shell, using both the seniority and supermultiplet calculations are summarized in Table 17a; the displacement energies calculated using these parameters are listed in columns 6 and 8 of Table 16. Excellent agreement is obtained between the calculated displacement energies, and also between the calculated and experimental values.

The anomalous behavior of the A=18 triplet appears to be analogous to the A=42 case,[57,67] both nuclei corresponding to n=2 in their respective shells (1d5/2 and 1f7/2). The behavior of both may be due to isospin mixing, but it is then unclear why only these multiplets are affected.

Table 17. Parameters obtained from fitting Coulomb displacement energies.

(a) 1d 5/2 Shell Seniority and Supermultiplet Scheme

Quantity	Value from least squares fit using: Seniority Scheme	Supermultiplet Scheme
λ	0.23 ± 0.03*	0.19 ± 0.03*
α	3673 ± 3 keV	3643 ± 3 keV
β	419 ± 6 keV	421 ± 6 keV
$\gamma^{(1)}$	8.14 ± 0.09 keV	14.40 ± 0.12 keV
$\gamma^{(2)}$	6.41 ± 0.03 keV	17.44 ± 0.15 keV

* This corresponds to an increase of ~9% in the p-p interaction radius from the beginning to the end of the shell.

(b) 1p shell Supermultiplet Scheme only.

Quantity	Value from least squares fit using: All $J^{\pi} = 3/2^{-}$ & even A data	All $(J^{\pi};T) = (3/2^{-};3/2)$ data
λ	0.28 ± 0.03	0.10 ± 0.03
α	941.9 ± 5 keV	1065.2 ± 6 keV
β	665.5 ± 6 keV	498.9 ± 5 keV
$\gamma^{(1)}$	27.4 ± 0.2 keV	63.2 ± 0.5 keV
$\gamma^{(2)}$	11.1 ± 0.1 keV	12.7 ± 0.1 keV

Another possible explanation is suggested by the poor agreement for A=19, where wave function calculations show strong admixtures of higher shells. Such admixtures appear to be appreciable only at the beginning of the (1d5/2)-shell.

b. Fitting of the supermultiplet scheme to the (1p)-shell. The seniority scheme was not used to fit the (1p)-shell data because it does not apply over the two (1p3/2) and (1p1/2) subshells. Also, due to the extremely high accuracy of some of the data in this shell, the χ^2 was strongly influenced by these values. To eliminate this strong dependence on such limited data, 10 keV were added in quadrature to all experimental errors prior to fitting the data. (Table 15 shows only the experimental error.)

The variation of χ^2 as a function of λ for the (1p)-shell was observed to be similar to that shown in Fig. 37. In this shell, only two cases were considered.

(I) All the single displacement energies listed in Table 15 except for mass 8 and 12, which for reasons identical to those discussed for mass 20 and 24, were replaced by their respective double displacement energies.

(II) All the single displacement energies for the $(J^{\pi};T)=(3/2^{-};3/2)$ data.

The values obtained for the parameters in the (1p)-shell using the supermultiplet scheme for the two cases are given in Table 17b. The calculated displacement energies obtained using these parameters are given in columns 6 and 8 of Table 15. The χ^2 per degree of freedom for

case (I) was found to be 33.9 and the χ^2 per degree of freedom for case (II) was found to be 0.72; both calculations were done with 10 keV added in quadrature to the experimental errors. A comparison of the calculations and the experimental data shows good agreement can be obtained using only the T=3/2 data.

The relatively poor fit (average error ~80 keV) obtained for case (I) is not surprising in view of the particle instability and strong isospin mixing which exists in some light nuclei. It appears likely that the unbound character of both mass 5 nuclei may give rise to significant Thomas-Ehrman shifts, that could readily account for the deviations observed.

Similarly, the instability of ^{6}Be appears to contribute to the larger deviation observed for the ^{6}Li-^{6}Be displacement energy as compared to that of the ^{6}He-^{6}Li displacement. The average error for the mass 7 T=3/2 quartet is also observed to be larger, even in the good fit in case (II). Because it was necessary to use excited states in the case of the A=13 and A=15 T=1/2 doublets, the simple approximation of the cancellation of core contributions may not be valid. Finally, Jänecke[68] has shown in a detailed analysis of T=3/2 and T=2 states that the observed deviations for these Coulomb displacements can be at least partly attributed to isospin mixing. The good fit obtained for case (II), which uses only the T=3/2 data, may indicate this mixing is strongly dependent on T but not A. The range of data fit, however, is relatively small.

3. Mass Predictions

Using the parameters listed in Table 17, it is possible to calculate any Coulomb displacement energy within the (1p)- and (1d5/2)-shells. Thus, if the mass of any member of a multiplet is known, the masses of the other members can readily be predicted. The masses of eight, as yet unmeasured, neutron deficient nuclei have been calculated in this manner. The results for both schemes are given in Table 18,[69] where the quoted errors include only the experimental error of the masses upon which the prediction is based. For example, the mass of ^{25}Si is obtained by adding the displacement energy, minus the neutron-hydrogen mass difference (0.7824 MeV) to the mass of the T=3/2 analogue state in ^{25}Al; since the experimental error quoted on that state is ±8 keV, that is the error quoted in Table 18. The agreement between calculations made using both coupling schemes is found to be very good; the worst deviation noted was 48 keV for ^{24}Si. Also shown in Table 18 are the mass predictions by Kelson and Garvey,[69] which are found to be consistently lower, except for mass 8.

Based on the predicted masses given in Table 18, the unreported nuclei, ^{20}Mg and ^{24}Si are expected to be stable since their last proton is bound by more than 2.70 MeV. The nuclei ^{22}Al and ^{23}Al are predicted to be stable to proton emission by ∿0.16 MeV, while the nuclei ^{19}Na and ^{8}C are predicted to be unstable by 0.36 and 4.00 MeV, respectively.

In a similar manner, the excitation energies of T=2 states in some T_z=0 and ±1 nuclei have been calculated, and the results are

Table 18. Mass predictions for neutron deficient nuclei within the (1p)- and (1d 5/2)-shells.

Nuclues	Mass excess calculated using: Seniority Scheme	Supermultiplet Scheme	Garvey-Kelson Prediction[a]
	(MeV ± keV)‡	(MeV ± keV)‡	
^{8}C	———	35.62 ± 120(35.54 ± 120)[b]	35.79
^{19}Na	12.965 ± 25*	12.968 ± 25*	12.87
^{20}Mg	17.509 ± 2	17.510 ± 2	17.40
^{21}Mg	10.916 ± 7	10.910 ± 7	10.79
^{22}Al	18.059 ± 30	———	17.93†
^{23}Al	6.743 ± 25	6.758 ± 25	6.71
^{24}Si	10.765 ± 5	10.813 ± 5	10.72
^{25}Si	3.828 ± 8	3.804 ± 8	3.77

‡ The errors quoted only include the experimental error in the masses upon which the prediction is based.

*The ground state mass excess is calculated assuming that the lowest $3/2^+$ state in ^{19}Na is at 0.095 MeV, as in its mirror, ^{19}O.

†This value is calculated for the Garvey-Kelson mass prediction using the new value for ^{22}F. [70]

(a)I. Kelson and G. T. Garvey, Phys. Lett. 23, 689 (1966).

(b)The value in parenthesis is calculated using the supermultiplet scheme and the $(J^{\pi};T) = (3/2^-; 3/2)$ data. The other value is based on the total $J^{\pi} = 3/2^-$ and even A data.

tabulated in Table 19 for the (1p)-shell. The T=2 state in ^{8}Be can decay through only one isospin allowed channel, to ^{6}He + 2p, to which it is predicted unbound by ~0.16 MeV. The T=2 state excitations predicted for nuclei in the (1d5/2) shell are given in Table 20. The mass-22 multiplet is assumed to have seniority=2, and consequently the relevant predictions for the T=2 excited states in the T_z=0 and ±1 nuclei depend upon whether the J of these states is even or odd. Since the ^{22}F ground state[70] probably has $J=1^{+}$, the predictions for the odd-J case are more likely correct.

Finally, the mass differences of all remaining members of multiplets within the (1p) and (1d5/2) shells have been calculated and are given in Tables 21 and 22 respectively. It should be emphasized that the values tabulated here are the mass differences, the neutron-hydrogen mass difference has been included. Thus, for example, if the mass of ^{21}O were known, the mass of its T=5/2 analogue in ^{21}F could be calculated in the seniority scheme by simply adding the value listed in the table; i.e., 2.712 MeV.

Table 19. Predicted excitations of unobserved T=2 analogue states in (1p) shell nuclei using the supermultiplet scheme.

Nucleus	Excitation energy of T=2 state calculated using:	
	All J^{π} = 3/2 & even A data (MeV ± keV)	All $(J^{\pi};T) = (3/2^{-};3/2)$ data (MeV ± keV)†
^{8}Li	10.72 ± 120	10.88 ± 120
^{8}Be	27.40 ± 120	27.59 ± 120
^{8}B	10.73 ± 120	10.85 ± 120

†The errors quoted only include the experimental errors in the masses upon which the prediction is based. (ie. ^{8}He mass excess = 31.65 ± 0.12 MeV).

Table 20. Predicted excitations of unobserved T=2 analogue states in $(1d_{5/2})$-shell nuclei.

Nucleus	J	Excitation energy of T = 2 state calculated using: Seniority scheme (MeV±keV)†	Supermultiplet scheme (MeV±keV)†
^{20}Na	0^+	6.492 ± 30	6.486 ± 30
^{22}Ne	even	14.011 ± 30*	-
	odd	13.987 ± 30	-
^{22}Na	even	14.760 ± 30	-
	odd	14.727 ± 30	-
^{22}Mg	even	13.978 ± 35	-
	odd	13.953 ± 35	-
^{24}Al	0^+	5.954 ± 9	5.971 ± 9

†The errors quoted only include the experimental error in the masses upon which the predictions depend.

*All mass-22 predictions depend upon the mass excess of ^{22}F being 2.828± 0.030 MeV.[70]

Table 21. Predicted mass differences between members of higher (>3/2) isobaric multiplets in the (1p)-shell using the supermultiplet scheme.

T	Mass difference between analogue states in:	Supermultiplet Scheme All $J = 3/2^-$; even A data (MeV)	All $(J;T) = (3/2^-;3/2)$ data (MeV)
2	$^{12}B^* - {}^{12}Be$	1.077	1.080
2	$^{12}C^* - {}^{12}B^*$	1.675†	1.596
2	$^{12}N^* - {}^{12}C^*$	2.273	2.111
2	$^{12}O - {}^{12}N^*$	2.872	2.627
5/2	$^{9}Li^* - {}^{9}He$	-0.016	0.109
5/2	$^{9}Be^* - {}^{9}Li^*$	0.604	0.617
5/2	$^{9}B^* - {}^{9}Be^*$	1.224	1.125
5/2	$^{9}C^* - {}^{9}B^*$	1.843	1.634
5/2	$^{9}N - {}^{9}C^*$	2.463	2.142
5/2	$^{11}Li^* - {}^{11}He$	0.582	0.710
5/2	$^{11}Be^* - {}^{11}Li^*$	1.177	1.210
5/2	$^{11}B^* - {}^{11}Be^*$	1.772	1.710
5/2	$^{11}C^* - {}^{11}B^*$	2.367	2.210
5/2	$^{11}N - {}^{11}C^*$	2.962	2.711
3	$^{10}Li^* - {}^{10}He$	-0.015	0.159
3	$^{10}Be^* - {}^{10}Li^*$	0.593	0.664
3	$^{10}B^* - {}^{10}Be^*$	1.200	1.168
3	$^{10}C^* - {}^{10}B^*$	1.807	1.672
3	$^{10}N^* - {}^{10}C^*$	2.414	2.176
3	$^{10}O - {}^{10}N^*$	3.021	2.681

†This value has been experimentally measured and has been included in the data fit.

Table 22. Predicted mass differences between different members of T = 5/2 and 3 isobaric multiplets in the $(1d_{5/2})$ shell.

T	Mass-difference between analogue states in:	Mass difference caluclated with Seniority scheme (MeV)	Supermultiplet scheme (MeV)
5/2	^{21}Al-$^{21}Mg^*$	4.492	4.508
5/2	$^{21}Mg^*$-$^{21}Na^*$	4.047	4.054
5/2	$^{21}Na^*$-$^{21}Ne^*$	3.602	3.600
5/2	$^{21}Ne^*$-$^{21}F^*$	3.157	3.145
5/2	$^{21}F^*$-^{21}O	2.712	2.691
5/2	^{23}Si-$^{23}Al^*$	4.893	4.911
5/2	$^{23}Al^*$-$^{23}Mg^*$	4.452	4.460
5/2	$^{23}Mg^*$-$^{23}Na^*$	4.012	4.010
5/2	$^{23}Na^*$-$^{23}Ne^*$	3.571	3.559
5/2	$^{23}Ne^*$-^{23}F	3.130	3.108
3	^{22}Si-$^{22}Al^*$	4.915	4.937
3	$^{22}Al^*$-$^{22}Mg^*$	4.472	4.484
3	$^{22}Mg^*$-$^{22}Na^*$	4.029	4.032
3	$^{22}Na^*$-$^{22}Ne^*$	3.586	3.579
3	$^{22}Ne^*$-$^{22}F^*$	3.144	3.127
3	$^{22}F^*$-^{22}O	2.701	2.674

VI. SUMMARY AND CONCLUSIONS

The (p,t) and (p,^{3}He) two nucleon transfer reactions have been utilized to produce high-isospin analogue states in (2s-1d) shell nuclei. The results obtained for T=2 (T=3) states in T_z=0 (1) and T_z=1 (2) nuclei are summarized in Table 3. A comparison of the cross sections of these $T_f=T_i+1$ states with that expected from DWBA predictions has shown excellent agreement throughout. As a result, it appears to justify the approximation that small kinematic effects in $B^M_{NL}(k_i,k_f)$ [see Eq. (II-1)] can be neglected when populating analogue states by the (p,t) and (p,^{3}He) reactions. The agreement obtained establishes this comparison as an unambiguous test for such $T_f=T_i+1$ analogue states.

In addition, the (p,t) reaction has been used to extend the known level information throughout the sd shell, particularly on ^{18}Ne and ^{34}Ar. These (p,t) results are summarized in Tables 1 and 5. The characteristic angular distributions observed in the (p,t) reaction permitted the assignment of numerous J^π values throughout the shell.

A detailed comparison of cross sections for analogue states produced in these reactions with $T_f=T_i$ was also carried out. Where the states compared were free of interferences, or where the relative magnitudes of the unresolved states could be predicted, the cross section ratio could indeed be utilized to distinguish between transitions involving j^2 and j_1j_2 pickup, and hence provide information on the structure of the final state. The cross section ratio for j_1j_2 states can in principle be used to provide information on the J^π of a state. However, in the data obtained in this work only a single case lends itself to this interpretation

(^{38}Ar 13.332 MeV - ^{38}Cl 2.752 MeV), and here statistics are inadequate to permit definite conclusions. This method could prove to be more useful in higher A nuclei.

Using the expressions for Coulomb energies as derived by Hecht,[8] general formulae for displacement energies were derived in two limiting coupling schemes. The resulting formulae were parameterized, and all available (1p)- and (1d5/2)-shell data were fit. Although the parameters obtained can provide information on the non-Coulomb charge dependent forces, the region of data fit was inadequate to permit any conclusions of this nature. The parameters were used, however, to predict a number of masses of unreported nuclei, and the excitations of high T states in these mass regions.

ACKNOWLEDGMENTS

I would like to express my sincere thanks to all those associated with the 88-inch cyclotron for their assistance in numerous ways. It is with particular pleasure that I thank:

Professor Joseph Cerny, my Research Director, for his continued interest, his guidance, and his encouragement in the course of this work;

Dr. John C. Hardy for his invaluable assistance with the experimental work and his many relevant and helpful discussions;

Dr. Sam W. Cosper and Dr. Robert L. McGrath for their assistance with the experimental equipment and their helpful discussions;

Dr. Bernard G. Harvey and Dr. David L. Hendrie for their interest in this work and several helpful discussions;

Mr. Fredrick S. Goulding and Mr. Donald A. Landis for providing the electronic equipment;

Mr. Robert Lothrop for the many detectors used in these experiments;

Mr. Creve C. Maples for this valuable discussions and several computer programs;

Dr. Gordon C. Ball, Dr. Gilbert W. Butler, Dr. Donald G. Fleming, Mr. George W. Goth, Mr. John E. Esterl, Mr. Gordon J. Wozniak, Mr. Richard G. Sextro and Mr. Richard J. Laforge for their assistance in the many shifts of data collection and their interesting and helpful discussions;

Dr. Nolan F. Mangelson, Dr. Chi Chang Lu, Dr. Mary F. Reed, Mr. Joel M. Moss, Mr. Michael S. Zisman and Mr. Joseph D. Sherman for their interest and their helpful discussions;

Mr. Claude Ellsworth and Mrs. Ruth-Mary Larimer for preparing several of the targets used;

Mr. John Meneghetti and his machine shop staff for their technical assistance;

Mr. John Bowen and the cyclotron crew for their co-operation;

My wife, Lili, for her understanding and her encouragement, and her courage to decipher my writing to type the first draft of this thesis.

This work was performed under the auspices of the United States Atomic Energy Commission.

REFERENCES

1. N. K. Glendenning, Ann. Rev. Nucl. Sci. 13, 191 (1963); Phys. Rev. 137, B102 (1965); ibid 156, 1344 (1967).

2. J. R. Rook and D. Mitra, Nucl. Phys. 51, 96 (1964).

3. M. H. MacFarlane and J. B. French, Rev. Mod. Phys. 32, 567 (1960).

4. D. G. Fleming, J. Cerny, C. C. Maples and N. K. Glendenning, Phys. Rev. 166, 1012 (1968).

5. J. C. Hardy, D. J. Skyrme and I. S. Towner, Phys. Lett. 23, 487 (1966); J. C. Hardy and I. S. Towner, Phys. Lett. 25B, 98 (1967).

6. J. Cerny, R. H. Pehl and G. T. Garvey, Phys. Lett. 12, 234 (1964).

7. G. W. Butler, J. Cerny, S. W. Cosper and R. L. McGrath, Phys Rev. 166, 1096 (1968).

8. K. T. Hecht, Nucl. Phys. A114, 280 (1968); ibid A102, 11 (1967).

9. C. L. Lin and S. Yoshida, Prog. Theor. Phys. (Tokyo) 32, 885 (1964); E. M. Henley and D. V. L. Yu, Phys. Rev. 133B, 1445 (1964); B. Bayman, Argonne National Laboratory Report, ANL-6878, 1964 (unpublished) p, 335; A. Y. Abul-Magd and M. El Nadi, Nucl. Phys. 77, 182 (1966).

10. A. de Shalit and I. Talmi, Nuclear Shell Theory, (Academic Press, N. Y., 1963).

11. T. A. Brody and M. Moshinsky, Tables of Transformation Brackets, (Monographia del Instituto de Fisica, Mexico, 1960).

12. C. Détraz, J. Cerny and R. H. Pehl, Phys. Rev. Lett. 14, 708 (1965); J. Cerny and R. H. Pehl, Phys. Rev. Lett. 12, 619 (1964).

13. I. S. Towner and J. C. Hardy, Nuclear Physics Laboratory, University of Oxford Report, ref. 19/68, (1968) unpublished.

14. N. M. Hintz, Argonne National Laboratory Report, ANL-6878, 1964 (unpublished) p. 425.

15. G. W. Butler, Thesis, Lawrence Radiation Laboratory Report UCRL-17783, 1967, (unpublished).

16. This material is non-radioactive luminous material manufactured by Shannon Luminous Materials Co., Los Angeles, California.

17. C. C. Maples and J. Cerny, Range Energy Tables, to be published.

18. Havar foil is composed of 42.5% Co, 20.0% Cr, 17.9% Fe, 13.0% Ni, 2.8% W, 2.0% Mo, 1.6% Mn, 0.2% C and trace Be.
It is manufactured by the Hamilton Watch Company, Metals Division, Lancaster, Pa.

19. F. S. Goulding, D. A. Landis, J. Cerny and R. H. Pehl, Nucl. Inst. Methods 31, 1 (1964).

20. LORNA is a data analysis program written by C. C. Maples.

21. H. Brunnader, J. C. Hardy and J. Cerny, Phys. Rev. 174, 1247 (1968).

22. F. Ajzenberg-Selove and T. Lauritzen, Nucl. Phys. A114, 1 (1968).

23. J. H. E. Mattauch, W. Thiele and A. H. Wapstra, Nucl. Phys. 67, 1 (1965); C. C. Maples, G. W. Goth and J. Cerny, Nucl. Data 2A, 429 (1966).

24. R. D. Gill, B. C. Robertson, J. L'Ecuyer, R. A. I. Bell, and H. J. Rose, Phys. Lett. 28B, 116 (1968).

25. E. Adelberger, Thesis, California Institute of Technology, unpublished.

26. J. H. Towle and G. J. Wall, Nucl. Phys. A118, 500 (1968).

27. N. F. Mangelson, B. G. Harvey and N. K. Glendenning, Nucl. Phys. A117, 161 (1968).

28. The program DWUCK was written by D. Kuntz, and modified for two-nucleon transfer reaction using the "zero-range interaction" approximation[1] by J. C. Hardy.

29. S. W. Cosper, H. Brunnader, J. Cerny and R. L. McGrath, Phys. Lett. 25B, 324 (1967).

30. J. W. Butler, L. W. Fagg, and H. D. Holmgren, Phys. Rev. 113, 268 (1959).

31. E. Adelberger and A. B. McDonald, Phys. Lett. 24B, 270 (1967); and erratum, Phys. Lett. 24B, 618 (1967).

32. H. M. Kuan, D. W. Heikkinen, K. A. Snover, F. Riess, and S. S. Hanna Phys. Lett. 25B, 217 (1967).

33. R. Block, R. E. Pixley, and P. Truöl, Phys. Lett. 25B, 215 (1967).

34. S. Mubarakmand, and B. E. F. Macefield, Nucl. Phys. A98, 97 (1967), and private communication to J. C. Hardy.

35. J. Dubois, Nucl. Phys. A104, 657 (1967).

36. G. T. Garvey, J. Cerny, and R. H. Pehl, Phys. Rev. Lett. 12, 726 (1964).

37. F. Riess, W. J. O'Connell, D. W. Heikkinen, H. M. Kuan, and S. S. Hanna, Phys. Rev. Lett. 19, 327 (1967).

38. G. T. Garvey and J. Cerny, to be published.

39. F. G. Kingston, R. J. Griffiths, A. R. Johnston, W. R. Gibson and E. A. McClatchie, Phys. Lett. 22, 458 (1966).

40. Supplied by Union Carbide Nuclear Company, Oak Ridge National Laboratory, Oak Ridge, Tenn.

41. P. M. Endt and C. Van der Leun, Nucl. Phys. A105, 1 (1967).

42. R. G. Miller, and R. W. Kavanagh, Phys. Lett. 22, 461 (1966); and Nucl. Phys. A94, 261 (1967).

43. W. R. McMurray, P. Van der Merve, and I. J. Van Heerden, Nucl. Phys. A92, 401 (1967).

44. M. Hagen, K. H. Maier and R. Michaelsen, Phys. Lett. 26B, 432 (1968).

45. J. Kouloumdjian, J. L'Ecuyer, and R. Fournier, Report No. LYCEN-6830 (1967).

46. M. E. O. de López, J. Rickards, and M. Mazari, Nucl. Phys. 51, 231 (1964).

47. P. R. Chagnon, Nucl. Phys. 59, 257 (1964).

48. J. D. Pearson, and R. H. Spear, Nucl. Phys. 54, 434 (1964).

49. R. D. MacFarlane, and A. Siivola, Nucl. Phys. 59, 168 (1964).

50. J. Cerny, private communication.

51. R. Jahr, J. A. H. Pfleger, and H. Zell, Phys. Lett. 25B, 113 (1967).

52. C. Daum, Nucl. Phys. 51, 244 (1965).

53. R. Jahr, K. Kayser, A. Kostka, and J. P. Wurm, Nucl. Phys. 76, 79 (1966).

54. B. Lawergren, Nucl. Phys. A96, 49 (1967).

55. P. M. W. Glaudemans, G. Weichers, and P. J. Brussaard, Nucl. Phys. 56, 548 (1964).

56. F. C. Erné, W. A. M. Veltman, J. A. J. M. Wintermans, Nucl. Phys. 88, 1 (1966).

57. J. Jänecke, Phys. Rev. 147, 735 (1966).

58. E. P. Wigner, Proc. Robert A. Welch Foundation Conference on Chemical Research 67, edited by W. O. Milligan, (The Robert A. Welch Foundation, Houston, 1958); S. Weinberg and S. B. Treiman, Phys. Rev. 116, 465 (1959); D. H. Wilkinson, Isobaric Spin in Nuclear Physics, edited by J. D. Fox and D. Robson, (Academic Press, New York, 1966) p. 30.

59. J. Jänecke, Nucl. Phys. A114, 433 (1968).

60. D. H. Wilkinson, Isobsric Spin in Nuclear Physics, edited by J. D. Fox and D. Robson, (Academic Press, New York, 1966), p. 30; Phys. Lett. 11, 243 (1964); ibid. 12, 348 (1964); Phys. Rev. Lett. 13, 571 (1964).

61. The formulae given in the two references differ in notation. Those formulae given in Table 1 of Nucl. Phys. A114, 280 (1968) may be shown equivalent to the quantities appearing in Eqs. 86-90 in Nucl. Phys. A102, 11 (1967), by utilizing the relationship:

$$\bar{V}_{even} = \frac{V_o}{j(2j+1)} + \frac{\bar{V}_{2(2j-1)(j+1)}}{j(2j+1)}$$

62. K. T. Hecht, Isobaric Spin in Nuclear Physics, edited by J. D. Fox and D. Robson, (Academic Press, New York, 1966) p. 823.

63. It should be noted that the formulae for $\nu=0$ and $\nu=1$ are simply generalizations of Eqs. 6 and 7 of Reference 59, where they are written exclusively for the (1f 7/2)-shell. The definitions of α,β and $\gamma^{(i)}$ used here are entirely equivalent.

64. E. Wigner, Phys. Rev. 51, 106 (1937).

65. H. A. Jahn, Proc. Roy. Soc. A201, 516 (1950).

66. H. A. Jahn and H. von Wieringen, Proc. Roy, Soc. A209, 502 (1951).

67. J. A. Nolen, J. P. Schiffer, N. Williams, D. von Ehrenstein, Phys. Rev. Lett. 18, 1140 (1967).

68. J. Jänecke, Isospin in Nuclear Physics, Ch. 8, ed. by D. H. Wilkinson, (North Holland publishing Co., Amsterdam)(to be published).

69. I. Kelson and G. T. Garvey, Phys. Lett. 23 689 (1966).

70. R. H. Stokes, and P. G. Young, to be published.

FIGURE CAPTIONS

Fig. 1. The general layout of the 88-inch cyclotron and the Cave 2 external beam facility.

Fig. 2. The detailed diagram of the scatterchamber, gas target and gas handling apparatus used in these experiments.

Fig. 3. A schematic diagram of the electronic setup used in conjunction with the two counter particle identifier: only system 1 is shown in its entirety, system 2 being identical.

Fig. 4. A representative particle identifier spectrum with router gates set as marked on the safety group (1), the triton group (2), the ^{3}He group (3) and the α-particle group (4).

Fig. 5. Energy spectra of the reactions ^{20}Ne(p,t)^{18}Ne and ^{20}Ne(p, ^{3}He)^{18}F, taken at θ_{LAB} = 26.8° for 2570 μCoulombs. The target was a 40:60 mixture of neon and methane, the neon being 99.9% enriched in ^{20}Ne. All peaks whose energies are marked (unbracketed) were used as calibrations.

Fig. 6. Energy spectra of the reactions ^{21}Ne(p,t)^{19}Ne and ^{21}Ne(p, ^{3}He)^{19}F taken at θ_{LAB} = 22.3° for 4880 μCoulombs. The neon target was enriched to 56.3% in ^{21}Ne, and included 21.1% ^{20}Ne and 22.6% ^{22}Ne. All peaks whose energies are marked (unbracketed) were used to establish the calibration.

Fig. 7. Angular distributions of the reactions ^{21}Ne(p,t)^{19}Ne and ^{21}Ne(p, ^{3}He)^{19}F leading to the T = 3/2 analogue states, the

$(p,{}^3He)$ cross sections having been multiplied by 0.93 to correct for kinematic effects. The angular distributions of the reaction $^{21}Ne(p,t)^{19}Ne$ leading to the 4.013 MeV and ground state, are shown for comparison. The dashed curves represent DWBA fits for the L values indicated, using the parameters given in Table 2. The ^{18}Ne g.s. is also shown.

Fig. 8. Energy spectra of the reactions $^{22}Ne(p,t)^{20}Ne$ and $^{22}Ne(p,{}^3He)^{20}F$ taken at $\theta_{LAB} = 36.2°$ for 9280 μCoulombs. The target was a 50:50 mixture of neon and methane, the neon being 92.0% enriched in ^{22}Ne. All peaks whose energies are unbracketed were used to establish the calibration.

Fig. 9. Energy spectra of the reactions $^{25}Mg(p,t)^{23}Mg$ and $^{25}Mg(p,{}^3He)$ ^{23}Na taken at $\theta_{LAB} = 24.1°$ for 970 μCoulombs. The target was 91.5% enriched in ^{25}Mg. All peaks whose energies are marked (unbracketed) were used as calibrations.

Fig. 10. Angular distributions of the reactions $^{25}Mg(p,t)^{23}Mg$ and $^{25}Mg(p,{}^3He)^{23}Na$ leading to the T = 3/2 analogue states, the $(p,{}^3He)$ cross section having been multiplied by 0.92 to correct for kinematic effects. The angular distributions of the (p,t) reaction leading to the $5/2^+$ 0.450 MeV state and to the $3/2^+$ ground states are also shown for comparison. The dashed curves represent DWBA fits for the L values indicated, using the parameters given in Table 2.

Fig. 11. Energy spectra of the reactions $^{26}Mg(p,t)^{24}Mg$ and $^{26}Mg(p,{}^3He)^{24}Na$ taken at $\theta_{LAB} = 22.3°$ for 3200 μCoulombs. The target was 99.2% enriched in ^{26}Mg. All peaks whose energies were marked (unbracketed) were used to establish calibration: see text.

Fig. 12. Energy spectra of the reactions $^{30}Si(p,t)^{28}Si$ and $^{30}Si(p, ^{3}He)^{28}Al$ taken at $\theta_{LAB} = 18.0°$ for 2150 μCoulombs. The target was 89.12% enriched in ^{30}Si; the remaining target components were 10.16% ^{28}Si and 0.72% ^{29}Si. The calibration was established using the resolved known states shown.

Fig. 13. Angular distributions of the reactions $^{30}Si(p,t)^{28}Si$ and $^{30}Si(p, ^{3}He)^{28}Al$ leading to the T = 2 analogue states, the $(p, ^{3}He)$ cross section data having been multiplied by 0.62 as suggested by Eq. IV-1. The distributions of the (p,t) reaction leading to the ^{28}Si ground and 1.780 MeV states are shown for comparison. The solid curves represent DWBA fits for L = 0 (analogue T = 2 and ground states) and L = 2 (1.780 MeV state) using the parameters given in Table 2.

Fig. 14. Energy level diagrams of known T = 1 states in mass-28 and mass-32. For clarity, the T = 0 levels in ^{28}Si and ^{32}S have been deleted, and the lowest T = 1 levels in all nuclei in the triad have been set equal.

Fig. 15. Energy spectra of the reactions $^{34}S(p,t)^{32}S$ and $^{34}S(p, ^{3}He)^{32}P$ taken at $\theta_{LAB} = 22.3°$ for 6380 μCoulombs. The target 67.92% enriched in ^{34}S, with 31.55% ^{32}S, 0.44% ^{33}S and 0.09% ^{36}S. The calibration for the T = 2 states was established using the clearly resolved known states shown.

Fig. 16. Energy spectra of the reactions $^{36}Ar(p,t)^{34}Ar$ and $^{36}Ar(p,^{3}He)^{34}Cl$ taken at $\theta_{LAB} = 24.1°$ for 3450 μCoulombs. The argon gas used was 99.6% enriched in ^{36}Ar. The excitations shown (bracketed) were determined in this work; the calibration was established using the unbracketed states and a CO_2 target run before and after the Ar experiments: see text.

Fig. 17. Energy spectra of the reactions $^{36}Ar(d,\alpha)^{34}Cl$, $^{38}Ar(d,\alpha)^{36}Cl$ and $^{40}Ar(d,\alpha)^{38}Cl$ all taken at $\theta_{LAB} = 22.3°$ for 2200 μCoulombs, 4000 μCoulombs and 5300 μCoulombs resp. The ^{36}Ar target was 99.6% enriched in ^{36}Ar, the ^{38}Ar target was 50.8% enriched in ^{38}Ar and the ^{40}Ar target was a natural argon target (99.6% ^{40}Ar).

Fig. 18. Energy level diagrams of the known states in mass-34. The ground states of ^{34}S and ^{34}Ar are normalized to the same energy as the ^{34}Cl ground state. Some levels not observed in these experiments are deleted.

Fig. 19. Angular distributions of the reactions $^{36}Ar(p,t)^{34}Ar$ and $^{36}Ar(p,^{3}He)^{34}Cl$ leading to T = 1 final states. The ^{3}He data have been multiplied by $2k_t/k_{^3He}$ as suggested by Eq. IV-1. The dashed curves through the triton data serve to guide the eye; the identical curves have been drawn through the ^{3}He data (arbitrarily normalized) to facilitate shape comparison.

Fig. 20. Angular distributions of the reactions $^{36}Ar(p,t)^{34}Ar$, $^{38}Ar(p,t)^{36}Ar$ and $^{40}Ar(p,t)^{38}Ar$ leading to $J^\pi = 0^+$ and 2^+ states.

The dashed curves are DWBA fits obtained using the parameters given in Table 2. The errors shown on the points are based purely on counting statistical errors, with no inclusion of background error.

Fig. 21. Angular distributions of the reaction $^{36}Ar(p, {}^{3}He)^{34}Cl$ leading to T = 0 final states. The dashed curves serve only to guide the eye; they have no theoretical significance.

Fig. 22. Angular distributions of the reactions $^{36}Ar(p,t)^{34}Ar$ and $^{36}Ar(p, {}^{3}He)^{34}Cl$ leading to final states of higher excitation. The curves through the data serve only to guide the eye. The errors on the data are purely counting statistical errors. No J^{π}; T could be assigned for these states from this work.

Fig. 23. Energy spectra of the reactions $^{38}Ar(p,t)^{36}Ar$ and $^{38}Ar(p, {}^{3}He)^{36}Cl$ taken at $\theta_{LAB} = 22.3°$ for 7562 μCoulombs. The argon gas was 50.8% ^{38}Ar; the other components were 23.3% ^{36}Ar and 25.9% ^{40}Ar. The excitations shown bracketed were determined in this work; the calibration was established using the known resolved states marked.

Fig. 24. Angular distributions of the reactions $^{38}Ar(p,t)^{36}Ar$ and $^{38}Ar(p, {}^{3}He)^{36}Cl$ leading to T = 1 and T = 2 analogue final states. The ^{3}He cross section data corresponding to the ^{36}Cl ground and 1.949 MeV states have been normalized to the triton data; that corresponding to the proposed state in ^{36}Cl at 3.12 MeV has been multiplied by the factor predicted assuming its formation by

$(2s\ 1/2)^2$ pickup. The ^{3}He data corresponding to the T = 2 analogue has been multiplied by the factor suggested by Eq. IV-1. The dashed curves through the triton data serve to guide the eye; the identical curve has been drawn through the ^{3}He data.

Fig. 25. Angular distributions of the reaction $^{38}Ar(p,t)^{36}Ar$ leading to T = 0 final states. The curve serves only to guide the eye.

Fig. 26. Energy spectra of the reactions $^{40}Ar(p,t)^{38}Ar$ and ^{40}Ar $(p, {}^3He)^{38}Cl$ taken at θ_{LAB} = 26.8° for 12553 μCoulombs. The target was a mixture (80:20) of natural argon (99.6% ^{40}Ar) and methane. The states shown bracketed were determined in this work; the calibration was established using the known resolved states.

Fig. 27. Angular distribution of the reactions $^{40}Ar(p,t)^{38}Ar$ and $^{40}Ar(p, {}^3He)^{38}Cl$ leading to T = 2 and T = 3 final states. The T = 2 ^{3}He data with corresponding triton data was multiplied by the factor predicted based on the configuration of the pickup forming the state. The T = 3 ^{3}He data have been multiplied by the factor suggested by Eq. IV-1. The dashed curves through the triton data serve to guide the eye; the identical curves have been drawn through the ^{3}He data.

Fig. 28. Angular distributions of the reaction $^{40}Ar(p, {}^3He)^{38}Cl$ leading to T = 2 final states whose triton analogues were not observed with sufficient cross section to permit comparisons. The dashed curves serve to guide the eye.

Fig. 29. Angular distributions of the reaction $^{40}Ar(p,t)^{38}Ar$ leading to T = 1 final states. The dashed curves serve to guide the eye.

Fig. 30. Energy spectra of the reactions $^{42}Ca(p,t)^{40}Ca$ and $^{42}Ca(p, ^{3}He)^{40}K$ taken at $\theta_{LAB} = 26.8°$ for 3554 μCoulombs. The target was 94.42% enriched in ^{42}Ca. The excitations of the T = 2 states were determined using those known resolved states shown as calibrations.

Fig. 31. Energy level diagram of the known T = 1 states in mass-20. The ^{20}F and ^{20}Na ground states have been normalized to the lowest T = 1 level in ^{20}Ne for comparison.

Fig. 32. Angular distributions of the reaction $^{22}Ne(p,t)^{20}Ne$ and $^{22}Ne(p, ^{3}He)^{20}F$ leading to T = 1 final states. The ^{3}He data have been multiplied by the factor predicted assuming j^2 pickup. The solid lines through the triton data serve to guide the eye: the identical lines have been drawn through the ^{3}He data. The broken lines represent DWBA fits, for L = 2 in the case of the ^{20}Ne 10.275 MeV state, and the L values indicated for the ^{20}Ne 12.250 MeV state. The parameters used are given in Table 2.

Fig. 33. Energy level diagram of the known T = 1 states in mass-24. The ^{24}Na and ^{24}Al ground states have been normalized to the lowest T = 1 level in ^{24}Mg to simplify comparison.

Fig. 34. Angular distributions of the reactions $^{30}Si(p,t)^{28}Si$ and $^{30}Si(p, ^{3}He)^{28}Al$ leading to T = 1 final states. The solid curves

serve to guide the eye; the identical curve has been drawn through the ^{3}He data. The dashed curves represent L = 0 (for the 10.700 MeV state) and L = 2 (for the 9.379 MeV and 10.909 MeV states) DWBA fits using the parameters in Table 2.

Fig. 35. Energy level diagram of the known T = 1 states in mass-36. The ^{36}Cl and ^{36}K ground states have been normalized to the lowest T = 1 state in ^{36}Ar to simplify comparison.

Fig. 36. Energy levels of the known T = 2 states in mass-38. The ^{38}Cl ground state has been normalized to the predicted excitation of the lowest T = 2 state in ^{38}Ar. The lowest T = 1 state in ^{38}K has been normalized to the ^{38}Ar ground state for comparison.

Fig. 37. A plot of the goodness of fit parameter (χ^2) versus the strength of the A dependence (λ) used in predicting Coulomb energy differences based on the seniority and supermultiplet energy equations for the (1d 5/2)-shell. The significance of the curves I, II, and III is discussed in section V-C of the text.

TECHNICAL INFORMATION DIVISION
LAWRENCE RADIATION LABORATORY
UNIVERSITY OF CALIFORNIA
BERKELEY, CALIFORNIA 94720